

วัสดุกำบังนิวตรอนแบบใหม่ที่ประกอบด้วยยางผสมของยางพาราธรรมชาติ-ยางสไตรีนบิวตาไดอีน
และไดโบรอนไตรออกไซด์

นางสาวชนวนิชญ์ จำปี



จุฬาลงกรณ์มหาวิทยาลัย

CHULALONGKORN UNIVERSITY

บทคัดย่อและแฟ้มข้อมูลฉบับเต็มของวิทยานิพนธ์ตั้งแต่ปีการศึกษา 2554 ที่ให้บริการในคลังปัญญาจุฬาฯ (CUIR)

เป็นแฟ้มข้อมูลของนิสิตเจ้าของวิทยานิพนธ์ ที่ส่งผ่านทางบัณฑิตวิทยาลัย

วิทยานิพนธ์นี้เป็นส่วนหนึ่งของการศึกษาตามหลักสูตรบริณูณาวิชากรรนศาสตรดุษฎีบัณฑิต

The abstract and full text of theses from the academic year 2011 in Chulalongkorn University Intellectual Repository (CUIR)
are the thesis authors' files submitted through the University Graduate School.

คณะวิศวกรรมศาสตร์ จุฬาลงกรณ์มหาวิทยาลัย

ปีการศึกษา 2557

ลิขสิทธิ์ของจุฬาลงกรณ์มหาวิทยาลัย

INNOVATIVE NEUTRON SHIELDING MATERIAL COMPOSING OF NATURAL RUBBER-
STYRENE BUTADIENE RUBBER BLENDS AND DIBORON TRIOXIDE

Miss Chayanit Jumpee



จุฬาลงกรณ์มหาวิทยาลัย
CHULALONGKORN UNIVERSITY

A Dissertation Submitted in Partial Fulfillment of the Requirements
for the Degree of Doctor of Engineering Program in Nuclear Engineering

Department of Nuclear Engineering

Faculty of Engineering

Chulalongkorn University

Academic Year 2014

Copyright of Chulalongkorn University

Thesis Title INNOVATIVE NEUTRON SHIELDING MATERIAL
 COMPOSING OF NATURAL RUBBER-STYRENE
 BUTADIENE RUBBER BLENDS AND DIBORON
 TRIOXIDE

By Miss Chayanit Jumpee

Field of Study Nuclear Engineering

Thesis Advisor Associate Professor Dr.Doonyapong Wongsawaeng

Accepted by the Faculty of Engineering, Chulalongkorn University in Partial
Fulfillment of the Requirements for the Doctoral Degree

..... Dean of the Faculty of Engineering

(Professor Dr.Bundhit Eua-arporn)

THESIS COMMITTEE

..... Chairman

(Associate Professor Dr.Supitcha Chanyotha)

..... Thesis Advisor

(Associate Professor Dr.Doonyapong Wongsawaeng)

..... Examiner

(Associate Professor Dr.Sunchai Nilsuwankosit)

..... Examiner

(Associate Professor Somyot Srisatit)

..... Examiner

(Associate Professor Nares Chankow)

..... External Examiner

(Dr.Phiphat Phruksarojanakun)

ชญาณิษฐ์ จำปี : วัสดุกำบังนิวตรอนแบบใหม่ที่ประกอบด้วยยางพาราธรรมชาติ-
ยางสไตรีนบิวตาไดอีนและไดโบรอนไตรออกไซด์ (INNOVATIVE NEUTRON SHIELDING
MATERIAL COMPOSING OF NATURAL RUBBER-STYRENE BUTADIENE RUBBER BLENDS
AND DIBORON TRIOXIDE) อ.ที่ปรึกษาวิทยานิพนธ์หลัก: รศ. ดร.ดุลยพงศ์ วงศ์แวง, 108 หน้า.

การทำงานเกี่ยวกับต้นกำเนิดรังสีนิวตรอนต้องมีความระมัดระวังเป็นพิเศษ เนื่องจากนิวตรอนเป็นอนุภาคที่ไม่มีประจุไฟฟ้าจึงมีอำนาจทะลุทะลวงสูง ดังนั้นการใช้วัสดุกำบังรังสีนิวตรอนจึงเป็นอีกวิธีหนึ่งในการป้องกันอันตรายจากรังสีนิวตรอนที่มีประสิทธิภาพ งานวิจัยนี้ได้ทำการออกแบบวัสดุกำบังรังสีนิวตรอนโดยใช้โปรแกรม Mote Carlo N Particle (MCNP) เพื่อเลือกวัสดุและรูปแบบที่เหมาะสมสำหรับเป็นวัสดุกำบังรังสีนิวตรอน โดยกำหนดให้มีความหนาของวัสดุที่ 1 ซม. และ 10 ซม. สำหรับกำบังเทอร์มัลนิวตรอน ($10^{-8} - 10^{-2}$ MeV) และทุกย่านพลังงานของนิวตรอน ($10^{-8} - 100$ MeV) ตามลำดับ ผลการออกแบบพบว่า วัสดุที่ดีที่สุดสำหรับกำบังเทอร์มัลนิวตรอนคือ วัสดุที่ประกอบด้วยยางพาราธรรมชาติ (NR) และยางเอสบีอาร์ (SBR) ในอัตราส่วน 1:1 และได้โดยรอนไตรออกไซด์ (B_2O_3) 60 part per hundred rubber (phr) ซึ่งสามารถลดTHONนิวตรอนจากต้นกำเนิด Am-Be ได้ที่ 53.91% และมีค่าภาคตัดขวางทั้งหมด (Total macroscopic cross section) 0.076 ซม.⁻¹ และวัสดุสำหรับกำบังรังสีนิวตรอนในทุกย่านพลังงาน ได้แก่วัสดุ 4 ชั้นที่ประกอบด้วยชั้นของยางพาราธรรมชาติและเหล็กออกไซด์ (Fe_2O_3) 100 phr หนาชั้นละ 2.5 ซม. สลับกับชั้นของยางพาราผสมกับยางสังเคราะห์เอสบีอาร์ในอัตราส่วน 1 : 1 และได้โดยรอนไตรออกไซด์ (B_2O_3) 10 phr หนาชั้นละ 2.5 ซม. ซึ่งสามารถลดTHONนิวตรอนจากต้นกำเนิด Am-Be ได้ที่ 72.56% และเมื่อเพิ่มวัสดุโลหะหนา 1 มม. เข้าไปเป็นโครงสร้างเพิ่มเติมทั้งด้านหน้าและด้านหลังของวัสดุกำบังรังสีนิวตรอนพบว่า แคดเมียมสามารถช่วยลดTHONรังสีนิวตรอนได้มากขึ้นที่สุด ซึ่งเมื่อเปรียบเทียบผลการกำบังรังสีนิวตรอนในทุกย่านพลังงานของวัสดุกำบังในรูปทรงสี่เหลี่ยมจัตุรัส ทรงกระบอกและทรงกลมที่มีปริมาตรเท่ากัน พบว่าวัสดุกำบังทรงกลมสามารถกำบังรังสีนิวตรอนได้ดีที่สุด จากนั้นจึงทำการทดลองชั้นรูปชั้นวัสดุกำบังรังสีนิวตรอนและนำไปถ่ายภาพด้วยนิวตรอนเพื่อดูการกระจายตัวของวัสดุคลื่น และกระเจิงรังสีนิวตรอนที่เติมลงไปในส่วนผสมของยาง ซึ่งพบว่ามีการกระจายตัวสม่ำเสมอทั่วทั้งชิ้นงาน และผลจากการประเมินรังสีแกมมาเมื่อใช้งานวัสดุกำบังรังสีนิวตรอนด้วยวิธี Prompt Gamma Neutron Activation Analysis (PGNAA) พบว่ามีการเกิดรังสีแกมมาทุติยภูมิปริมาณต่ำชั้นมาที่พลังงาน 478 keV ดังนั้นวัสดุกำบังรังสีที่ออกแบบนี้สามารถนำไปประยุกต์ใช้กำบังรังสีนิวตรอนได้อย่างมีประสิทธิภาพ

ภาควิชา วิศวกรรมนิวเคลียร์

ลายมือชื่อนิสิต _____

สาขาวิชา วิศวกรรมนิวเคลียร์

ลายมือชื่อ อ.ที่ปรึกษาหลัก _____

ปีการศึกษา 2557

5371841821 : MAJOR NUCLEAR ENGINEERING

KEYWORDS: NEUTRON SHIELDING / THERMAL NEUTRON / MCNP / NATURAL RUBBER / SBR / DIBORON TRIOXIDE / IRON(III) OXIDE

CHAYANIT JUMPEE: INNOVATIVE NEUTRON SHIELDING MATERIAL COMPOSING OF NATURAL RUBBER-STYRENE BUTADIENE RUBBER BLENDS AND DIBORON TRIOXIDE.
ADVISOR: ASSOC. PROF. DR.DOONYAPONG WONGSAWAENG, 108 pp.

Utilization of neutron sources requires careful safety precaution because neutrons have no electric charge and have high penetrating power. Therefore, the use of neutron shielding material is one of the methods to effectively prevent neutron radiation hazard. In this research work, neutron shielding materials were designed using the Monte Carlo N-Particle (MCNP) code in order to select proper materials and dimensions for neutron shielding. Thicknesses of 1 cm and 10 cm were chosen for shielding thermal neutron (10^{-8} - 10^{-2} MeV) and neutron in the entire energy spectrum (10^{-8} - 100 MeV), respectively. Simulation results indicated that the best shielding material for thermal neutron composed of natural rubber (NR) and SBR rubber blend in the 1:1 ratio with 60 part per hundred rubber (phr) diboron trioxide (B_2O_3), which can reduce the neutron dose from the Am-Be source by 53.91% with the total macroscopic cross section of 0.076 cm^{-1} . For shielding neutron in the entire energy spectrum, the best shielding material was four alternating layers of NR with 100 phr iron (III) oxide (Fe_2O_3) and of NR and SBR blend in the 1:1 ratio with 10 phr diboron trioxide (B_2O_3), each layer having 2.5 cm in thickness. This shielding material can reduce the neutron dose by 72.56%. Addition of 1 mm cadmium sheets on the front and back sides offered the most additional neutron shielding performance. Comparison of the cubical, cylindrical and spherical shapes of the neutron shielding material with the same volume revealed that the spherical shape offered the best shielding performance for neutron in the entire energy spectrum. The optimal neutron shielding materials were fabricated and neutron radiography was performed to determine the homogeneity of the absorbing and scattering materials added to the rubber matrix. Result revealed good homogeneity throughout the shielding materials. Assessment of the produced secondary gamma ray by Prompt Gamma Neutron Activation Analysis (PGNAA) revealed a low-dose 478 keV gamma ray. Therefore, the designed shielding material can be utilized to effectively shield against neutrons.

Department: Nuclear Engineering

Student's Signature

Field of Study: Nuclear Engineering

Advisor's Signature

Academic Year: 2014

ACKNOWLEDGEMENTS

I would like to express my profound gratitude to Assoc. Prof. Dr. Doonyapong Wongsawaeng, my advisor, for valuable advices, continued suggestions, caring, patience, and for his excellent guidance which help me all the time of research and writing of this dissertation. Your advice on both research as well as on my career have been priceless. Not only the research methodologies but also many other methodologies in life. I would not have achieved this far and this thesis would not have been completed without all the support that I have always received from him.

I offer my sincere appreciation for the learning opportunities, kind support and valuable advices provided by all lecturers and staff members at the Nuclear Engineering Department, Faculty of Engineering, Chulalongkorn University.

I would like to thank the Graduate School, Chulalongkorn University, and The Commission on Higher Education under Strategic Scholarships for Frontier Research Network for the Ph.D. Program Thai Doctoral Degree for the funding support of my Ph.D. study and research work.

I would like to thank the Rubber research institute of Thailand, Department of agriculture for the equipment supports.

I also thank my friends for providing support and friendship that I needed.

Finally, a special thanks to my family. My hard-working parents have sacrificed their lives for my sister and myself and provided unconditional love and care. I thank tremendously my father Mr. Wichian Jumpee, my mother Mrs. Tassanee Jumpee, my younger sister Ms. Tichanun Jumpee. Words cannot express how grateful I am to them. I would also like to thank my best friend Mr. Chanwit Pinkome who was always my support in the moment when there was no one respond my queries. At the end I would like to express my appreciation to all close relatives for their invaluable help and constant encouragement during the full course of my study.

CONTENTS

	Page
THAI ABSTRACT	iv
ENGLISH ABSTRACT	v
ACKNOWLEDGEMENTS	vi
CONTENTS.....	vii
LIST OF TABLES	xii
LIST OF FIGURES.....	xiii
CHAPTER 1	1
INTRODUCTION	1
1.1 Background and rationale	1
1.2 Research objective	3
1.3 Scope of Dissertation.....	3
CHAPTER 2	4
THEORY AND LITERATURE REVIEW.....	4
2.1 Neutron.....	4
2.1.1 Neutron Sources	4
2.1.1.1 Spontaneous fission Radioisotopes	4
2.1.1.2 Alpha particles packed in a low-Z elemental matrix (α, n).....	5
2.1.1.3 High energy photons co-located with beryllium or deuterium (γ, n)	5
2.1.1.4 Plasma focus and plasma pinch devices	5
2.1.1.5 Light ion accelerators	6
2.1.1.6 High energy photo-neutron/photo-fission systems	6

	Page
2.1.1.7 Nuclear fission reactors.....	6
2.1.1.8 Spallation at particle accelerators.....	6
2.1.1.9 Nuclear fusion systems	7
2.1.2 Neutron Division (by Energy Level)	7
2.1.3 Neutron Detection.....	8
2.1.3.1 Neutron detection by neutron capture	8
2.1.3.2 Neutron detection by elastic scattering	8
2.1.4 Uses.....	8
2.1.5 Interaction between Neutrons and Matter (14)	9
2.1.5.1 Elastic Scattering (n, n).....	9
2.1.5.2 Inelastic Scattering. ($n, n'+\gamma$)	10
2.1.5.3 Transmutation (n, p), (n, α)	10
2.1.5.4 Neutron-Proton Reaction (n, p).....	11
2.1.5.5 Neutron-Alpha Reaction (n, α)	11
2.1.5.6 Radiative Capture (n, γ).....	11
2.1.5.7 Fission	13
2.1.6 Neutron cross section (15).....	13
2.1.6.1 Target type	15
2.1.6.2 Incident particle energy dependence	15
2.1.6.3 Target temperature dependence	15
2.1.6.4 Reaction type.....	16
2.1.7.5 Scattering cross-section.....	16
2.1.6.6 Absorption cross section	17

	Page
2.2 Monte Carlo N-Particle code (MCNP)	21
2.2.1 The Monte Carlo Method.....	21
2.2.1.1 <i>MCNP input for problem</i>	22
2.2.1.2 <i>The output</i>	23
2.2.1.3 <i>Estimation of Monte Carlo Errors</i>	24
2.3 Rubber.....	25
2.3.1 Natural rubber (19).....	25
2.3.1.1 <i>Natural Rubber Latex</i>	25
2.3.1.2 <i>Dry/Solid Rubber</i>	26
2.3.1.3 <i>Chemical Structure of Natural Rubber</i>	26
2.3.1.4 <i>Properties of Natural Rubber</i>	27
2.3.1.5 <i>Mixing natural rubber with other polymers</i>	30
2.3.2 Styrene-butadiene(19).....	31
2.3.2.1 <i>Chemical Structure, Production and Properties of Styrene-Butadiene-Rubber(SBR)</i>	31
2.3.2.2 <i>Mixing with chemical rubber</i>	34
2.3.2.3 <i>Mixing SBR with other polymers</i>	34
2.3.2.4 <i>Applications</i>	34
2.4 Borate minerals.....	35
2.4.1 Boracite	38
2.4.2 Boron Oxide	39
METHODOLOGY	40
3.1 Materials.....	40

	Page
3.2 Boron detection in potash ore core by alpha track etch method.....	42
3.3 Material selection by MCNP simulation.....	42
3.3.1 Optimization the type of neutron shielding materials.....	42
3.3.2 Optimization of the amount of neutron absorber/scatter.....	45
3.3.3 Comparison of the neutron shielding performance between innovative neutron shielding materials and other ordinary neutron shielding materials	45
3.3.4 Additional material for improving the total neutron shielding performance	46
3.3.5 Shape effect of neutron shielding material	47
3.4 Fabrication of the shielding materials.....	47
3.4.1 Material's homogeneity verification.....	49
3.5 Experimental work on neutron attenuation.....	49
3.6 Secondary gamma radiation analysis by prompt gamma neutron activation analysis (PGNAA).....	50
CHAPTER 4	52
RESULT AND DISCUSSION.....	52
4.1. Boron detection in potash ore core by alpha track etch	52
4.2. Material selection by MCNP simulation.....	54
4.2.1 Optimization of the type of neutron shielding materials.....	54
4.2.2 Optimization of the amount of neutron absorber/scatter.....	58
4.2.3 Comparison of the neutron shielding performance between innovative neutron shielding materials and other ordinary neutron shielding materials	61

	Page
4.2.4 Additional material for improving the total neutron shielding performance	68
4.2.5 Different shapes of neutron shielding material.....	69
4.3. Fabrication of rubber compound.....	72
4.4. Neutron transmission test	79
4.5 Secondary gamma radiation determination	81
CHAPTER 5	83
CONCLUSION	83
5.1 Conclusion	83
5.2 Suggestion and future studies.....	85
APPENDICES	86
APPENDIX A.....	87
Neutron cross sections of common materials (24).....	87
APPENDIX B	90
Neutron Flux-to-Dose Rate Conversion Factors and Quality Factors.....	90
Photon Flux-to-Dose Rate Conversion Factors.....	91
APPENDIX C.....	93
NEUTRON SOURCE	93
APPENDIX D.....	95
EXAMPLE OF MCNP INPUT FILE	95
REFERENCES.....	104
VITA	108

LIST OF TABLES

Table 1: Radioisotopes which decay with alpha particles packed in a low-Z elemental matrix.....	5
Table 2: Neutron classification by energy level(13).....	7
Table 3: Guidelines for Interpreting the Relative Error R*.....	24
Table 4: General properties of boracite	38
Table 5: Properties of boron oxide	39
Table 6 : Main compositions of considered neutron shielding materials (40 phr each of B_2O_3 , PbO_2 and Fe_2O_3)	44
Table 7: The composition of ordinary neutron shielding material.....	46
Table 8: Ingredients for fabrication of most appropriate rubber compounds	49
Table 9: Optimized composition of innovative neutron shielding materials.....	61
Table 10: The calculated transmission factor of various neutron shielding material	68
Table 11: Properties of vulcanized rubber sample.....	73

CHULALONGKORN UNIVERSITY

LIST OF FIGURES

Figure 1: Elastic Scattering (n, n)	9
Figure 2: Inelastic Scattering. ($n, n' + \gamma$)	10
Figure 3: Neutron-Proton Reaction (n, p)	11
Figure 4: Neutron-Alpha Reaction (n, α)	11
Figure 5: Radiative Capture (n, γ) of hydrogen becomes to deuterium.....	12
Figure 6: Radiative Capture (n, γ) of deuterium becomes to tritium	12
Figure 7: Interaction between neutron beam and target area	14
Figure 8: Relation between U-235 fission cross-section and neutron energy(16)...	15
Figure 9: The Monte Carlo Method	22
Figure 10: Chemical structure of natural rubber.....	26
Figure 11: Chemical structure of SBR.....	31
Figure 12: Somboon sylvinitic ore type of potash ; Asia Pacific Potash Corporation company, Udon Thani province , Thailand.....	37
Figure 13: Boracite, Mineralogisches Museum Bonn	38
Figure 14 :The vertical section of potash core sample (Somboon type) with the CR 39 track etch detector plates (size = 1 cm x 1 cm) at the positions A, B, C and D..	42
Figure 15: Schematic representation of the Monte Carlo model.....	45
Figure 16: The two roll mill (Kodaira Seisakusho Co.,Ltd ; model : R 11-3 FF) at The Rubber Research Institute of Thailand.....	48
Figure 17: The electrically-heated hydraulic compression machine : PR2D-W500L500 PM (CHAREON TUT CO.,LTD).....	48
Figure 18: Geometry of the neutron transmission test	50
Figure 19: The top view of prompt gamma radiation counting system.....	51

Figure 20 :The vertical section of potash core sample (Somboon type) that was attached with the CR 39 track etch detector plates at the positions A, B, C and D.....	53
Figure 21: Micrographs of CR-39 etched alpha tracks, showing much higher track densities at potash core positions A (a) and B (b) compared to positions C (c) and D (d).....	53
Figure 22: (a) Neutron dose equivalent rate (neutron energy 10^{-8} – 100 MeV), (b) Secondary gamma dose equivalent rate and (c) total dose equivalent rate on the outer surface of 1 cm radius sphere shielding sample.	55
Figure 23: Neutron dose equivalent rate [(rem/hr)/neutron] spectra of total neutron energy range (10^{-8} – 100 MeV) on the outer surface of 1 cm rubber shielding materials.....	56
Figure 24: (a) Neutron dose equivalent rate (neutron energy 10^{-8} – 100 MeV), (b) Secondary gamma dose equivalent rate and (c) total dose equivalent rate on the outer surface of 10 cm radius sphere shielding sample.....	57
Figure 25: Neutron dose equivalent rate [(rem/hr)/neutron] spectra of total neutron energy range (10^{-8} – 100 MeV) on the outer surface of 10 cm rubber shielding materials.....	58
Figure 26: (a) The neutron dose equivalent rate and secondary gamma (photon) dose equivalent rate on the outer surface of spherical neutron shielding material at different amount of neutron absorber (Part per hundred rubber; phr) for 1 cm of sample #2 and (b) total dose equivalent rate (both neutron and photon) from <i>thermal neutron source</i> (10^{-8} – 10^2 MeV)	59
Figure 27: Total dose rate on the outer surface of sphere neutron shielding at different amounts of neutron absorbers for sample#10 from <i>entire energy range of neutron source</i> (10^{-8} – 100 MeV)	60
Figure 28: (a) The neutron and secondary gamma (photon) dose equivalent rate (<i>from thermal neutron source</i> ; 10^{-8} – 10^2 MeV) and (b) transmission factor (I/I_0) of	

total dose equivalent rate on the outer surface of 1 cm radius sphere shielding materials.....	63
Figure 29: Neutron dose equivalent rate [(rem/hr)/neutron] spectra for thermal neutron (10^{-8} – 10^{-2} MeV) at the outer surface of 1 cm radius sphere shielding materials.....	64
Figure 30: (a) The neutron and secondary gamma (photon) dose equivalent rate (from entire energy neutron source; 10^{-8} – 100 MeV) and (b) transmission factor (I/I_0) of total dose equivalent rate on the outer surface of 10 cm radius sphere shielding materials.....	66
Figure 31: Neutron dose equivalent rate [(rem/hr)/neutron] spectra at the outer surface of 10 cm thick ordinary neutron shielding materials and the innovative neutron shielding material (sample #10).....	67
Figure 32: The column chart of dose equivalent rate for (a) entire energy of neutron, (b) secondary gamma ray and (c) total dose of neutron and gamma ray with various additional metal plates	69
Figure 33: Drawing of cross section of various shapes for neutron shielding material sample #10 for MCNP modeling	70
Figure 34: The transmission factor of various shapes of neutron shielding material with and without cadmium sheets.....	71
Figure 35: The neutron dose distribution at each plane ($15 \times 15 \text{ cm}^2$) of cube detector around each shielding shape.....	71
Figure 36: (a) Front view and (b) side view of 1 cm (NR+SBR+B ₂ O ₃ 60 PHR: sample #2) shielding material samples trial-produced to fabricate slab shape. (c) Neutron radiograph of this shielding material (front view).	73
Figure 37: (a) The background counting intensity profile at various positions on the image plate (no material) and (b) the neutron radiograph with indicated profile's positions.	74

Figure 38: (a) The counting intensity profile at various positions on 1 cm thick sample #10 and (b) neutron radiograph with indicated profile's positions.....	75
Figure 39: SEM micrographs of the surface of the vulcanized rubber (NR+SBR+B ₂ O ₃ 60 PHR) for magnifications of 200x (a) and 1,000x (b) showing the blooming of B ₂ O ₃ particles (and boric acid) (red arrows) on the rubber surface without encasing in a thin layer of conventional rubber compound.	76
Figure 40: The front view of each layer of neutron shielding material: (a) NR+Fe ₂ O ₃ 100 phr, (b) NR+SBR+B ₂ O ₃ 5 phr, (c) the side view of 4 layers of sample #10 (2.5 cm each) and (d) neutron radiograph of this 10 cm neutron shielding material (front view).	77
Figure 41: (a) The counting intensity profile at various positions on 10 cm thick sample #10 and (b) neutron radiograph with indicated profile's positions.....	78
Figure 42: SEM micrographs of the surface of the vulcanized rubber (NR+SBR+Fe ₂ O ₃ 100 PHR) for magnifications of 200x (a) and 10,000x (b).....	79
Figure 43: The relationship between transmitted neutron and material thickness of (a) sample #2 and (b) sample #10.	80
Figure 44: (a) Gamma ray spectrum of ²⁴¹ AmBe neutron source (background) and (b) secondary gamma ray spectrum from neutron interaction with sample #2 and sample #10.....	82

CHAPTER 1

INTRODUCTION

1.1 Background and rationale

Neutrons have been widely used in medical, agricultural and industrial applications. For example, they are used to produce radiopharmaceuticals, improve plant seed, measure soil humidity and take photographs of materials with low atomic mass numbers. Since neutrons have no electric charge, they can travel through the electron cloud and directly interact with the atomic nucleus. During collision, a neutron can transfer almost all of its energy to a nucleus having a similar mass to it, e.g., hydrogen. Human body has high water content, so there are many hydrogen atoms in our bodies. The mass of hydrogen nucleus is very close to that of neutron, therefore, exposure to free neutrons can be hazardous since the interaction of neutrons with molecules in the body can cause disruption to molecules and atoms, and can also cause reactions which give rise to other forms of radiation such as protons which has high Linear Energy Transfer (LET).⁽¹⁾ The normal precautions of radiation protection apply: avoid exposure, stay as far from the source as possible, and keep exposure time to a minimum. Since neutrons have unique properties and strong penetrating power, some particular thought must be given on how to protect from neutron exposure. For other types of radiation, e.g., alpha particles and gamma rays, materials of high atomic numbers and high densities offer good shielding. Lead is frequently used. However, this approach will not work with neutrons, since the absorption of neutrons does not increase with atomic number, as it does with alpha, beta and gamma radiations. Neutron shielding needs some materials which have atomic mass close to that of neutron.⁽²⁾ For example, hydrogen-rich materials are often used to shield against neutrons, since hydrogen atoms both scatter and slowdown neutrons. After slowing down, neutrons may then be absorbed with an isotope which has a high affinity for slow neutrons such as boron-10.

Several experimental works prepared polymeric compositions containing materials with high neutron cross section to study their thermal neutron shielding properties. Materials made of polyethylene or epoxy resin mixed with boron compound (ilmenite and colemanite) are widely used as neutron shielding materials.(3) (4) Concrete is the most widely used construction material in the world for radiation shielding as well. There are several studies that have investigated the engineering and radiation (both gamma ray and neutron) shielding properties of concrete containing colemanite (or hematite). (5), (6), (7) However, they usually exhibit sizable weight and volume resulting in low-flexibility performances. Flexible polymers such as natural rubber were used as the matrix of neutron shielding materials, but they only shield against thermal neutrons.(8), (9)

In many areas of Thailand, there is a lot of natural rubber cultivation. This rubber is a hydrocarbon polymer containing a large number of hydrogen atoms and can easily be fabricated into flexible materials. In addition, borate minerals such as boracite, the boron compounds, are found in the Northeast of Thailand.(10) Thus, not only is the production of neutron shielding materials comprising of natural rubber/synthetic SBR blends and a borate material useful for neutron-related work, but it also utilizes domestic resources.

The most effective neutron shielding material can be obtained by appropriately mixing high hydrogen-content materials, heavy elements and thermal neutron absorbers together. High hydrogen-content materials can undergo elastic scattering with fast and intermediate-energy neutrons. Heavy elements can undergo inelastic scattering with fast neutrons and can attenuate the secondary gamma ray emission. Finally, neutron absorbers function to greatly reduce the number of thermal neutrons.

In this experimental work, rubbers, which are low-cost hydrocarbon polymers that can easily be fabricated into many different products and shapes, were selected as the substrate of the composite together with a low-cost neutron absorbing material, which is B_2O_3 . Fe_2O_3 (commonly known as rust), a very low-cost and usually disregarded material, was also utilized as the heavy element in the composite.

The method of calculation for neutron shielding can be found in references (11), (12). This research work incorporated inelastic scattering and shielding of

secondary gamma ray into the simulation part of the work. The compositions of neutron shielding materials were optimized by Monte Carlo simulations using the MCNP5 code considering the neutron flux encompassing the entire range of interaction energy and accounting for secondary gamma ray emissions.

Neutron attenuation experiments were carried out in order to verify neutron and secondary gamma ray shielding performances of the designed neutron shielding materials by using a simulated neutron source (energy 1×10^{-8} – 100 MeV) and an Am-Be neutron source.

1.2 Research objective

To develop and fabricate the neutron shielding material composing of natural rubber-styrene butadiene rubber blends and diboron trioxide

1.3 Scope of Dissertation

- 1.3.1 Utilize diboron trioxide derived from borate mineral available in Thailand.
- 1.3.2 Fabricate the neutron shielding material using natural rubber-styrene butadiene rubber blends and diboron trioxide
- 1.3.3 Estimate neutron attenuation using at least 1 neutron source.
- 1.3.4 Model the composition for neutron shielding materials by using MCNP transport code.

CHAPTER 2

THEORY AND LITERATURE REVIEW

2.1 Neutron

Production of neutron shielding material in this research work necessitates the study and understanding of the features and information related to neutrons. This section, therefore, discusses the following topics: information of neutrons, interaction of neutrons with matter, cross section of neutron and attenuation of neutron energy and neutron sources.

A neutron is an elementary particle with no electric charge and possesses a mass of 1.0086654 atomic mass unit (amu) or 1.67492×10^{-27} kg. The half-life of free neutron is about 10.2 minutes. All atom nuclei (except hydrogen) compose with neutrons and protons. In atomic nucleus is necessary to have neutrons for binding the protons together by the strong force because protons cannot bind with each other due to their mutual electric repulsion being stronger than the attraction of the strong force. The number of neutrons is the neutron number and determines the isotope of an element. For example, the abundant boron-11 isotope has 5 protons and 6 neutrons, while the rare boron-10 isotope has 5 protons and 6 neutrons. Neutron is not a chemical element, the free neutron is sometimes included in tables of nuclides. It is then considered to have an atomic number of zero and a mass number of one, and is sometimes referred to as neutronium which has the symbol n or 0_1n .

2.1.1 Neutron Sources

A neutron source is a device that emits neutrons. There are several of different sources, ranging from small size radioactive sources to neutron research facilities and research reactors.

Nowadays, the widely-used neutron sources can be categorized as follows:

2.1.1.1 *Spontaneous fission Radioisotopes*

The spontaneous isotope can undergo fission through natural processes by emitting free neutron. The most common spontaneous fission radioisotope is californium-252 that can emit free neutron energy 10^7 - 10^9 neutrons per second.

2.1.1.2 Alpha particles packed in a low-Z elemental matrix (α, n)

When alpha particles interact with low atomic weight material for example beryllium, carbon. Oxygen and lithium could produce free neutron. Therefore neutron source could be construct by mixing low atomic weight isotope with the radioisotope which emits alpha particles for example Americium-241 or radium. The useful lifetime for these types of sources is due to the half-life of the radioisotope that emits the alpha particles.

Table 1: Radioisotopes which decay with alpha particles packed in a low-Z elemental matrix

Neutron source	Half life	Neutrons/Second-Curies
$^{210}\text{Po-Be}$	138 days	3.0×10^6
$^{226}\text{Ra-Be}$	1,620 years	1.5×10^7
$^{238}\text{Pu-Be}$	86.4 years	2.2×10^6
$^{239}\text{Pu-Be}$	2.43 years	1.6×10^6
$^{241}\text{Am-Be}$	458 years	2.2×10^6

2.1.1.3 High energy photons co-located with beryllium or deuterium (γ, n)

Gamma radiation with an energy exceeding the neutron binding energy of a nucleus can eject a neutron. A examples and its decay products is:



2.1.1.4 Plasma focus and plasma pinch devices

The plasma focus neutron source produces controlled nuclear fusion by creating a dense plasma within which ionized deuterium and/or tritium gas is heated to temperatures sufficient for creating fusion.

2.1.1.5 Light ion accelerators

Neutrons could be produced by using particle accelerators source (hydrogen, deuterium or tritium ion) and targets of low-Z materials for example deuterium, tritium, lithium, and beryllium.

2.1.1.6 High energy photo-neutron/photo-fission systems

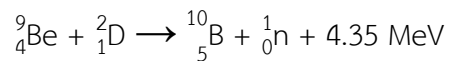
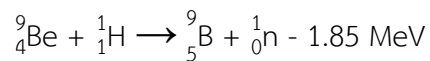
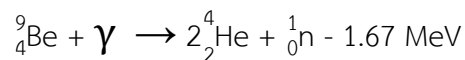
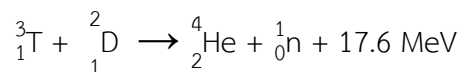
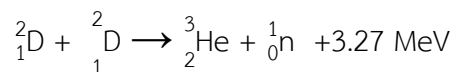
The interaction between matter and photon which has energy above the nuclear binding of them, could emit a neutron (photodisintegration) or undergoes fission (photo-fission). Typically, photons begin to produce neutrons upon interaction with normal matter at energies of about 7 - 40 MeV. Therefore high energy photon (megavoltage) radiotherapy facilities may produce neutron radiation as well. Moreover high energy electrons (over 50 MeV) may produce neutrons by a mechanism similar to that of photo-neutrons.

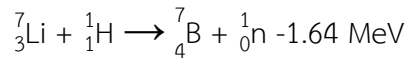
2.1.1.7 Nuclear fission reactors

The nuclear reactor produces very large quantities of neutrons by fission reaction. The uranium-235 fissile isotope is typically used in nuclear power reactors. .

2.1.1.8 Spallation at particle accelerators

A high-flux source in which protons that have been accelerated to high energies hit a target material, prompting the emission of neutrons. There are many reactions for using in these accelerators, for example:





2.1.1.9 Nuclear fusion systems

The combining of the heavy isotopes of hydrogen or nuclear fusion has the potential to produce large quantities of neutrons. There are a few of large scale nuclear fusion systems also exist including the National Ignition Facility (NIF) in the USA, Joint European Torus (JET) in the UK, and the International Thermonuclear Experimental Reactor (ITER) experiment in France.

2.1.2 Neutron Division (by Energy Level)

Neutrons come in many energy levels depending upon the sources. The interaction between neutrons and matters varies with the type of matter and the neutron energy level. Thus, in order to understand the neutron behaviors, it is customary to divide the neutron energy level into the following groups (some may overlap):

Table 2: Neutron classification by energy level(13)

Type of neutron	Energy Level
Cold neutron	< 0.003 eV
Thermal neutron	0.003 eV – 0.4 eV
Epithermal neutron	0.4 eV – 100 eV
Intermediated (resonance) neutron	100 eV – 200 keV
Fast neutron	200 keV – 10 MeV
High energy (relativistic) neutron	> 10 MeV

2.1.3 Neutron Detection

Neutrons can create an ionization track that is detectable by elastic scattering with atoms, but the experiments are difficult to carry out. The common method to detect neutrons can be categorized according to the nuclear processes relied upon, mainly elastic scattering or neutron capture.

2.1.3.1 Neutron detection by neutron capture

The nuclides have a high probability to absorb neutrons could be released energy by neutron capture reactions, then these energy would be converted to electrical signals. The neutron capture creates the compound nucleus emits more easily detectable radiation, such as an alpha particle. The nuclides $^{3}_{2}\text{He}$, $^{6}_{3}\text{Li}$, $^{10}_{5}\text{B}$, $^{233}_{92}\text{U}$, $^{235}_{92}\text{U}$, $^{237}_{93}\text{Np}$ and $^{239}_{94}\text{Pu}$ are useful for this purpose.

2.1.3.2 Neutron detection by elastic scattering

Neutrons could undergo elastic scattering with nuclei, during collision, a neutron can transfer almost all of its energy to a nucleus having a similar mass to it for example hydrogen nucleus. Recoiling nuclei can ionize and excite further atoms through collisions then could be produced scintillation light or charge for detecting the signal.

2.1.4 Uses

The neutrons have been widely used in many applications. For example, they are used to produce radiopharmaceuticals by neutron capture reaction including neutron activation analysis, improve plant seed, measure soil humidity by elastic scattering detection and take photographs of materials with low atomic mass numbers. In particular, knowledge of neutrons and their behavior has been important in the development of nuclear reactors and nuclear weapons.

2.1.5 Interaction between Neutrons and Matter (14)

Neutrons carry no electric charge. It is a highly-penetrating radiation because it can pass through the electron cloud of an atom and interact directly with the atomic nucleus. Thus, living tissues can be severely damaged by neutrons. In addition, neutrons can activate the stable nuclei to become radioactive nuclei.

This section introduces five reactions that can take place when a neutron interacts with a nucleus. In the first two, known as scattering reactions, a neutron is obtained from each reaction. In the remaining reactions, known as absorption reactions, the neutron is absorbed into the nucleus and a different type of radiation emerges.

2.1.5.1 Elastic Scattering (n, n)

An elastic scattering is similar to a billiard ball collision. A neutron collides with a nucleus, transfers some energy to it, and bounces off in a different direction. (Sometimes it absorbs the neutron and then reemits it, conserving the kinetic energy.) The fraction of its initial energy lost depends on whether it hits the target nucleus head-on or at an angle, exactly like the cue ball striking a ball on the billiard table. The target nucleus gains the energy lost by the neutron, and then moves away at an increased speed.

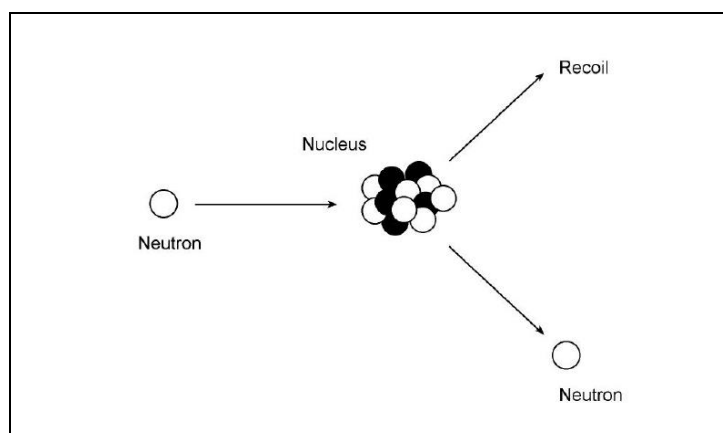


Figure 1: Elastic Scattering (n, n)

Light nuclei are the most effective for slowing down neutrons. A neutron colliding with a heavy nucleus rebounds with little loss of speed and transfers very little energy. This is similar to firing the cue ball at a cannon ball. On the other hand, neutrons will not be scattered by the light electron clouds surrounding the nucleus, but will travel straight through, much like throwing a baseball through a fog.

2.1.5.2 Inelastic Scattering. ($n, n' + \gamma$)

A neutron may strike a nucleus and be temporarily absorbed, forming a compound nucleus. This will be in an excited state. It may de-excite by emitting another neutron of lower energy, together with a gamma photon, which takes the remaining energy. This process is called inelastic scattering. It generally happens only when high-energy neutrons interact with heavy nuclei and has little practical importance for reactor operation.

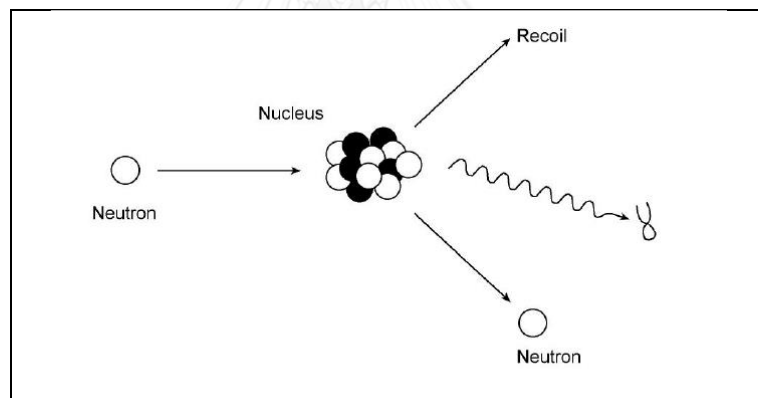


Figure 2: Inelastic Scattering. ($n, n' + \gamma$)

2.1.5.3 Transmutation (n, p), (n, α)

A neutron may be absorbed by nucleus and forming a compound nucleus, which then de-energizes by emitting a charged particle, either a proton or an alpha particle. This produces a nucleus of a different element. Such a reaction is called a transmutation. Transmutation is the transformation of one element into another by a nuclear reaction. For example:

2.1.5.4 Neutron-Proton Reaction (n, p)

Oxygen-16 captures a neutron and emits a proton to form nitrogen-16:

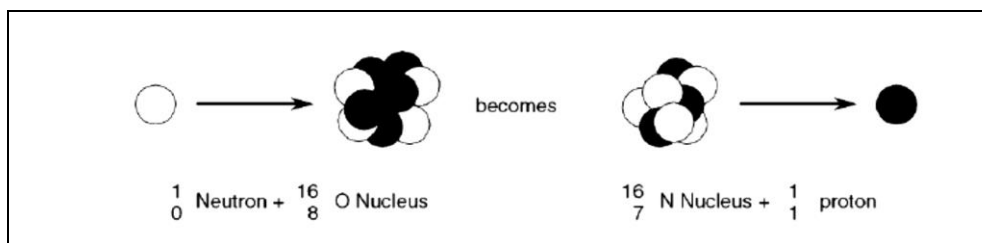


Figure 3: Neutron-Proton Reaction (n, p)

The product, nitrogen-16, is radioactive with a half-life of 7.1 seconds. So this example represents an activation reaction. N-16 is a beta emitter, but more importantly, it also emits very penetrating, high-energy gamma rays.

2.1.5.5 Neutron-Alpha Reaction (n, α)

Neutrons captured by boron-10 and become to lithium-7 and emit an alpha particle by following reaction:

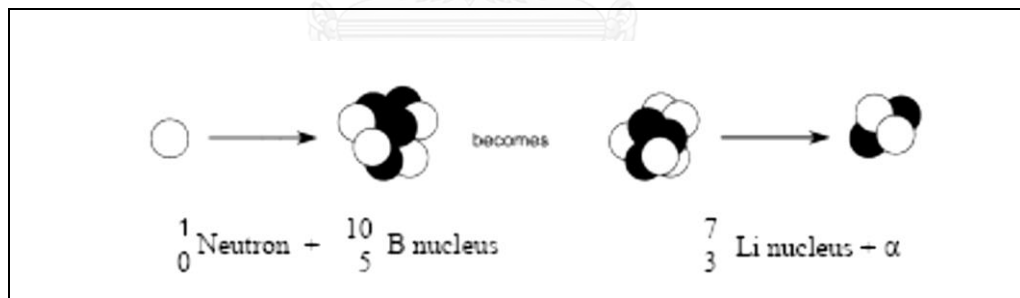


Figure 4: Neutron-Alpha Reaction (n, α)

2.1.5.6 Radiative Capture (n, γ)

The compound nucleus that was formed by nucleus capturing with neutron emits only a gamma photon. This mean the product nucleus is an isotope of the same element as the original nucleus. Its mass number increases by one. This is the most common nuclear reaction.

Example: The simplest radiative capture occurs when hydrogen absorbs a neutron to produce deuterium (heavy hydrogen).

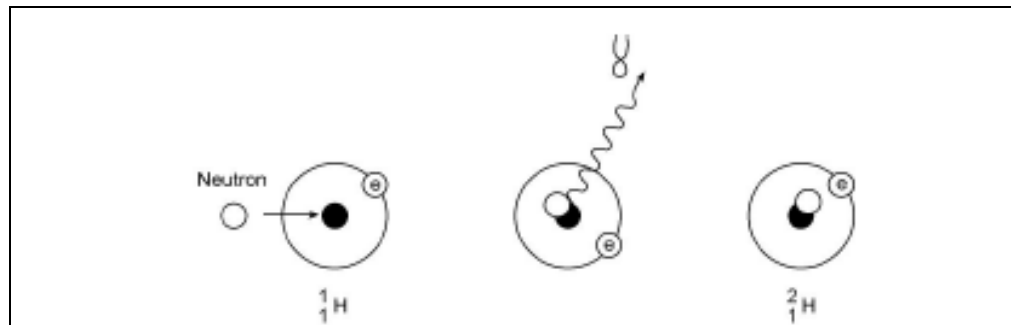


Figure 5: Radiative Capture (n, γ) of hydrogen becomes to deuterium

The deuterium formed is a stable nuclide. However, many radiative capture products are radioactive and are beta-gamma emitters. Deuterium itself undergoes a radiative capture reaction to form tritium;

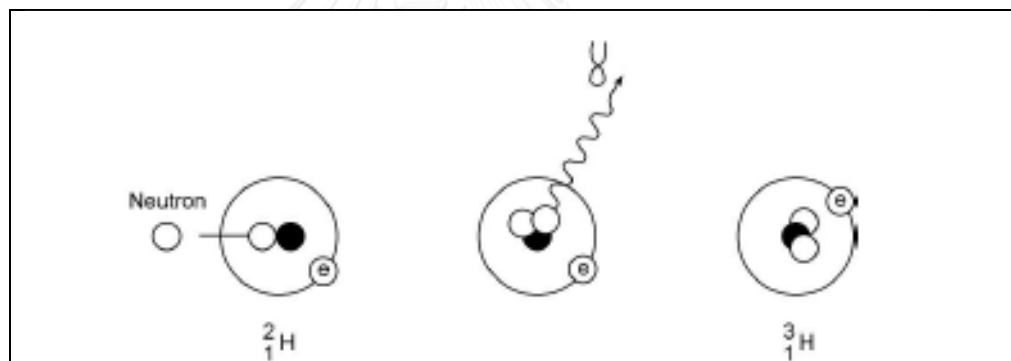


Figure 6: Radiative Capture (n, γ) of deuterium becomes to tritium

The tritium isotope is unstable and is a major radiation hazard in CANDU reactors.

Stable cobalt-59 undergoes radiative capture to form highly radioactive Co-60:



Cobalt-60 has a long half-life (5½ years) and emits very penetrating gamma radiation when it decays, making it a serious hazard among activated corrosion

products. Normal steel usually contains a small amount of cobalt, but the concentration in reactor grade materials is limited to reduce the radiation hazard. Cobalt-60 is an isotope commonly used in radiation treatment of cancer.

2.1.5.7 Fission

Nuclear fission is a nuclear reaction in which a large nuclei breaks apart into two smaller nuclei, releasing a great deal of energy including producing free neutron and photon. The two nuclei produced are most often of comparable size, typically with a mass ratio around 3:2 for common fissile isotopes.

Fission is usually induced by a neutron, although it is occasionally seen as a form of spontaneous radioactive decay, especially in very high-mass-number isotopes.

The exothermic reaction of heavy element fission can release large amounts of energy both as electromagnetic radiation such as gamma radiation and as kinetic energy of the fragments. In order to produce energy from fission reaction, the total binding energy of the resulting elements must be greater than that of the starting element.

2.1.6 Neutron cross section (15)

In nuclear and particle physics, the concept of a neutron cross section is used to express the chance of interaction between an incident neutron and a target nucleus. The standard unit for measuring the cross section is barn, which is equal to 10^{-28} m^2 or 10^{-24} cm^2 .

It can be explained by considering the uniform neutron beam (I_0) hitting a thin plate with a cross sectional area A , thickness x and density N atoms per unit volume, as shown in Figure 7.

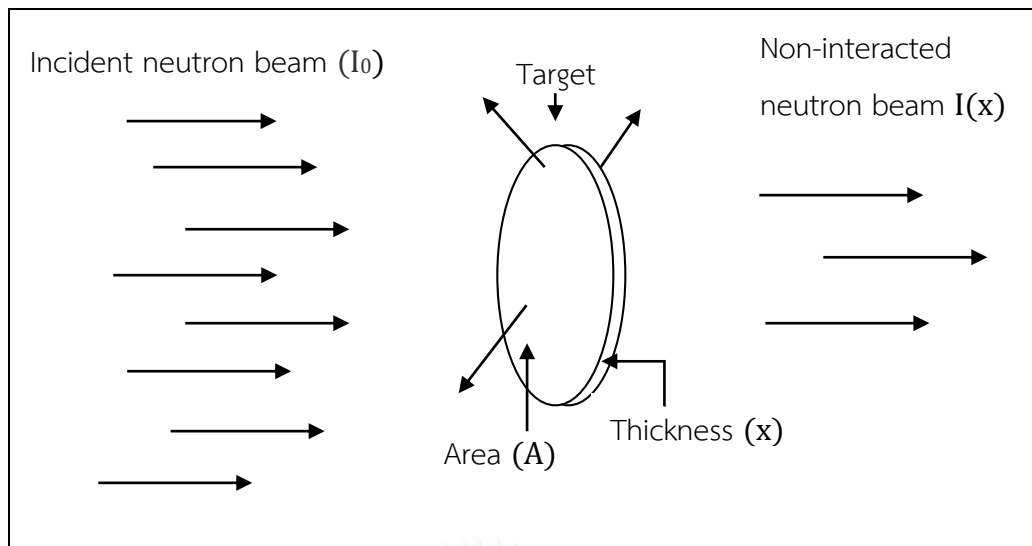


Figure 7: Interaction between neutron beam and target area

The intensity of neutrons (I_0) that pass through the target area (A) per second can be expressed as I_0A , but only a fraction of neutrons undergoes interaction with the target nuclei. The interaction rate depends on the atomic density of the target (N), the type of interaction, the thickness of the target (X) and the chance of interaction between an incident neutron and a target nucleus that called the microscopic cross section of neutron (σ) for such interaction.

Therefore it can be summarized by the following expression:

$$\text{Interaction rate (interaction/second)} = \sigma N A X I_0 \quad (2)$$

Solving equation (2) for σ :

$$\sigma = \frac{\text{Interaction rate}}{N A X I_0} \quad (3)$$

The term NAX is equal to the total number of atoms in the target, and it follows that σ is the interaction rate per atom in the target per unit intensity of the incident neutron beam.

Therefore the probability of an interaction, depends on:

2.1.6.1 Target type

The neutron cross section is defined for a given type of target particle. For example, the absorption cross section of boron-10 is much higher than that of boron-11. This is the reason why some neutron shielding material use enriched boron-10 instead of natural boron

2.1.6.2 Incident particle energy dependence

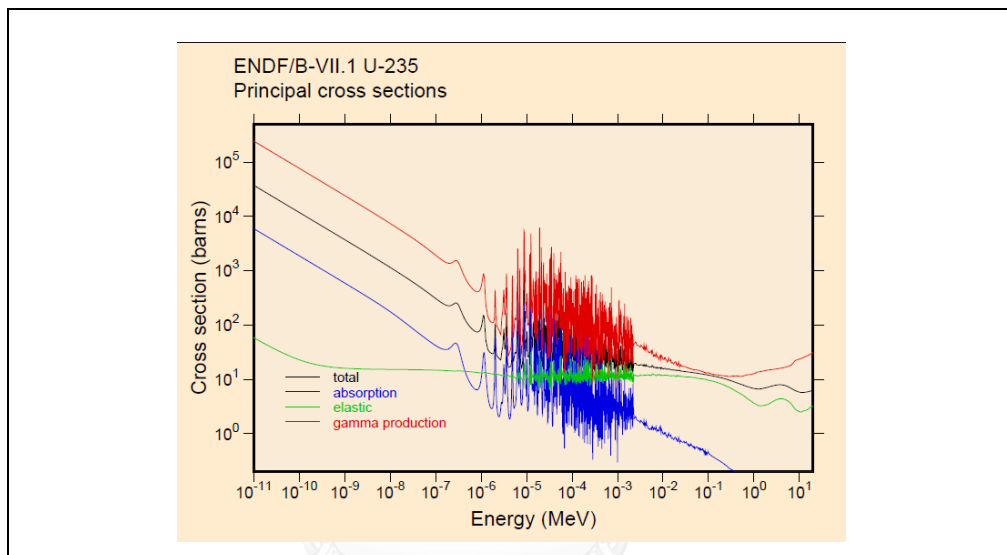


Figure 8: Relation between U-235 fission cross-section and neutron energy(16)

For a given target and reaction, the cross section is strongly dependent on the neutron speed. In the extreme case, the cross section can be, at low energies, either null (the energy for which the cross section becomes significant is called threshold energy) or, on the contrary, much larger than the cross section at high energies. For example from Figure 8 shows at the range of neutron energy below 10^{-7} MeV (low energy) the U-235 fission cross-section is higher than that at high neutron energy range

2.1.6.3 Target temperature dependence

Typically the cross sections are usually measured at room temperature (20°C). To account for the dependence with temperature of the medium, the following formula is used:

$$\sigma = \sigma_0 \left(\frac{T_0}{T} \right)^{\frac{1}{2}} \quad (4)$$

Where σ is the cross section at temperature T and σ_0 is the cross-section at temperature T_0 . (T and T_0 are in Kelvin)

2.1.6.4 Reaction type

The incident neutron can interact with a target element with independent of the type of reaction expression by the total cross section σ_t . However there are some particles interact with the target and continue travelling and some of them disappears after the interaction. For that reason, the scattering cross section (σ_s) and absorption cross sections (σ_A) are defined and the total cross section (σ_t) is simply the sum of the two partial cross sections:

$$\sigma_t = \sigma_s + \sigma_A \quad (5)$$

$$\sigma_t = \sigma_{(n,n)} + \sigma_{(n,n')} + \sigma_{(n,\gamma)} + \sigma_{(n,\alpha)} + \sigma_{(n,p)} + \sigma_{(n,f)} + \dots \quad (6)$$

where

$\sigma_{(n,n)}$ = Elastic scattering cross section

$\sigma_{(n,n')}$ = Inelastic scattering cross section

$\sigma_{(n,\gamma)}$ = Radiative capture cross section

$\sigma_{(n,\alpha)}$ = Alpha transmutation cross section

$\sigma_{(n,p)}$ = Proton transmutation cross section

$\sigma_{(n,f)}$ = Fission cross section

2.1.7.5 Scattering cross-section

The scattering cross-section represents the Elastic Scattering cross section and the Inelastic Scattering cross-section. The scattering cross-section varies with the atomic number of the element.

2.1.6.6 Absorption cross section

The absorption cross-section is the total neutron cross section except the scattering cross-section. It can be explained that when a neutron is absorbed by a nucleus, the atomic nucleus moves up on the table of isotopes by one position. And the atomic nucleus is highly energized. This energy has to be by several mechanisms as follows.

1. To eject the neutron from the nucleus. Because when the neutron is emitted immediately, it acts the same as in other scattering events.
2. To emit gamma radiation.
3. To decay β^- particle, where a neutron is converted into a proton, an electron and an electron-type antineutrino
4. To release the energy as kinetic motion of the fission fragments, also emitting between one and five free neutrons

Macroscopic cross section(15)

In the Figure 7 the target of thickness X is placed in a neutron beam of intensity I_0 . Since the target is small, the neutrons that interact in the target would be lost from the beam, and only those neutrons that haven't interacted in the target would pass through the target that composes of atomic density N and total microscopic cross section of neutron σ_t .

Let $I(x)$ be the intensity of non-interacted neutrons after penetrating the distance x into the target. In traversing an additional distance dx , the intensity of the neutron beam will be decreased by the number of neutron that has interacted in the sheet of thickness dx . This decrease in intensity is expressed by

$$-dI(x) = N\sigma_t I(x)dx \quad (7)$$

Where (σ_t) is the total microscopic cross section of neutrons in unit of barn (b), where $1 \text{ barn} = 10^{-24} \text{ cm}^2$.

Integration of Equation (7) yields :

$$\int -dI(x) = \int N\sigma_t I(x)dx$$

$$I(x) = I_0 e^{-N\sigma_t x} \quad (8)$$

Therefore the intensity of non-interacted beam decreases exponentially with distance inside the target. And the intensity of the non-interacted beam transmitting from the target is expressed in Equation (8)

From Equation (8): $I(x) = I_0 e^{-N\sigma_t x}$

The product of atom density (N) and cross section, in the exponential term, occurs quite frequently in the equation of reactor physics and is given the special symbol Σ , called the *macroscopic cross section*. In particular, the product $N\sigma_t = \Sigma_t$ is called *the macroscopic total cross section*

In terms of Σ_t , Equation (7) can be written as

$$-dI(x) = \Sigma_t I(x)dx \quad (9)$$

Dividing this expressing by $I(x)$,

$$\frac{-dI(x)}{I(x)} = \Sigma_t dx \quad (10)$$

The quantity $\frac{dI(x)}{I(x)}$ in Equation (10) is equal to the fraction of neutrons that have penetrated the distance x into the target without interacting then interact in the distance dx . Expressed in other terms, this is equivalent to the *probability* that a neutron which survives up to x , interacts in the next dx . Thus, in view of Equation (10) $\Sigma_t dx$ is the probability of interaction in dx , and it follows that Σ_t is the *probability per unit path length* that a neutron will undergo some sort of interaction. In a similar manner, it is easy to show that Σ_s , the macroscopic scattering cross section, is equal to probability per unit path length that a neutron will undergo elastic scattering. Analogous interpretations hold for the other macroscopic cross sections.

From Equation (8), $I(x)$ refers to those neutrons that haven't interacted in penetrating the distance x inside the target. The ratio of non-interacted neutron beam and incident neutron beam can be given by:

$$\frac{I(x)}{I_0} = e^{-N\sigma_t x} = e^{-\Sigma_t x} \quad (11)$$

This ratio is equal to the probability that neutron can travel through the distance x without interacting. Then let $p(x)dx$ be the probability that a neutron would have its first interaction in the distance dx in the target thickness x . This is equal to the probability that neutron survives up to x without interaction times the probability that it does in fact interact in the additional distance dx . Since Σ_t is the probability of interaction per path length, $p(x)dx$ is given by :

$$\begin{aligned} p(x)dx &= (e^{-\Sigma_t x})(\Sigma_t dx) \\ &= \Sigma_t e^{-\Sigma_t x} dx \end{aligned} \quad (12)$$

The first interaction probability distribution function $p(x)$ can be used in number of ways. For instance, the probability $P(a, b)$ that a neutron would have its first interaction between $x = a$ and $x = b$ is simply the integral of $p(x)dx$ between these limits as expressed by:

$$\begin{aligned} P(a, b) &= \Sigma_t \int_a^b e^{-\Sigma_t x} dx \\ &= e^{-\Sigma_t a} - e^{-\Sigma_t b} \end{aligned} \quad (13)$$

In particular, the probability that a neutron will interact at least once in traveling through an infinitely thick medium is obtained by placing $a = 0$ and $b = \infty$. Thus,

$$P(0, \infty) = \Sigma_t \int_0^\infty e^{-\Sigma_t x} dx = 1, \quad (14)$$

as would be expected.

The distance that a neutron moves between interactions is called a free path, and the average distance between interactions is known as the mean free path. This quantity that is usually designated by the symbol λ is simply the average value of x , the distance traversed by neutron without interaction, over the interaction probability distribution $p(x)$, that is,

$$\begin{aligned}\lambda &= \int_0^\infty xp(x)dx \\ &= \Sigma_t \int_0^\infty xe^{-\Sigma_t x}dx \\ &= 1/\Sigma_t\end{aligned}\quad (15)$$

The macroscopic cross section of mixed isotopes or elements can be calculated from

$$\Sigma_{\text{mix}} = \Sigma_1 + \Sigma_2 + \Sigma_3 + \dots \quad (16)$$

$$\Sigma_{\text{mix}} = N_1\sigma_1 + N_2\sigma_2 + N_3\sigma_3 + \dots \quad (17)$$

where

Σ_{mix} = Macroscopic cross section of the mixed material (or isotope)

$\Sigma_1, \Sigma_2, \Sigma_3, \dots$ = Macroscopic cross section of isotope or element 1, 2, 3,..., respectively

N_1, N_2, N_3, \dots = Atomic density of isotope or element 1, 2, 3,..., respectively

$\sigma_1, \sigma_2, \sigma_3, \dots$ = Microscopic cross section of isotope or element 1, 2, 3,..., respectively.

2.2 Monte Carlo N-Particle code (MCNP)

MCNP and the monte carlo method(17)

MCNP is a general purpose Monte Carlo, N-Particle user code maintained by the Diagnostics Applications Group at Los Alamos National Laboratory. MCNP can accommodate coupled neutron, photon, and electron transport. It can be used for several cases with continuous energy, generalized geometry and time dependent

Monte Carlo Method vs. Deterministic Method

There are a lot of difference transport methods between Monte Carlo methods and Deterministic methods. The Deterministic methods is the discrete ordinates method, solve the transport equation for the average particle behavior moreover it typically give fairly complete information (for example, flux) throughout the phase space of the problem. On the other hand, Monte Carlo obtains answers by simulating individual particles and recording some aspects (tallies) of their average behavior and supplies information only about specific tallies requested by the user.

2.2.1 The Monte Carlo Method

The interaction of nuclear particles with matter is a statistical process. Monte Carlo can be used to duplicate theoretically a statistical process and is particularly useful for complex problems that cannot be modeled by computer codes that use deterministic methods. The individual probabilistic events that comprise a process are simulated sequentially. The probability distributions governing these events are statistically sampled to describe the total phenomenon. In particle transport, the Monte Carlo technique is a numerical experiment. It consists of actually following each of many particles from a source throughout its life to its death in some terminal category (absorption, escape, etc.). Probability distributions are randomly sampled using transport data to determine the outcome at each step of its life.

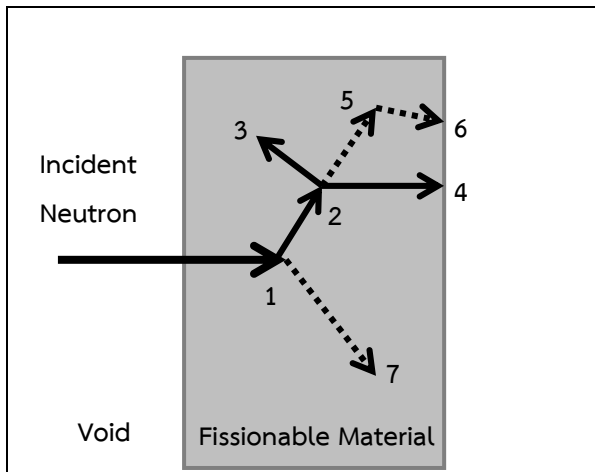


Figure 9: The Monte Carlo Method

Figure 9 represents the neutron incident on a slab of material that can undergo fission. In this example, the event 1 is a neutron collision and is randomly scattered in the various directions with the physical scattering distribution. And also produce a photon and temporarily stored, or banked, for later analysis. At event 2, two neutron and one photon were occurred by fission reaction. One neutron and the photon are banked for later analysis. The first fission neutron is captured at event 3 and terminated. The banked neutron is now retrieved and, by random sampling, leaks out of the slab at event 4. The fission-produced photon has a collision at event 5 and leaks out at event 6. The remaining photon generated at event 1 is now followed with a capture at event 7. Note that MCNP retrieves banked particles such that the last particle stored in the bank is the first particle taken out. This neutron history is now complete. As more and more such histories are followed, the neutron and photon distributions become better known. The quantities of interest (whatever the user requests) are tallied, along with estimates of the statistical precision (uncertainty) of the results.

2.2.1.1 MCNP input for problem

The main MCNP input file contains information about the problem in areas such as:

1. The geometry specification

2. The description of materials and selection of cross-section evaluations,
3. The location and characteristics of the neutron, photon, or electron source,
4. The type of answers or tallies desired, and
5. Any variance reduction techniques used to improve efficiency.

The basic constants unit used in MCNP are :

1. Lengths in centimeters,
2. Energies in MeV,
3. Times in shakes (10^{-8} sec),
4. Temperatures in MeV (kT),
5. Atomic densities in units of atoms/barn-cm,
6. Mass densities in g/cm³,
7. Cross sections in barns (10^{-24} cm²),
8. Heating numbers in MeV/collision, and
9. Atomic weight ratio based on a neutron mass of 1.008664967 amu. In these units, Avogadro's number is $0.59703109 \times 10^{24}$.

To define a problem in MCNP an input file, providing the geometry and all necessary data, is needed. The form of this file is defined in the manual (18) and will be reproduced only very briefly. Each input file has three sections. The first section specifies the geometrical cells used in the calculation. The second section defines all surfaces and marcobodies used for cell definition and the third section specifies all other data necessary.

2.2.1.2 The output

The standard output file contains a reproduction of the input file and all messages printed to the console. Upon successful completion or interruption of the calculation it is amended with various data tables, some on request only. It is always amended by an overview of the global statistics of the run and the tally data.

More information on the output files and their structure can be found in the MCNP5 user's manual : volume II (18).

2.2.1.3 Estimation of Monte Carlo Errors

The relative error values (R) are exhibited in the output accompanied by a second number of MCNP tallies. These R is defined to be estimated standard deviation (1SD) of the mean divided by the estimated mean. For a well-behaved tally, R will be proportional to $\frac{1}{\sqrt{N}}$ where N is the number of histories. Thus, to reduce R , we are necessary to increase the total number of histories. For a poorly behaved tally, R may increase as the number of histories increases. The estimated relative error can be used to form confidence intervals about the estimated mean, allowing one to make a statement about what the true result is. The Central Limit Theorem states that as N approaches infinity there is a 68% chance that the true result will be in the range $\bar{x}(1 \pm R)$ and a 95% chance in the range $\bar{x}(1 \pm 2R)$. It is extremely important to note that these confidence statements refer only to the precision of the Monte Carlo calculation itself and not to the accuracy the result compared to the true physical value. A statement regarding accuracy requires a detailed analysis of the uncertainties in the physical data, modeling, sampling techniques, and approximations, etc., used in a calculation. The guidelines for interpreting the quality of the confidence interval for various values of R are listed in Table 3.

*Table 3: Guidelines for Interpreting the Relative Error R^**

Range of R	Quality of the Tally
0.5 to 1.0	Not meaningful
0.2 to 0.5	Factor of a few
0.1 to 0.2	Questionable
< 0.10	Generally reliable
< 0.05	Generally reliable for point detectors

* $R = S_{\bar{x}}/\bar{x}$ and represents the estimated relative error at the 1σ level.

These interpretations of R assume that all portions of the problem phase space are being sampled well by the Monte Carlo process.

2.3 Rubber

The main material used for neutron moderation in this dissertation is the polymeric hydrocarbon compound with high hydrogen atom content such as natural rubber and styrene butadiene rubber (SBR). Therefore, understanding the information and features of these polymers is necessary for their suitable and effective use.

2.3.1 Natural rubber (19)

Natural rubber or Para rubber is an elastic hydro carbon polymer derived from milky latex (combined with approximate 30% by weight of dry rubber content, DRC) which is produced by the para rubber tree (*Hevea brasiliensis*). The purified form of natural rubber is the chemical poly-isoprene, which can also be produced synthetically. Natural rubber is used extensively in many applications and products, as is synthetic rubber. It is normally very stretchy and extremely waterproof and flexible. The natural rubber is typically divided into two types as follows:

2.3.1.1 Natural Rubber Latex

The fresh natural rubber latex that can be obtained from rubber trees contains water. It is unsuitable for using in any industries. Therefore, this rubber latex is usually centrifuged to reduce the amount of its water content until the latex containing dry rubber increases from 30% to 60% by weight, which is now called concentrated latex. Since the latex comprises of a small number of organic compounds such as proteins and phosphor lipids, these compounds can be rotten by microorganisms or bacteria, which produces carbon dioxide, methane or nitrogen gases or compounds. Therefore, ammonia is usually added to natural rubber latex to preserve it. The latex preserved by high concentration of ammonia (0.7%) combined with other chemicals is called High Ammonia Latex (HA latex). On the other hand, Low Ammonia latex (LA latex) contains low concentration of ammonia (0.2%) and 0.02% of ZnO/TMTD or 0.2% of Boric acid or 0.2% of Santobrite.

2.3.1.2 Dry/Solid Rubber

Dry rubber is produced by adding acid agent (acetic acid, formic acid or sulfuric acid) into fresh rubber latex. The acid agent makes rubber particles clot and separates solid content from the liquid content. Then, the rubber humidity is removed by a suitable method to protect mold from occurring. Dry rubbers come in many types such as Rubber Sheet, Crepe Rubber and Technically Classified Rubber.

2.3.1.3 Chemical Structure of Natural Rubber

Natural rubber is the natural polymer of long chain isoprene (C_5H_8) (most often cis-1, 4-polyisoprene) with a molecular weight of 200,000 to 400,000 daltons. The density is 0.93 g/cm^3 at 20°C . It has the glass transition temperature, T_g , of approximately -72°C . Therefore, when natural rubber is kept at temperature below -72°C , the properties change from a flexible material into a brittle solid like glass.

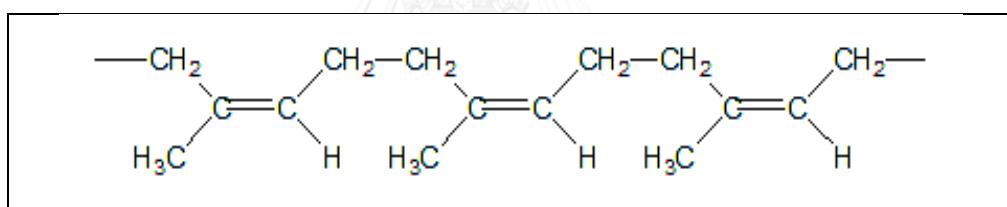


Figure 10: Chemical structure of natural rubber

CHULALONGKORN UNIVERSITY

From figure 10, an isoprene consists of a double bond and an α -methylene group, which are sensitive to the vulcanization reaction with sulfur agent. Furthermore, this double bond is easily reacted with other chemical agents such as oxygen or ozone (especially at high temperature), which can result in degradation of its properties.

The typical arrangement of natural rubber molecules is amorphous, but keeping it at low temperature (below 20°C) for a long period of time can regulate its molecule, a phenomenon called “low temperature crystallization.” This crystallization can harden the rubber and it cannot homogeneously mix with other chemicals. However, when crystallized rubber is heated, the crystal will be demolished and the rubber will become softer as temperature increases. For the crystallization as a result

of rubber strain (strain-induced crystallization), it occurs when rubber is strained or pulled more than 2-3 times its normal length. The strain-induced crystallization can turn the rubber from transparent to opaque, but it can also improve mechanical properties such as increasing tensile strength, tear strength and abrasion resistance.

2.3.1.4 Properties of Natural Rubber

Elasticity

Elasticity is the dominant feature of natural rubber. Vulcanized natural rubber exhibits high elasticity. When an external force acts upon the rubber and is then removed, the rubber quickly restores its normal form (size and shape).

Tack

Pre-vulcanized natural rubber has a good tack property, which is necessary to assemble certain parts of certain products together such as automobile tires, etc.

Tensile strength

Natural rubber easily crystallizes when it is strained. These occurring crystals can reinforce the rubber, so it exhibits high tensile strength (~20 MPa or more) even without any rubber filler agent. Moreover, adding reinforcing filler to rubber can increase the tensile strength. The tensile strength of natural rubber is higher than that of the majority of synthetic rubbers.

Tear strength

Because when natural rubber is strained, it simply crystallizes, so it exhibits high tear strength both at room temperature and elevated temperature.

Dynamic properties

Natural rubber has good dynamic properties because it has small amount of energy (heat) loss while in use. In addition, it exhibits high fatigue resistance.

Abrasion resistance

Natural rubber has high abrasion resistance, but it is lower than that of synthetic styrene butadiene rubber (SBR).

Electrical insulation

Natural rubber is a very good electrical insulator with a specific resistivity of 10^{15} - 10^{16} ohm•cm.

Liquid and chemical resistance

Since natural rubber consists of non-polar hydrocarbon polymer, pre-vulcanized rubber can be dissolved in non-polar solvents such as benzene, hexane and toluene. The solubility will decrease when rubber is vulcanized with 3D chemical bond, which can block the dissolution process. Thus, when 3D vulcanized natural rubber is immersed in non-polar solvents, it only swells. However, this swelling can degrade mechanical properties of rubber. Therefore, natural rubber is intolerant with petroleum oil or non-polar solvents, but it can tolerate with polar-solvents such as acetone or alcohol. Furthermore, diluted acid and base (except concentrated nitric acid and sulfuric acid) can't degrade it.

Aging properties

Because natural rubber molecules contain a large number of double bonds, natural rubber is sensitive to oxygen (via oxidation reaction) with an aid of sunlight as a catalyst. Natural rubber is also not ozone-resistant. A lot of micro-cracks will occur at the surface of natural rubber (perpendicular to the direction of stretch) when it is stretched or exposed to ozone for a long period of time. Therefore, during production of natural rubber material, some anti-degradants and wax are usually added into the material to improve the aging properties.

Low-temperature flexibility

Natural rubber exhibits good flexibility even when bent at a very low temperature.

Compression set

Natural rubber has a low compression set both at room temperature and medium-to-high temperature. However, at low temperature, the compression set of natural rubber increases because of the crystallization effect that decreases the flexibility property of natural rubber. Because natural rubber isn't tolerant with heat, at high temperatures, the compression set increases and influences the degradation of the rubber.

Mixing

There are some limits of using crude rubber because it has rather poor mechanical properties and because its physical properties change with temperature. The crude natural rubber will be soft and sticky when it is heated, but when it is exposed to low temperature it will become hard and brittle. Thus, in utilizing crude natural rubber, it is necessary to add other chemical agents, for example, sulfur or carbon black as a catalyst. The mixed rubber (with chemical agent) is called “rubber compound,” which is then fabricated under heat and pressure in the mould. This process is called vulcanization and the rubber from this process is known as vulcanized rubber. Vulcanized rubber properties are stable with changing temperature and mechanical properties are also improved.

Although natural rubber is vulcanized by using peroxide chemicals or by exposing it to high-energy radiation, sulfur is usually used in the rubber industry. Natural rubber requires more sulfur agent but less accelerator agent (catalyst agent) compared with synthetic rubber. This is because there are some organic compounds agents present in natural rubber which can accelerate the vulcanization process.

Mixing natural rubber with chemical agents is difficult because natural rubber is a solid material that is very hard, sticky and viscous. Thus, it is necessary to masticate the rubber to cut off the rubber molecules and decrease its viscosity before mixing with other chemical agents. The mastication process is essentially a mechanical process to shear rubber molecules using a two-roll mill device with an internal mixer. Typically, at low temperature, one can masticate the rubber with high efficiency because the rubber exhibits high viscosity which allows a large amount of shear force to be generated, so rubber molecules are easily torn apart (or cut). At high temperature, the rubber exhibits low viscosity and the shear force is reduced during mastication. However, adding a small amount of peptizing agent can increase the rubber mastication efficiency because the agent can block the recombination reaction of broken rubber molecules.

The service temperature of natural rubber is -55°C to 70°C. However, keeping natural rubber at low temperature for a long period of time can make the rubber

crystallize and become hard, reducing its elasticity. On the contrary, extended use of natural rubber at high temperature can degrade its mechanical properties as the rubber is degraded by heat.

2.3.1.5 Mixing natural rubber with other polymers

Natural rubber is a non-polar polymer, so it can be homogeneously mixed with non-polar rubbers such as styrene butadiene rubber (SBR), poly-isoprene rubber (IR) and butadiene rubber (BR). Furthermore, it can be mixed with a small amount of nitrile rubber (NBR) by using a low acrylo-nitrile NBR grade or by adding a small quantity of compatibilizer. Mixing natural rubber with synthetic rubber offers several advantages, mainly because it can combine the features of both rubbers together. Natural rubber has a high tack and high dynamic properties, allows easy fabrication and has low accumulated heat during usage. Synthetic rubber exhibits high-abrasion resistance (when mixed with BR), high-heat resistance (when mixed with NBR or ethylene-propylenediene monomer; EPDM), high-petroleum resistance (when mixed with NBR) and high anti-aging with ozone (when mixed with EPDM).

However, careful consideration must be made when mixing natural rubber with other polymers on the factors that affect the rubber compound properties such as rubber viscosity and vulcanization process. Commonly, before mixing different types of rubber together, each rubber type is usually masticated to have the same initial viscosity. In addition, when mixing natural rubber with synthetic rubber which has a small number of double bonds in molecules (for example, Butyl rubber, IIR, EPDM), one should select a suitable vulcanization process. Otherwise, different rubber types may be separated into different phases during vulcanization. Moreover, one should consider the dispersion of chemical filler or accelerator in the rubber when mixing together rubbers with different polar structures.

2.3.2 Styrene-butadiene(19)

Styrene-Butadiene or **Styrene-Butadiene-Rubber** (SBR) is a synthetic rubber copolymer consisting of styrene and butadiene. It has been widely used for producing vehicle tire. It has a good resistance with abrasion. When it was protected by some additive it could be a good aging stability material. There are mainly two processes to produce SBR: (a) from solution by ionic polymerization reaction or (b) emulsion that the reaction is via free radical polymerization.

2.3.2.1 Chemical Structure, Production and Properties of Styrene-Butadiene-Rubber(SBR)

Styrene-Butadiene or Styrene-Butadiene-Rubber (SBR) is a synthetic rubber copolymer consisting of styrene monomer (23-40%) and butadiene monomer. These two monomers are arranged with random pattern (random copolymer). Furthermore, as the molecular chain arrangement of SBR is amorphous, crystallization hardly occurs when it is stretched, so it has low tensile strength. It has good abrasion resistance and good aging stability when protected by additives.

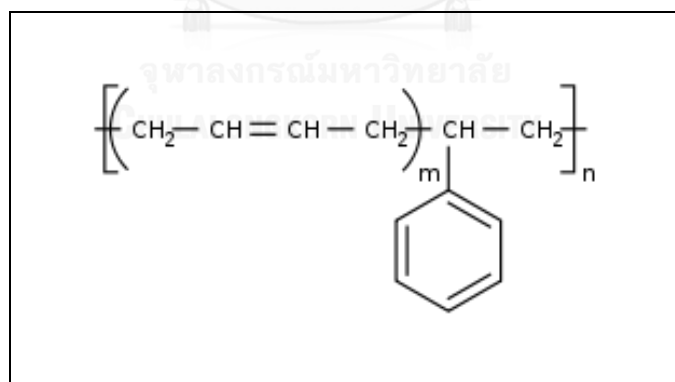


Figure 11: Chemical structure of SBR

Rubber industries often use SBR produced from polymerization process in the emulsion form (emulsion polymerization), and this rubber is called E-SBR. In some cases, the SBR may be produced from solution polymerization procedure and its name is L-SBR.

E-SBR is divided into two groups by the production temperature: (1) cold E-SBR where the production temperature is about 5 °C and (2) hot E-SBR where the production temperature is about 50°C or more. Commercial SBR has the Mooney viscosity ML 1+4 at 100°C in the range of 30-120, or an average molecular weight in the range of 250,000 - 800,000. The low-viscosity SBR is easily mixed in the roll mill device and, thus, can be homogeneously blended with additive agent or oil. In addition, it shrinks less than extruded rubber. The surface is also smoother than high-viscosity SBR. The pre-vulcanized SBR with a high-viscosity grade exhibits higher green strength than a low-viscosity one; therefore, it has a small number of pores and more filler (additive) agent can be added into the SBR. These reasons make the price of SBR products made from low-viscosity grade SBR decreasing.

The SBR density is 0.93 g/cm³ at room temperature. It offers more uniform quality and fewer amounts of trace elements than natural rubber. Moreover, it is not necessary to masticate before mixing with chemical agents because it has low molecular weight. In addition, it has less tendency to become scorched during processing since SBR exhibits slower vulcanization and oxidization rates than natural rubber.

Tack

SBR has a low tacky property, so in tire productions it is necessary to combine SBR with natural rubber with high tacky. Adding tackifier (such as petroleum resin, coumarone resin or phenoric resin) can help improve this drawback of SBR.

Elasticity

SBR has lower elasticity than natural rubber. Its elasticity will decrease when the proportion of styrene increases.

Tensile strength

Because SBR cannot crystallize when stretched, it has low tensile strength (lower than natural rubber about 7-10 times without reinforcing filler). However, adding reinforcing filler can help increase the tensile strength to about that of natural rubber (or lower).

Tear strength

The SBR has very low tear strength, especially at high temperature, because when it is stretched, it cannot crystallize. Therefore, it is often added with reinforcing filler to increase the tear strength.

Abrasion resistance

Reinforced SBR with reinforcing filler such as carbon black exhibits about 10-20 % more abrasion resistance than that of natural rubber.

Aging properties

SBR has a lot of double bonds in its molecule, so it is quickly degraded when exposed to oxygen, ozone, sunlight and heat. When SBR is degraded, it becomes harder because cross-linking reaction occurs more than chain-scission reaction. Adding anti-aging chemical into SBR can extend its useful life. Moreover, improving the vulcanization process to Efficiency Vulcanization (EV) or Semi-Efficiency Vulcanization (semi-EV) can increase anti-aging property from heat.

Oil and chemical resistance

SBR is a non-polar polymer like natural rubber. Therefore, it has low resistance to petroleum and hydrocarbon solvents, but it is tolerant with diluted acid, base, alcohol, water, salt and silicone oil.

Electrical insulator

SBR is a very good electrical insulator because it is a non-polar rubber. It has a specific electrical resistance in the range of 10^{14} - 10^{15} ohm.cm.

Rebound resilience

SBR has a rebound resilience property much lower than that of natural rubber. During its transformation, it will lose energy in the form of heat (high hysteresis). So, when using SBR in a dynamic field, it will accumulate heat more than natural rubber. These reasons make the SBR unsuitable for using in large tires production.

Service temperature

Normally, SBR can be used in the temperature range of -50 -100°C. Because crystallization cannot occur at low temperatures, SBR does not become hard when keeping or using at low temperatures for a long period of time.

2.3.2.2 Mixing with chemical rubber

Typically, the characteristics of mixing SBR with chemical rubber are similar to that of natural rubber. However, one has to add accelerator (catalyst) agent into SBR more than one does into natural rubber because SBR has a slower vulcanization rate.

2.3.2.3 Mixing SBR with other polymers

SBR is a non-polar rubber, so it can easily be mixed with other non-polar rubbers. SBR is usually mixed with BR or natural rubber in the tire industry since BR can increase the abrasion resistance. Moreover, it can decrease the accumulation heat when functioning as vehicle tires. By properly adding natural rubber, it can improve mechanical and dynamic properties. For SBR mixing with polar rubber such as NBR, it is possible only when using a low-acrylonitrile NBR grade.

2.3.2.4 Applications

The SBR is used widely in vehicle tires, shoe heels and sole. In addition it is a material that competes with natural rubber. Emulsion latex SBR is usually used in coated papers, bind pigmented coatings and etc.

2.4 Borate minerals

The boron is typically used for neutron shielding material especially in oxides of boron form such as boron monoxide (B_2O), boron suboxide (B_6O) and boron trioxide (B_2O_3) which is the most common form.

Boron found in nature is usually in the form of borate mineral. Borate is a compound of the borate ion with metallic elements. It is sometimes also combined with silicate and forms complex borosilicate minerals like tourmalines.

Borate minerals were formed by high temperature contact and reaction of boron with different elements in rocks during the intrusion of hydrothermal solutions (accompanying magma) into other formations, or weathering or water entry and reaction at the outcrops, edges, or near faults of other borate deposits. Boron can form very different compounds by comparatively small changes in the solution's mineral content, concentration, pH, time to reach equilibrium, temperature, water availability or pressure. Boron is not a major element in the earth's crust and waters, averaging only 3-20 ppm in upper continental crust.

Principal Sedimentary Borate Minerals (20)

Shallow lake deposits formed by precipitation and evaporation Boron (United States), Kirka (Turkey) and Tincalayu (South America)

Mineral	Formula	B_2O_3 content (wt %)
Primary		
Borax	$Na_2O \cdot 2B_2O_3 \cdot 10H_2O$	36.5
Ulexite	$Na_2O \cdot 2CaO \cdot 5B_2O_3 \cdot 16H_2O$	43.0
Secondary		
Kernite	$Na_2O \cdot 2B_2O_3 \cdot 4H_2O$	51.0

Mineral	Formula	B ₂ O ₃ content (wt %)
Ulexite	Na ₂ O·2CaO·5B ₂ O ₃ ·16H ₂ O	43.0
Colemanite	2CaO·3B ₂ O ₃ ·5H ₂ O	50.8
Szaibelyite	Liaoning Province (China)	41.4
	2MgO·B ₂ O ₃ ·H ₂ O	

*Formed by Precipitation from Cooling Hot-Spring Fluids Argentina and Death Valley
(United States)*

Mineral	Formula	B ₂ O ₃ content (wt %)
Primary		
Ulexite	Na ₂ O·2CaO·5B ₂ O ₃ ·16H ₂ O	43.0
Secondary		
Proberite	Na ₂ O·2CaO·5B ₂ O ₃ ·10H ₂ O	49.6
Colemanite	2CaO·3B ₂ O ₃ ·5H ₂ O	50.8

Source: American Ceramic Society Bulletin, Vol. 81, No. 8

Common Borate Minerals

- Kernite - Na₂B₄O₇·4H₂O
- Borax - Na₂B₄O₇·10H₂O
- Ulexite - NaCaB₅O₉·8H₂O
- Colemanite - Ca₂B₅O₁₁·5H₂O
- Boracite Mg₃B₇O₁₃Cl

Main Sources of Borates

Most of the borates in the world are supplied by Rio Tinto Borax from the southern United States. The company was established by Francis Marion Smith in 1883

which was then known as The Harmony Borax Works. In 1872, Mr. Smith found borates in the Nevada desert.

Death Valley in California is famous for borate mining. Atacama Desert in Chile also contains mineable borate concentrations.

For the borate minerals source in Thailand are found in a few amounts of boracite in the northeastern portion. Boracite are typically occurred by an uncommon component of bedded sedimentary salt and potash deposits of marine origin, the boron probably derived from nearby volcanic activity(21). There are some studies reported that the small amount of boracite is found with the Udon Sylvinit type potash ore in the province of Udon Thani, Thailand.(22) And also found boracite as a accessory minerals in Tachyhydrite and Carnallite type of potash ore in Chalerm Phrakiat District, Nakhon Ratchasima Province(23)



Figure 12: Somboon sylvinitic ore type of potash ; Asia Pacific Potash Corporation company, Udon Thani province , Thailand

2.4.1 Boracite

Boracite ($Mg_3B_7O_{13}Cl$) is a magnesium borate mineral. It occurs as blue green, colorless, gray, and yellow to white crystals in the orthorhombic - pyramidal crystal system. It occurs as well formed crystals and dispersed grains often embedded within gypsum and anhydrite crystals. It has a Mohs hardness of 7 to 7.5 and a specific gravity of 2.9. It has a conchoidal fracture and does not show cleavage. It is soluble in water.

Boracite is typically found in evaporite sequences associated with gypsum, anhydrite, halite, sylvite, carnallite, kainite and hilgardite. The name of boracite is derived from its boron content (19 to 20% boron by mass).



Figure 13: Boracite, Mineralogisches Museum Bonn

Table 4: General properties of boracite

Category	Tektoborates
Chemical formula	$Mg_3B_7O_{13}Cl$
Molecular weight (g/mole)	392.03
Strunz classification	06.GA.05
Composition (%)	$B_2O_3 = 62.15$ (Boron = 19.3) $FeO = 1.09$ $MgO = 25.71$ $MgCl_2 = 12.14$

2.4.2 Boron Oxide

Table 5: Properties of boron oxide

Properties	Boron trioxide (most common)	Boron monooxide	Boron suboxide
Molecular formula	B_2O_3	B_2O	B_6O
Molar mass	69.6182 g/mol	37.621 g/mol	80.865 g/mol
CAS Registry Number	1303-86-2	12505-77-0	
Appearance	white, glassy solid	Unstable phase	Reddish icosahedral twinned crystals
Density	2.460 g/cm ³ , liquid; 2.55 g/cm ³ , trigonal; 3.11–3.146 g/cm ³ , monoclinic		2.56 g/cm ³
Melting point	450 °C (842 °F; 723 K) (trigonal) 510 °C (tetrahedral)		2,000 °C (3,630 °F; 2,270 K)
Boiling point	1,860 °C (3,380 °F; 2,130 K), sublimates at 1500 °C		NA
Solubility in water	1.1 g/100mL (10 °C) 3.3 g/100mL (20 °C) 15.7 100 g/100mL (100 °C)		NA
Solubility	partially soluble in <u>methanol</u>		NA
Acidity (pKa)	~ 4		NA

CHAPTER 3

METHODOLOGY

3.1 Materials

- 3.1.1 Potash core sample (Somboon type)
- 3.1.2 Solid state nuclear track detector (CR-39)
- 3.1.3 Microscope system
- 3.1.4 Californium-252 (^{252}Cf) neutron source
- 3.1.5 Monte Carlo N-Particle (MCNP5) program
- 3.1.6 Natural rubber (STR 5L)
- 3.1.7 Styrene Butadiene Rubber (SBR 1502 from BST elastomer Co., Ltd. Thailand)
- 3.1.8 Chemical for rubber processing
 - 3.1.8.1 Zinc oxide
 - 3.1.8.2 Steric acid
 - 3.1.8.3 Wingstay-L
 - 3.1.8.4 Dibenzothaizylenedisulphide (MBTS)
 - 3.1.8.5 Tetramethylthigramdisulphide (TMTD)
 - 3.1.8.6 Diphenyl Guanidine (DPG)
 - 3.1.8.7 Sulfur
- 3.1.9 Two-roll mill of 8" x 20" in diameter
- 3.1.10 Diboron trioxide powder (B_2O_3)
- 3.1.11 Iron dioxide powder (Fe_2O_3)
- 3.1.12 Lead dioxide powder (PbO_2)
- 3.1.13 Boric acid
- 3.1.14 (Americium-241/Beryllium-9, $^{241}\text{Am}/\text{Be}$) neutron source
- 3.1.15 Gamma counting system
 - 3.1.15.1 High-purity Germanium (HPGe) Detectors

3.1.15.2 Counting system : Multichannel analyzer, Amplifier, High voltage power supply

3.1.16 Neutron counting system

3.1.16.1 ^6Li Glass scintillator neutron detector

3.1.16.2 Counting system : Pre Amplifier ; PAD 814A, Amplifier, High Voltage power supply, Multi-channel analyzer (MCA) ; DSA2000 and Microcomputer

3.1.17 Neutron radiography system

3.1.17.1 Thermal neutron beam at Thai Research Reactor TRR-1/M1

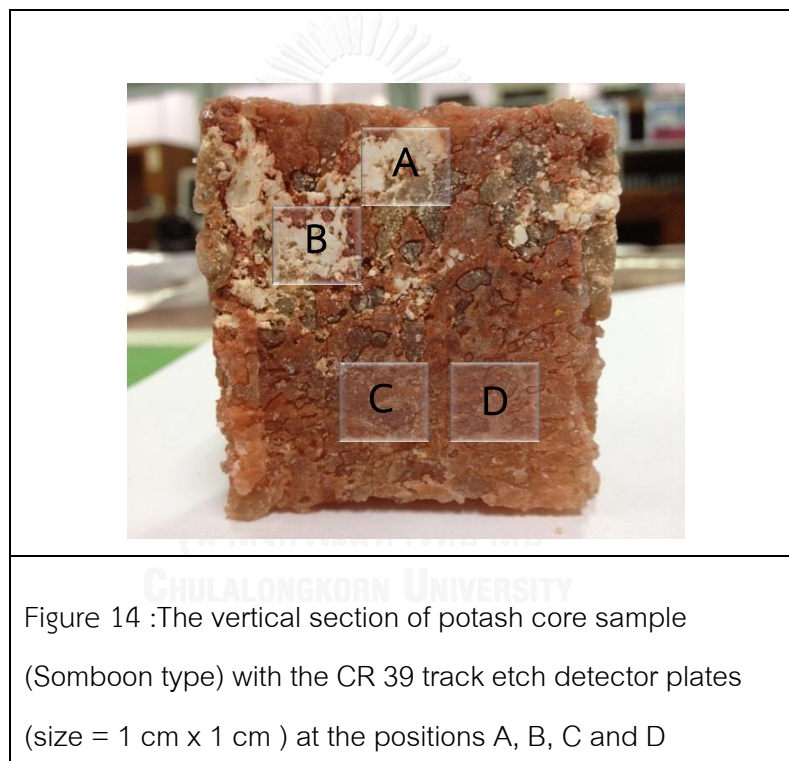
3.1.17.2 Neutron imaging plate (ND 2040)

3.1.17.3 Image reader (BAS 2500)



3.2 Boron detection in potash ore core by alpha track etch method

The vertical section of potash core sample (Somboon type) was put in close contact with the CR 39 track etch detector plates (show in Figure 14), which is sensitive to alpha particles. They were subsequently wrapped with plastic sheet and covered with plastic zip lock bag for waterproofing. They were then exposed to ^{252}Cf neutron source contained in water and polyethylene tank for 24 hours. The CR-39 detector plates were etched in a 7 M NaOH solution at 70°C for 2 hours to reveal tracks. Then, the tracks were observed under an optical microscope.



3.3 Material selection by MCNP simulation

3.3.1 Optimization the type of neutron shielding materials.

The main raw materials were selected from simple elements or compound materials, taking into consideration cost, radiation shielding performances and physical. The main compositions of the selected neutron shielding material to shield against the entire range of neutron energy and secondary gamma ray emission are listed in Table 6.

Although Gadolinium (Gd) is the best neutron shielding material, it not be used in this work because it is very expensive. They consisted of natural rubber (NR), styrene butadiene rubber (SBR-1502) and neutron absorber/scattering agent 40 phr of each agent was used for each sample because preliminary fabrication indicated that at 40 phr, rubber still exhibited desirable properties. The lead or iron content is desirable for inelastic neutron scattering to effectively bring the neutron energy down to lower-energy regions. In addition, lead and iron are used for attenuation of gamma radiation. Neutrons in the lower-energy regions can be moderated by hydrogen and other light elements by elastic scattering. In the thermal energy region, boron (as B_2O_3) is used for neutron absorption. Because the interaction between a thermal neutron and boron-10 produces a secondary gamma ray from the following interaction: Thermal neutron + B-10 \rightarrow He-4 + Li-7* (478 keV gamma ray), without the gamma ray attenuating material (Pb or Fe), this neutron shielding material would itself become a significant source of gamma radiation.

For each sample in Table 6, the input card of the MCNP5 transport code was appropriately prepared for testing and comparison of shielding properties of different materials. A simplified model was employed: a single radiation source, an isotropic emission of simulated neutron source with energy 10^{-8} – 100 MeV, was located at the center of a sphere filled with the shielding material as shown in Figure 15. The shielding material was considered for shielding the neutron dose equivalent rate [(rem/hr)/source strength] and the secondary gamma dose equivalent rate [(rem/hr)/source strength]. The human biological dose equivalent rate were conversed from particle flux by using FLUX-TO-DOSE CONVERSION FACTORS base on the action of the International Commission on Radiological Protection [ICRP-21] (see in Appendix A). The spherical model of radius 1 cm or 10 cm was chosen for neutron shielding in the thermal region or in the entire-energy range, respectively, to ensure that all neutron particles interacted with the shielding material at least one time before leaving

the system. For each shielding material, the dose equivalent rate per source strength was estimated on the outer surface of the sphere.

Table 6 : Main compositions of considered neutron shielding materials (40 phr each of B_2O_3 , PbO_2 and Fe_2O_3)

Sample No.	No. of layers	Material composition	Density (g/cm ³)	Element content (part per hundred rubber; phr)							
				H	C	¹⁰ B	¹¹ B	O	Fe	Pb	
0	0	No material (Air)	0.00120					Air*			
1	1	NR+SBR	0.987	10.378	89.622	-	-	-	-	-	-
2	1	NR+SBR+ B_2O_3	1.210	10.378	89.622	2.460	9.963	27.577	-	-	-
3	1	NR+SBR+ PbO_2	1.343	10.378	89.622	-	-	5.351	-	34.649	
4	1	NR+SBR+ Fe_2O_3	1.301	10.378	89.622	-	-	12.023	13.988	-	
5	1	NR+SBR+ $B_2O_3+PbO_2$	1.273	10.378	89.622	1.230	4.982	16.464	-	17.325	
6	1	NR+SBR+ $B_2O_3+Fe_2O_3$	1.254	10.378	89.622	-	-	19.800	27.977		
Multi-layer samples											
		Layer 1		Layer 2		Layer 3		Layer 4		Layer 5	
7	4	Sample 2		Sample 3		Sample 2		Sample 3		-	
8	4	Sample 2		Sample 4		Sample 2		Sample 4		-	
9	4	Sample 3		Sample 2		Sample 3		Sample 2		-	
10	4	Sample 4		Sample2		Sample4		Sample 2		-	
11	5	Sample 2		Sample 3		Sample 2		Sample 3		Sample 2	
12	5	Sample 2		Sample 4		Sample 2		Sample 4		Sample 2	
13	5	Sample 3		Sample 2		Sample 3		Sample 2		Sample 3	
Comparative materials											
		Composition		Density (g/cm ³)				% isotope			
14	1	Boron (B)		7.874			¹⁰ B= 19.9		¹¹ B= 80.1		
15	1	Iron (Fe)		2.34				Natural Fe = 100			

* (21) Air's composition (weight fraction) ; Carbon : Nitrogen : Oxygen : Argon

0.000124 : 0.755268 : 0.231781 : 0.012827

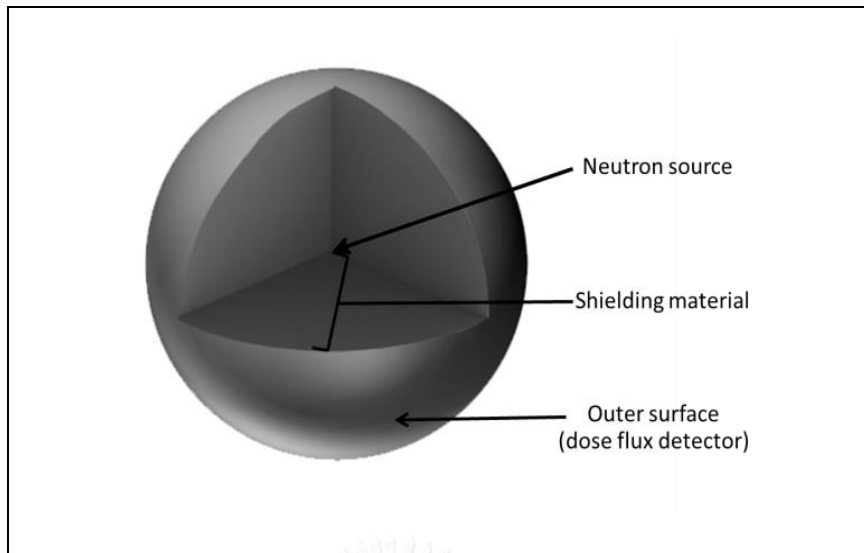


Figure 15: Schematic representation of the Monte Carlo model

3.3.2 Optimization of the amount of neutron absorber/scatter

The amount of neutron absorber/scatter of the best neutron shielding performance for thermal neutron and total range of neutron energy, which were investigated in section 3.3.1, were varied to determine the optimum amount. A simulation of 1 cm thick sample#2 with varying amount of B_2O_3 added from 0 to 70 phr was determined. The reason of setting maximum amount of B_2O_3 at 70 phr because in preliminary fabrication indicated that more than 70 phr the rubber compound would be lost of elasticity properties. For the 10 cm thick shielding material sample#10 with varying amounts of B_2O_3 added from 0 to 70 phr and Fe_2O_3 added from 0 to 100 phr was determined. The reason why the amount of Fe_2O_3 added was limited to 100 phr was because during a trial fabrication test, the rubber became very rigid at 100 phr and more, making it much less flexible.

3.3.3 Comparison of the neutron shielding performance between innovative neutron shielding materials and other ordinary neutron shielding materials

The neutron shielding performance of ordinary neutron shielding materials (listed in table 7) such as concrete, water, polyethylene (PE), borated PE and certain materials from research works (8),(9) were determined compare with 1 cm and 10 cm

thickness of the innovative neutron shielding materials using the MCNP transport code. The composition of these materials were listed in Table 2.

The dose transmission factor is defined as the ratio of the shielded neutron dose to the unshielded neutron dose:

$$\text{Dose Transmission Factor} = \frac{\text{Dose with shielding material (I)}}{\text{Dose without shielding material (I}_0\text{)}}$$

A small value of the transmission factor is better than a large value.

Table 7: The composition of ordinary neutron shielding material.

Material	Density (g/cm ³)	Element Content (%)						
		H	C	¹⁰ B	¹¹ B	O	Fe	Etc.
Regular concrete*	2.30	1.0	-	-	-	53.20	1.4	Na 2.90
								Al 3.40
								Si 33.7
								Ca 4.4
Water*	1.00	11.189	-	-	-	88.811	-	-
Polyethylene (PE)*	0.93	14.372	85.628	-	-	-	-	-
Borated PE*	1.00	12.536	77.464	1.99	8.01	-	-	-
B ₄ C 20 phr/NR and carbon black 40 phr (8)	1.181	7.400	82.818	1.937	7.846	-	-	-
H ₃ BO ₃ 30 phr/NR and carbon black 40 phr (9)	1.453	7.826	75.389	0.611	2.475	13.699	-	-

* (21) Compendium of Material Composition Data for Radiation Transport Modelling.

3.3.4 Additional material for improving the total neutron shielding performance

The 10 cm thick optimum neutron shielding material for total neutron was added by various 1 mm thick metal sheets that were reasonably easy to machine and has high-Z element. Additions were at the front side (close to the neutron source) of the sphere shielding sample (see Figure 15), the back side (outer surface of the sphere) and both sides. The neutron dose equivalent rate was investigated at the outer surface of the sphere sample to compare the neutron shielding capability.

3.3.5 Shape effect of neutron shielding material

Different shapes (rectangle, cylinder and sphere) with the same volume of neutron shielding material with and without the thin layer of metal sheet were analyzed for neutron shielding performance.

3.4 Fabrication of the shielding materials

Composite materials shown in Table 6, which were the most appropriate rubber compounds after MCNP simulation of all compounds listed in Table 1, were fabricated by trial and error, as it was unpredictable which composition would result in a stable compound. All rubber mixtures were prepared in a two-roll mill (see Figure 16) of 8 inch x 20 inch in diameter with the working distance of 300 mm (speed of slow roll 18 rpm) and the gear ratio of 1:4. Powders of B_2O_3 , PbO_2 and Fe_2O_3 were appropriately introduced into the blend according to the recipe of compositions given in Table 2. Mixing time was about 25 minutes. After compounding, the stock was left for 24 hrs to mature. The sheets were cut into slabs and then compression molded by an electrically-heated hydraulic presser (Figure 17) at 160 ± 2 °C and 4 MPa for a suitable duration of each sample.

The rubber samples' physical properties (tensile strength and tear resistant) were tested following standard methods at The Rubber Research Institute of Thailand in order to determine the best rubber recipe of each sample.



Figure 16: The two roll mill (Kodaira Seisakusho Co.,Ltd ; model : R 11-3 FF) at The Rubber Research Institute of Thailand.



Figure 17: The electrically-heated hydraulic compression machine : PR2D-W500L500 PM (CHAREON TUT CO.,LTD)

Table 8: Ingredients for fabrication of most appropriate rubber compounds

Ingredient (phr)	Samples						
	1	2(2.1)	4(4.1)	10			
				Layer 1	Layer 2	Layer 3	Layer 4
NR	50	50(100)	50(100)	100	50	100	50
SBR-1502	50	50(0)	50(0)	0	50	0	50
ZnO	5	5	5	5	5	5	5
Steric acid	2	2	2	2	2	2	2
Wingstay-L	1	1	1	1	1	1	1
B ₂ O ₃	0	60	0	0	10	0	10
Fe ₂ O ₃	0	0	100	100	0	100	0
MBTS ^a	1.2	1.2	1.2	1.2	1.2	1.2	1.2
TMTD ^b	1	1	1	1	1	1	1
DPG ^c	0.5	0.5	0.5	0.5	0.5	0.5	0.5
Sulfur	2.5	2.5	2.5	2.5	2.5	2.5	2.5
Compression molded time	8	30	4	4	15	4	15

^a Dibenzothaizyledisulphide, ^b Tetramethylthigramdisulphide , ^c Diphenyl Guanidine

3.4.1 Material's homogeneity verification

The homogeneity of each shielding material sample was verified by neutron radiography at the Thai Research Reactor TRR-1/M1, which is a TRIGA-type reactor. A neutron imaging plate (ND 2040) attached to the shielding material by an aluminium tape was exposed to the neutron beam for 4 minutes. The neutron flux and the Cd ratio at the position of the shielding material were approximately $9 \times 10^5 \text{ n cm}^{-2} \text{ s}^{-1}$ and 100, respectively. The neutron imaging plate was processed by an image reader (BAS 2500).

3.5 Experimental work on neutron attenuation

The neutron attenuation experiment was carried out at the Radiation Measurement Laboratory at the Nuclear Engineering Department, Faculty of Engineering, Chulalongkorn University to assess neutron shielding performances of the selected shielding materials shown in Table 2. Shielding materials were slab shaped

with thicknesses of 1 cm and 10 cm and dimensions of 15 cm x 15 cm. These slabs were stacked together to a height of 20 cm. The Am-Be neutron source whose strength was $3.08 \times 10^{5\text{rela}w}$ n cm⁻² s⁻¹ was placed at the bottom of the polyethylene (PE) source holder with a distance of 40 cm from the neutron detector, as illustrated in Figure 18. The neutron measurement was performed using a NE-905 glass scintillation neutron detector connected to a counting system.

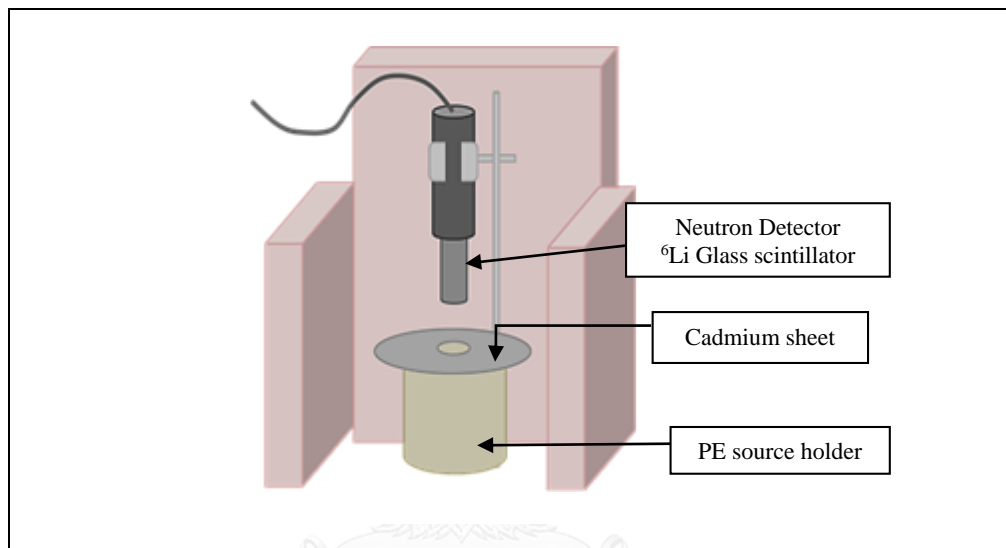


Figure 18: Geometry of the neutron transmission test

3.6 Secondary gamma radiation analysis by prompt gamma neutron activation analysis (PGNAA)

The slab shape of the shielding material with dimensions of 15 cm x 15 cm was placed in front of the neutron source holder to expose with Am-Be neutron source located in the middle hole of the cylindrical polyethylene (PE) source holder. The source holder was placed in the horizontal position so that the neutron source to slab sample material distance (SSD) is 12 cm. The spectra profile of gamma radiation was collected for 60 minutes by high purity germanium (HPGe) gamma radiation detector system. The detector was placed in the perpendicular position with respect to the neutron source holder, as illustrated in Figure 19.

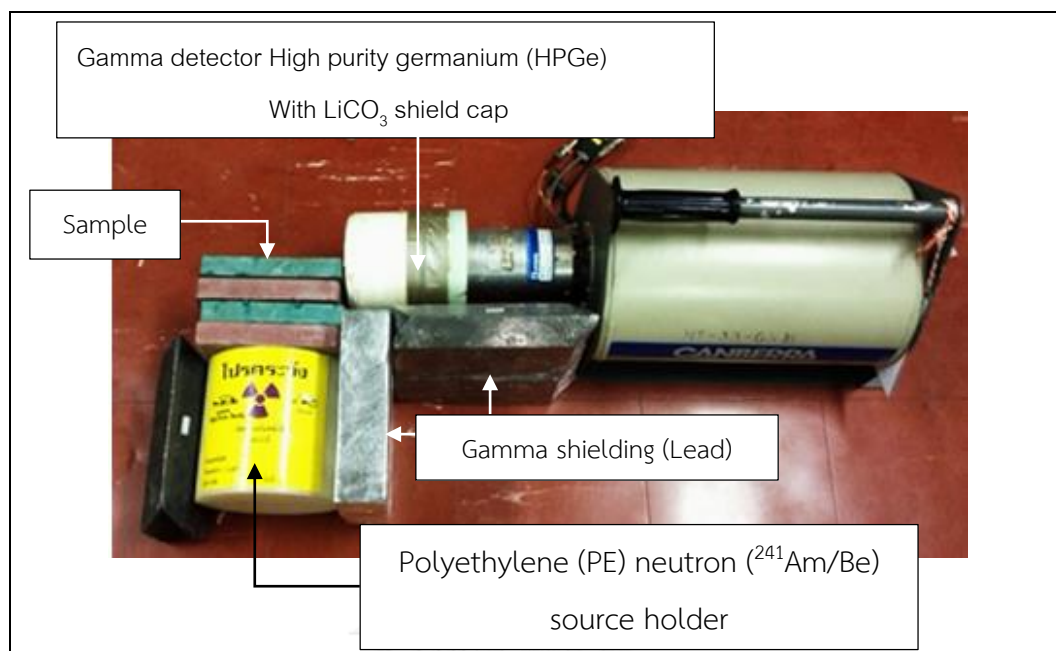


Figure 19: The top view of prompt gamma radiation counting system



CHAPTER 4

RESULT AND DISCUSSION

4.1. Boron detection in potash ore core by alpha track etch

The etched tracks of CR-39 detector plates (at positions A, B, C and D) after being bombarded with thermal neutrons were observed under optical microscope with magnification 100 as show in Figures 21 (a), (b), (c) and (d). Figures 21(a) and (b) representing positions A and B, respectively, exhibited a white color representing numerous tracks. These tracks appearing in high densities originated from alpha particles passing through plastic CR-39, creating hidden damages to its polymer chains. These damages can be made visible and can increase in size after etching the CR-39 polymer plate with NaOH solution. A number of alpha (${}^4\text{He}$) particles were created by thermal neutrons bombarding the material that composed of boron-10 (${}^{10}\text{B}$), following the interaction: $\text{Thermal neutron} + {}^{10}\text{B} \rightarrow {}^4\text{He} + {}^7\text{Li}^*$. Therefore, with a huge quantity of ${}^{10}\text{B}$ present in the material, numerous alpha tracks in the CR-39 detector plate were created as well. For the images of etched tracks shown in Figures 21 (c) and (d), which were attached at positions C and D on the potash core having brown color, less particle tracks were observed compared to Figures 21 (a) and (b). Therefore, the Somboon type potash core which exhibited white color contained an elevated amount of boron compared to the region with brown color.

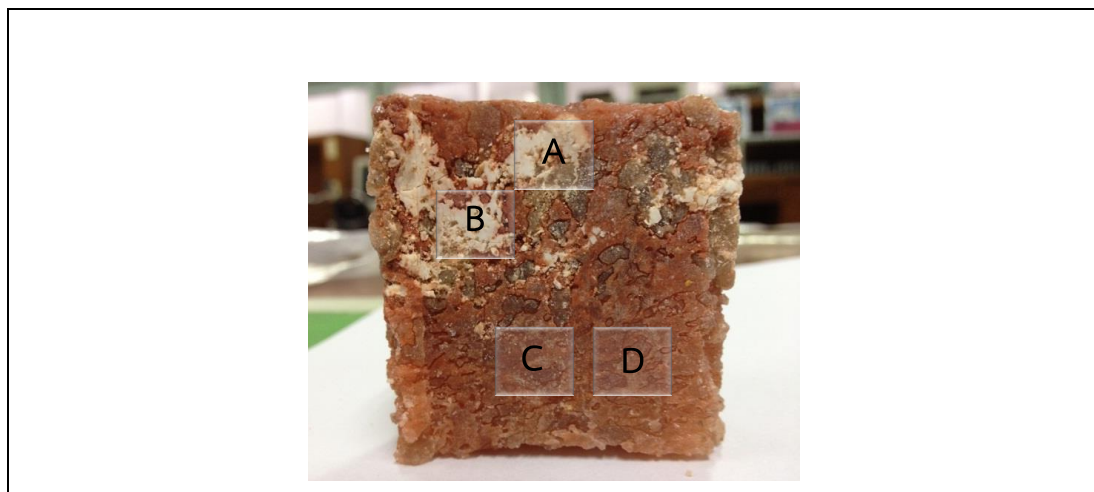


Figure 20 :The vertical section of potash core sample (Somboon type) that was attached with the CR 39 track etch detector plates at the positions A, B, C and D

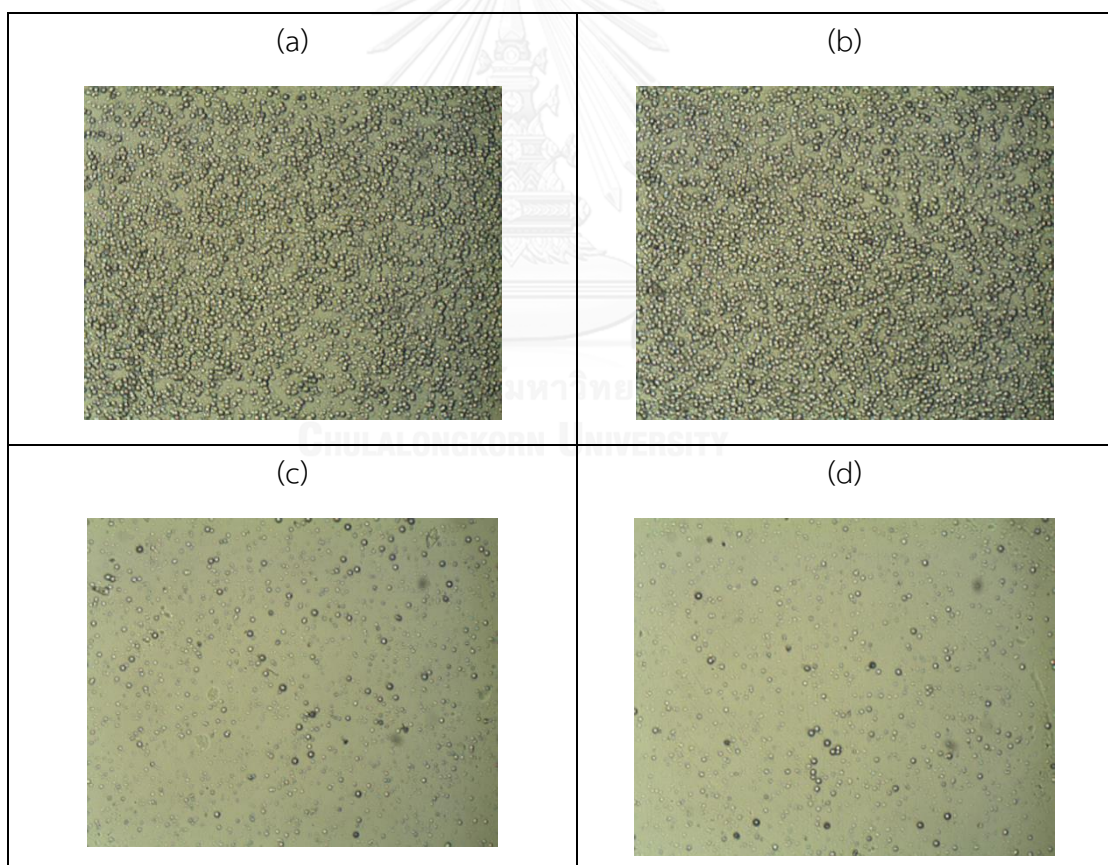


Figure 21: Micrographs of CR-39 etched alpha tracks, showing much higher track densities at potash core positions A (a) and B (b) compared to positions C (c) and D (d).

4.2. Material selection by MCNP simulation

4.2.1 Optimization of the type of neutron shielding materials

Results from the MCNP transport code revealed that the 1 cm thick sample #2 (NR+SBR+B₂O₃) and 10 cm thick sample #10 (4 alternating layers of NR+Fe₂O₃/NR+SBR+B₂O₃) exhibited excellent neutron and secondary gamma ray shielding performances, as seen in Figures 22 and 24.

Figure 23 illustrates the neutron shielding efficiencies at different energy regions. For sample #2, the best shielding efficiency occurred in the thermal energy range ($10^{-8} - 10^{-2}$ MeV) because boron exhibits a high thermal neutron absorption cross-section. Although some fast neutrons could interact with hydrogen atoms in the rubber composition to become thermal neutrons, the number of interaction is very few because the thickness of 1 cm was smaller than the mean free path of fast neutrons in rubber. Thus, only thermal neutrons could be absorbed by this material, which also had the highest boron content. The standard deviation (SD) associated with each data point was not shown in the spectra because the relative error from MCNP tallies was less than 0.01, which means that the quality of the tally was generally reliable (see detail in Table 4).

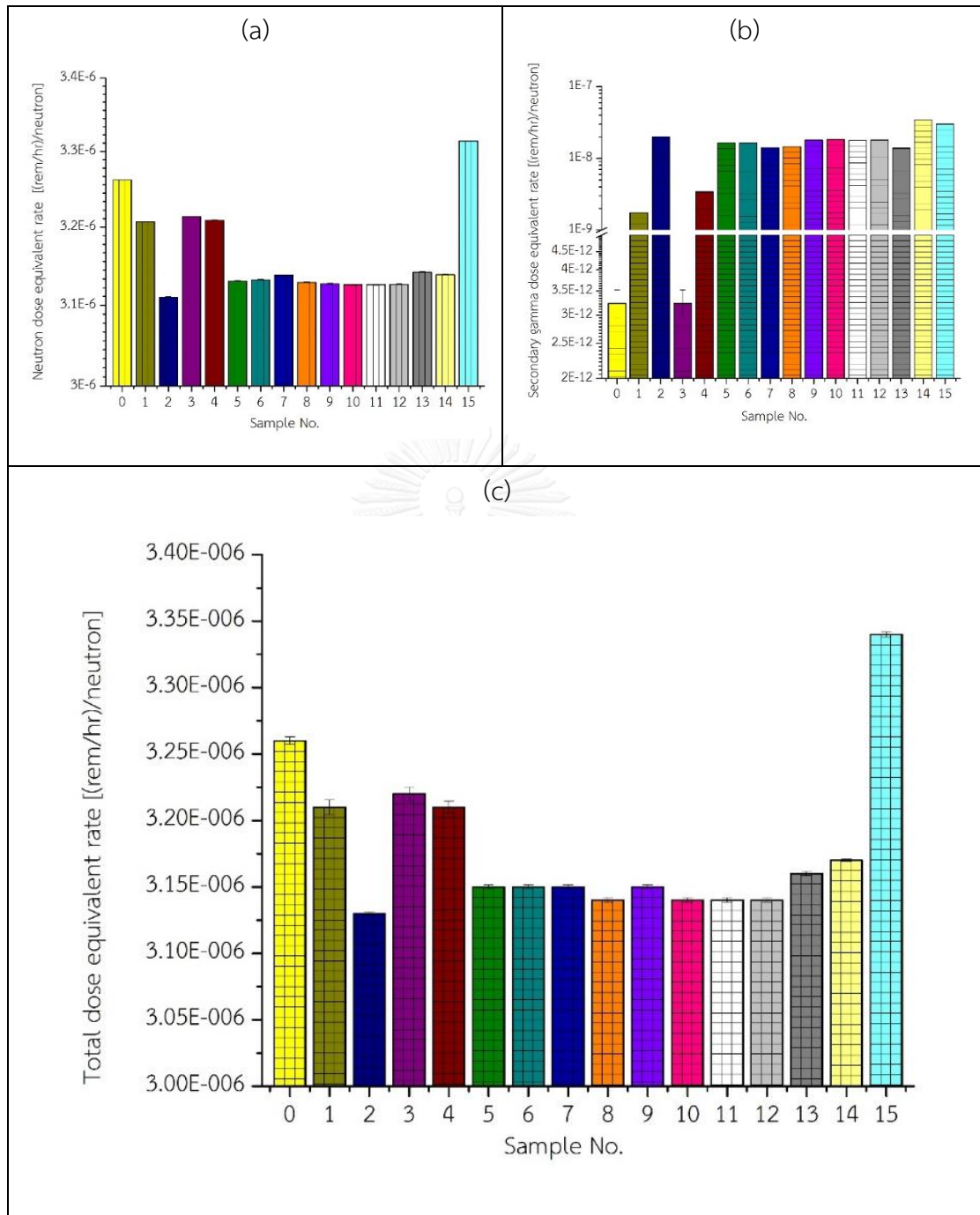


Figure 22: (a) Neutron dose equivalent rate (neutron energy 10^{-8} – 100 MeV), (b) Secondary gamma dose equivalent rate and (c) total dose equivalent rate on the outer surface of 1 cm radius sphere shielding sample.

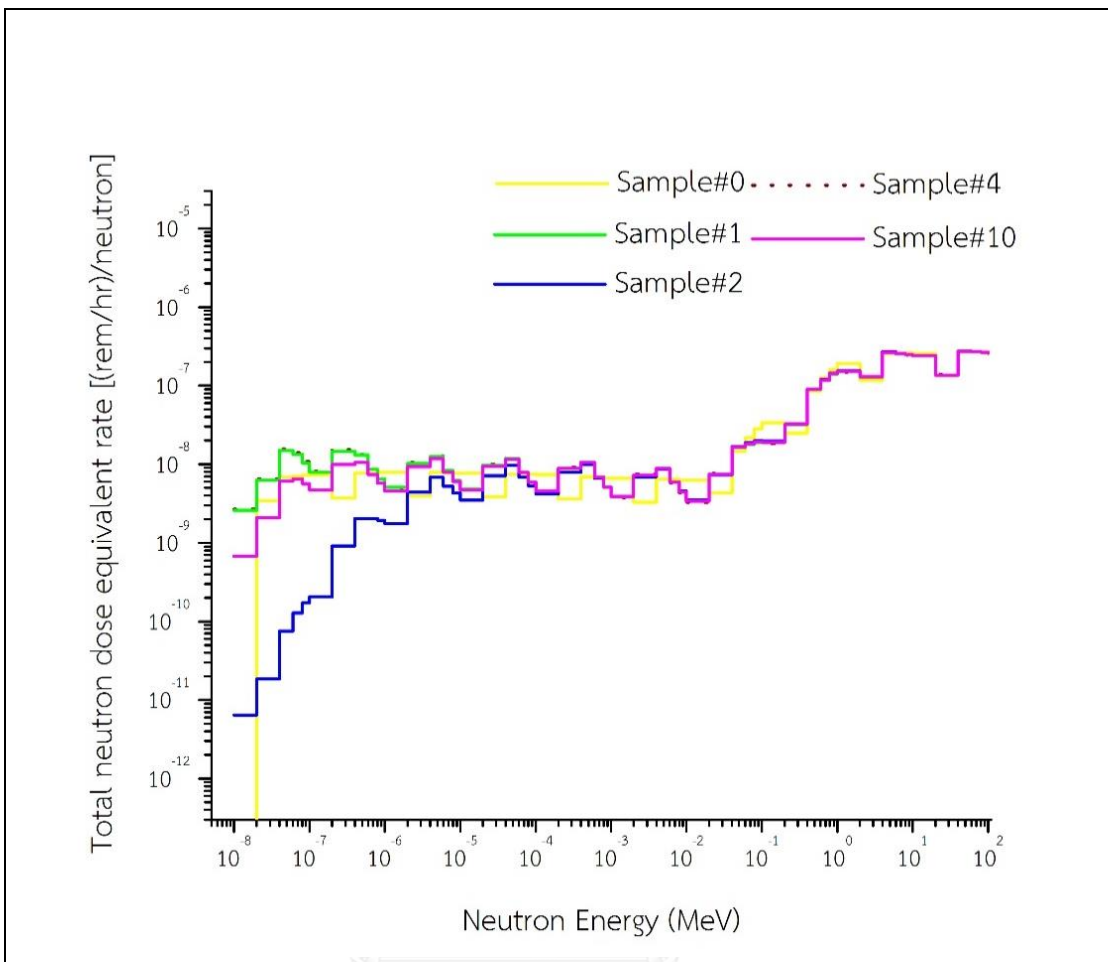


Figure 23: Neutron dose equivalent rate [(rem/hr)/neutron] spectra of total neutron energy range (10^{-8} – 100 MeV) on the outer surface of 1 cm rubber shielding materials.

For the 10 cm thick sample #10, fast neutrons could undergo inelastic scattering with iron and elastic scattering with hydrogen present in the rubber to become thermal neutrons and finally be absorbed by boron that has high thermal neutron absorption cross-section ($^{10}\text{B} = 3843$ barn).

Figure 25 illustrates that in the fast neutron regime (10^{-1} – 100 MeV), although not clearly visible in this Figure, sample #10 outperformed sample #2 because the total neutron dose equivalent rate was lower in the entire fast neutron energy range. Moreover, for sample #10, it also performed better than the NR/SBR rubber compound (sample #1) and NR/SBR/ Fe_2O_3 (sample #4) in the thermal energy range due to the presence of the boron compound.

Therefore 1 cm of sample #2 and 10 cm of sample #10 are suitable for thermal neutron ($10^{-8} - 10^{-2}$ MeV) shielding and all-energy neutron ($10^{-8} - 100$ MeV) shielding, respectively.

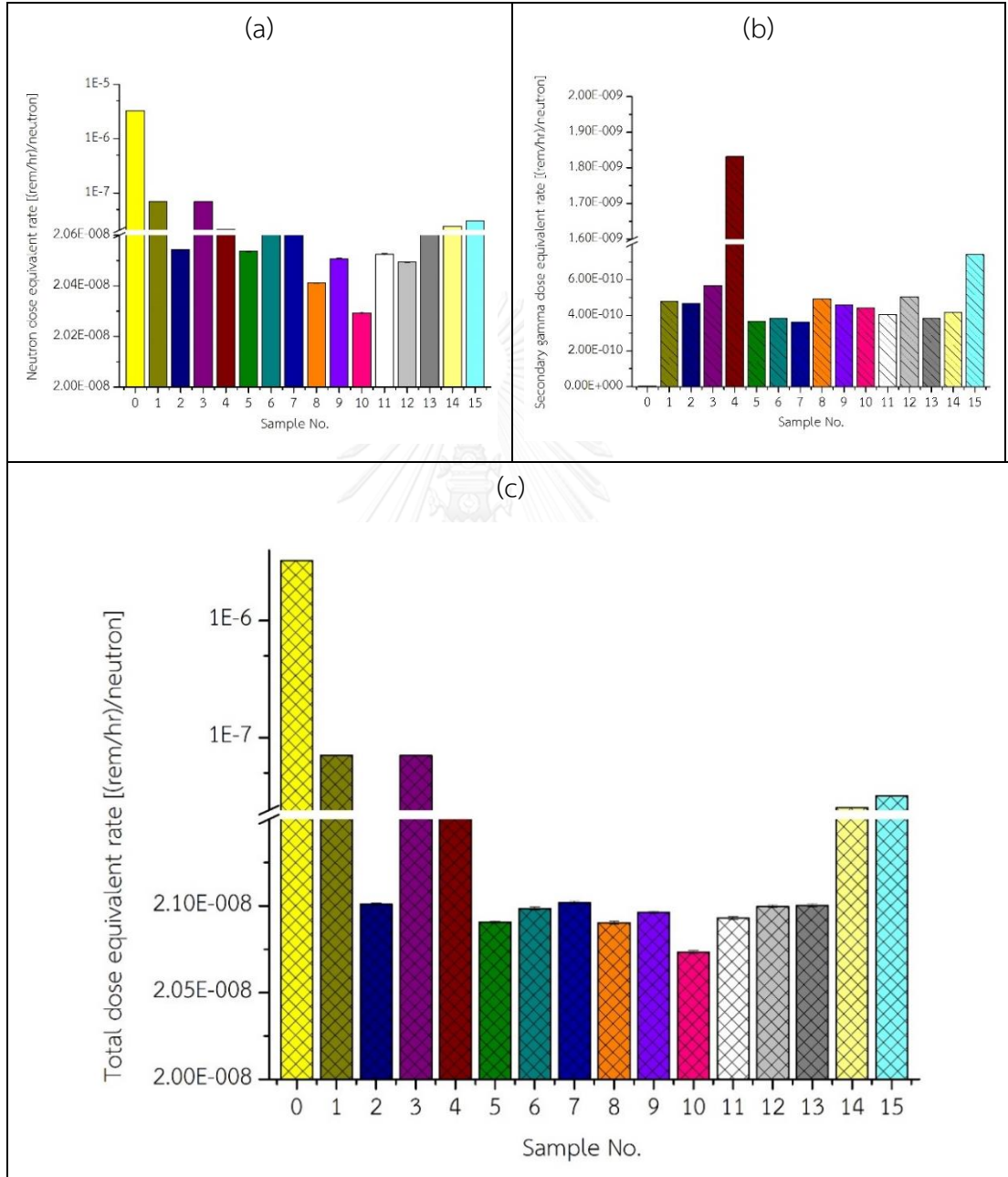


Figure 24: (a) Neutron dose equivalent rate (neutron energy $10^{-8} - 100$ MeV), (b) Secondary gamma dose equivalent rate and (c) total dose equivalent rate on the outer surface of 10 cm radius sphere shielding sample.

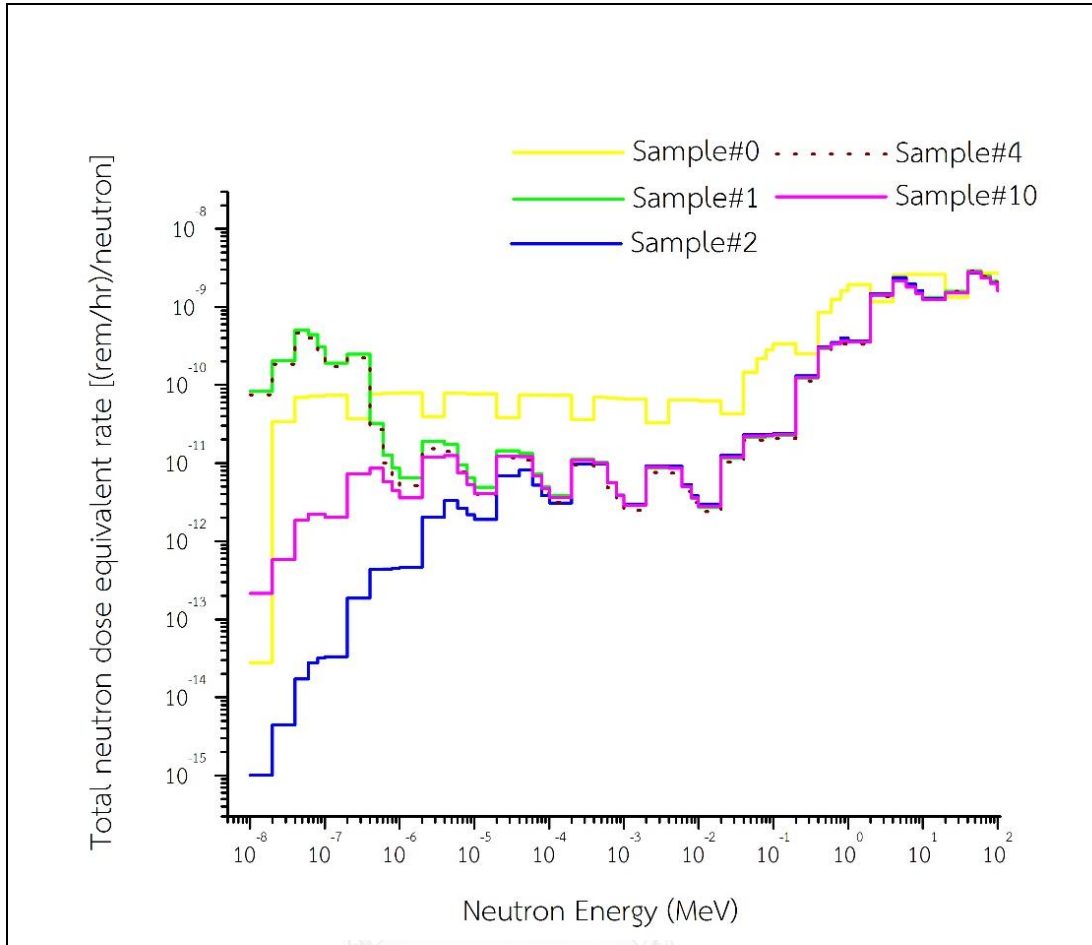


Figure 25: Neutron dose equivalent rate [(rem/hr)/neutron] spectra of total neutron energy range (10^{-8} – 100 MeV) on the outer surface of 10 cm rubber shielding materials.

4.2.2 Optimization of the amount of neutron absorber/scatter

To further determine the optimized amount of B_2O_3 and Fe_2O_3 additions, a thermal neutron attenuation simulation of a 1 cm thick sample #2 with varying amounts of B_2O_3 from 0 to 70 phr was performed. Results are shown in Figures 26(a) and (b). As more B_2O_3 was added, the total dose equivalent rate became reduced and appeared to saturate after about 60 phr. Thus, the most appropriate B_2O_3 addition for sample #2 was chosen to be 60 phr.

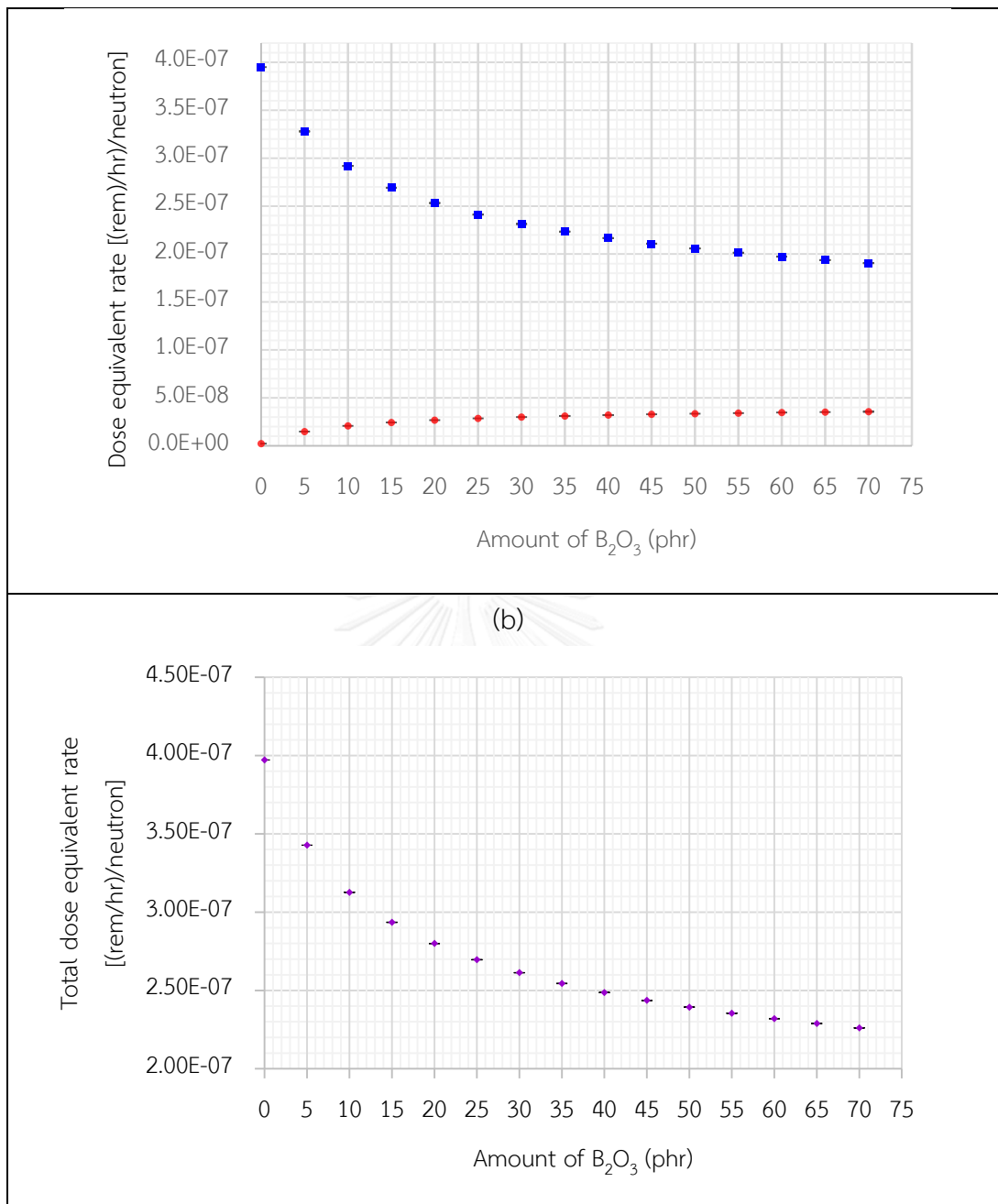


Figure 26: (a) The neutron dose equivalent rate and secondary gamma (photon) dose equivalent rate on the outer surface of spherical neutron shielding material at different amount of neutron absorber (Part per hundred rubber; phr) for 1 cm of sample #2 and (b) total dose equivalent rate (both neutron and photon) from *thermal neutron source ($10^8 - 10^2$ MeV)*

A simulation of a 0 cm thick sample #10 with varying amounts of B_2O_3 from 0 to 70 phr and Fe_2O_3 from 0 to 100 phr was performed. The reason why the amount of added Fe_2O_3 was limited to 100 phr was because during a trial fabrication test, the rubber became very rigid at 100 phr and more, making it much less flexible. Results in Figure 27 revealed that the most appropriate amounts were 100 phr of Fe_2O_3 and 10 phr of B_2O_3 .

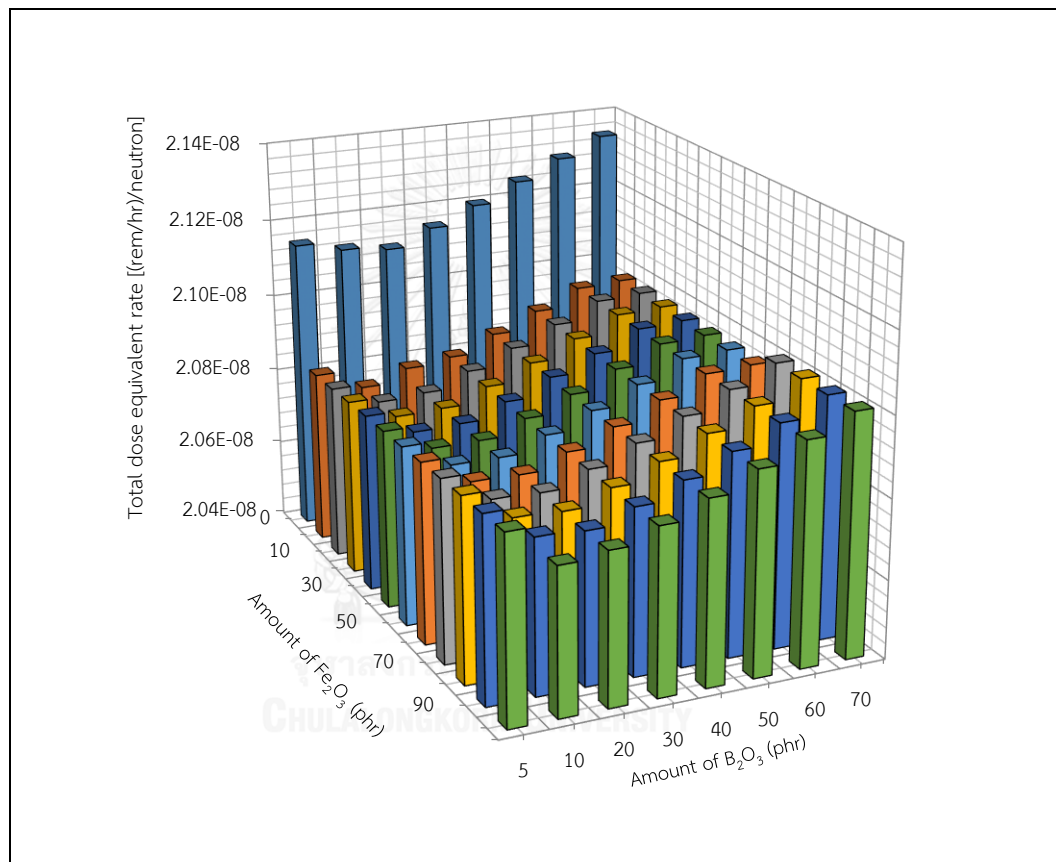


Figure 27: Total dose rate on the outer surface of sphere neutron shielding at different amounts of neutron absorbers for sample#10 from *entire energy range of neutron source ($10^8 - 100 MeV$)*

Table 9: Optimized composition of innovative neutron shielding materials

Material	Density (g/cm ³)	Element Content (%)					
		H	C	B-10	B-11	O	Fe
Sample#2 NR+SBR+B ₂ O ₃ 60 phr	1.2950	6.486	56.013	2.306	9.341	25.854	
Sample#10							
		Layer 1					
NR+Fe ₂ O ₃ 100phr	1.6796	5.189	44.811	-	-	15.029	34.971
		Layer 2					
NR+SBR+B ₂ O ₃ 10 phr	1.0580	9.435	81.475	0.559	2.265	6.267	-
		Layer 3					
NR+Fe ₂ O ₃ 100phr	1.6796	5.189	44.811	-	-	15.029	34.971
		Layer 4					
NR+SBR+B ₂ O ₃ 10 phr	1.0580	9.435	81.475	0.559	2.265	6.267	-

4.2.3 Comparison of the neutron shielding performance between innovative neutron shielding materials and other ordinary neutron shielding materials

Thermal neutron

Results from the MCNP transport code revealed that the 1 cm thick borated PE exhibited the best shielding performances. The second best performance was sample#2 (NR+SBR+B₂O₃ 60 phr; density: 1.295 g/cm³), B₄C/NR and H₃O₃/NR as seen in Figure 28. This is due to both the presence of boron, which has high absorption cross section for thermal neutron, and the highest hydrogen content. Because the interaction between thermal neutron and boron-10 produces a secondary gamma radiation from the following interaction: ${}^1_0n + {}^{10}_5B \rightarrow {}^4_2He + {}^7_3Li^*$ (gamma 478 keV), the sample#2 produced the maximum secondary gamma ray. However, as sample#2 was made from rubber, it exhibited the best flexibility compared to other materials.

Figure 29 illustrated the neutron dose equivalent rate spectra at the back surface of the shield for various materials in the energy region of thermal to epithermal

neutron. Although epithermal neutrons (10^{-5} - 10^{-2} MeV) could undergo elastic scattering with hydrogen atoms in concrete, water and PE to become thermal neutrons, these interactions were few. Moreover, these thermal neutrons cannot be absorbed by these materials without boron or other elements with high thermal neutron absorption cross section, so these materials produce more neutron dose than those with boron constituent.



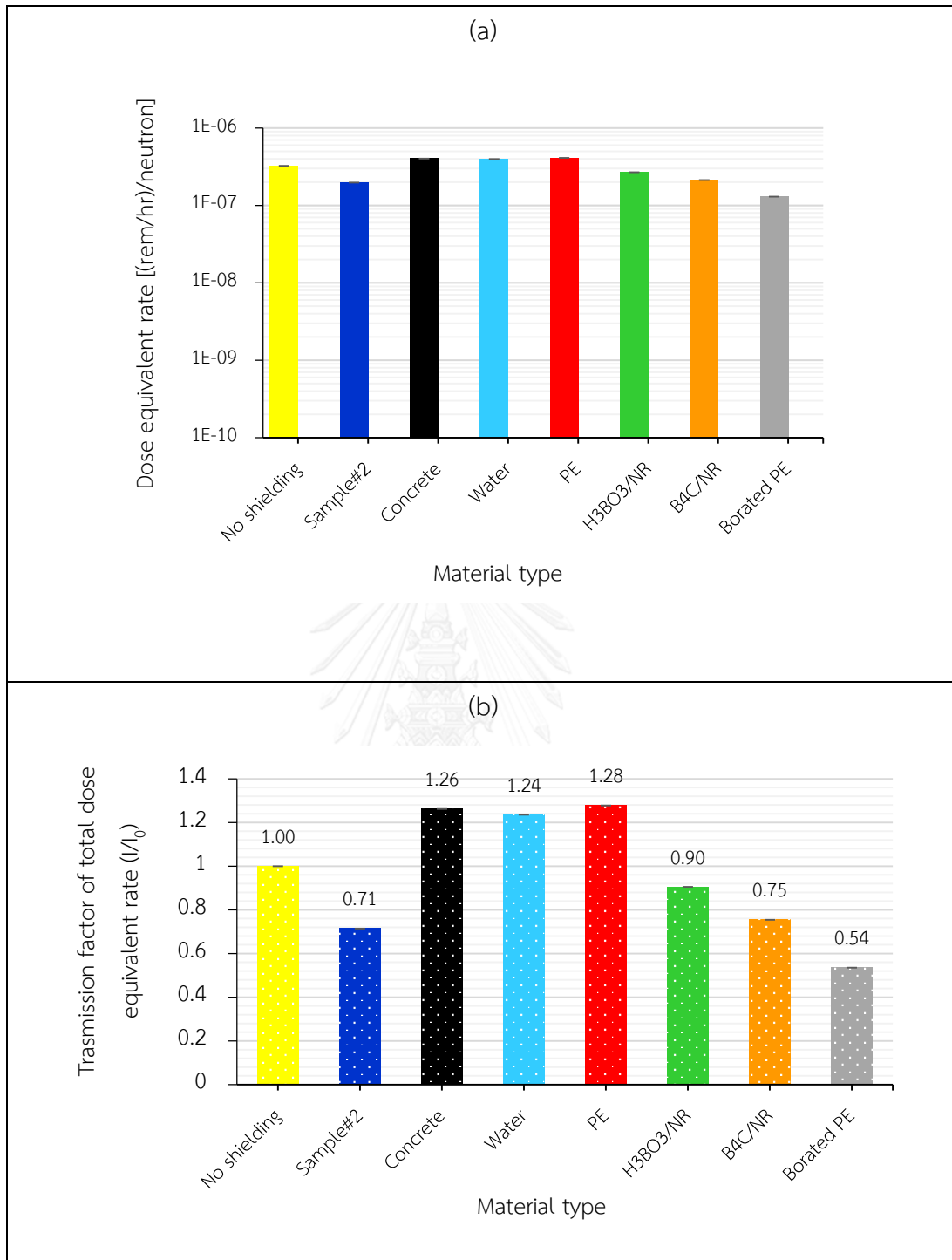


Figure 28: (a) The neutron and secondary gamma (photon) dose equivalent rate (from thermal neutron source; $10^{-8} - 10^{-2}$ MeV) and (b) transmission factor (I/I_0) of total dose equivalent rate on the outer surface of 1 cm radius sphere shielding materials.

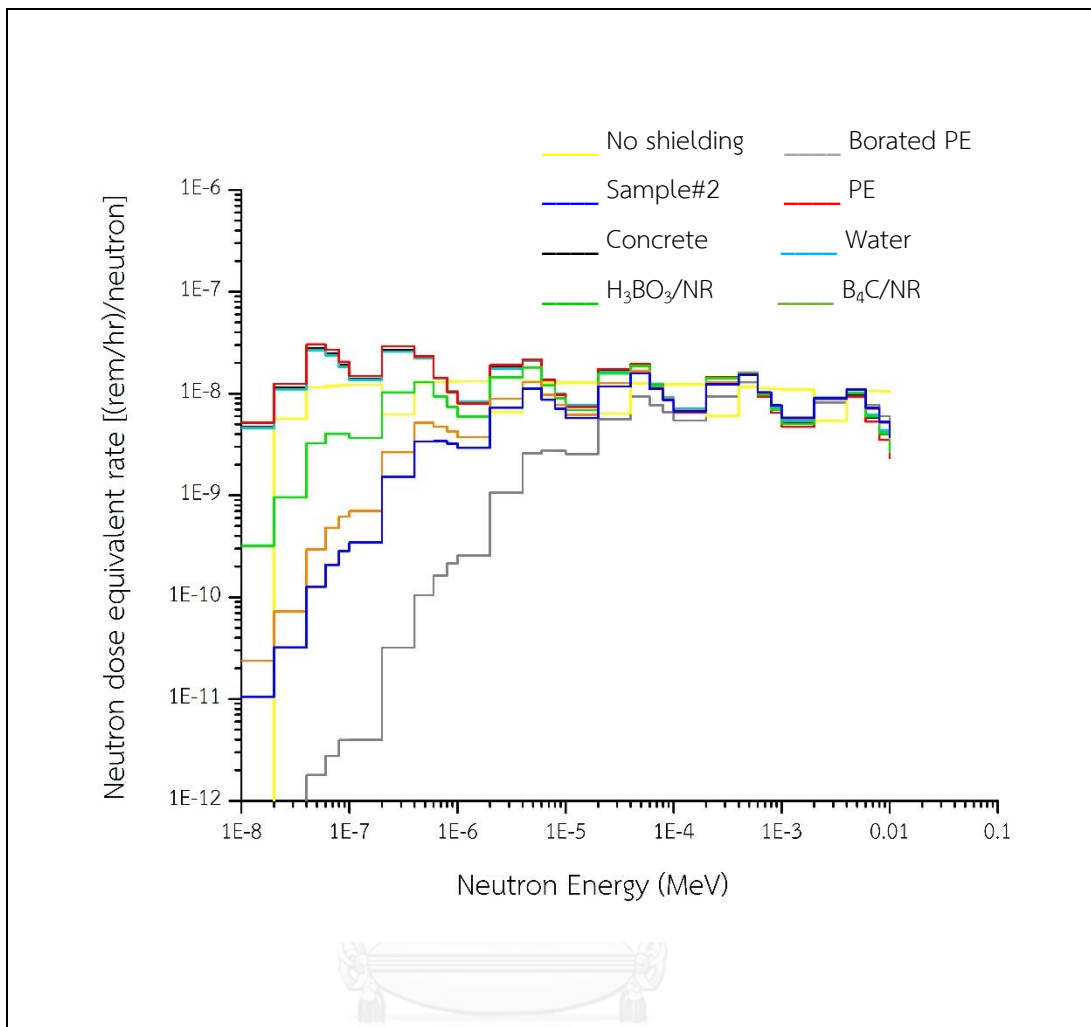
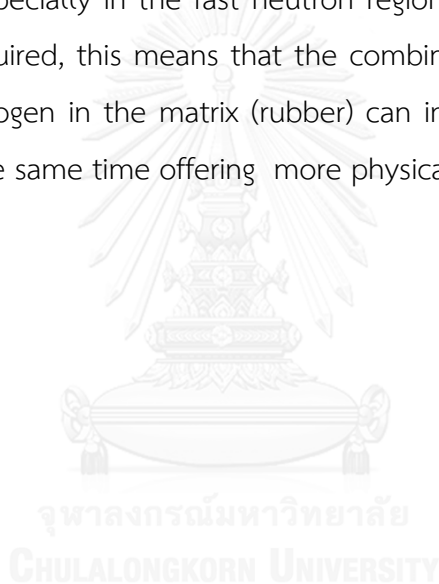


Figure 29: Neutron dose equivalent rate [(rem/hr)/neutron] spectra for thermal neutron ($10^{-8} - 10^{-2}$ MeV) at the outer surface of 1 cm radius sphere shielding materials.

Entire neutron energy

The MCNP simulation of total neutron attenuation for 10 cm thick materials revealed that the innovative neutron shielding #10 exhibited the best shielding performance with the transmission factor of 0.64 as shown in Figure 30(b). Although the neutron shielding performance of sample#10 is slightly less than that of concrete, the secondary gamma ray was produced from concrete even more (shown in Figure 30(a)) since fast neutrons interact with high-Z elements. Thus, sample #10 offered the best total dose equivalent rate (neutron and secondary gamma).

Figure 31 revealed the MCNP result of total neutron attenuation of 10 cm thick materials. In the thermal neutron region, the neutron equivalent dose rate of borated PE was significantly lower than that of sample #10 and others. This was due to the effect of boron which borated PE contained the most (see Table 7). However, when considering the fast neutron region (above 0.1 MeV), the better shielding performance was revealed in both materials that had high content of low-Z elements [*hydrogen in PE (C_2H_4) and oxygen in water, iron(III) oxide (Fe_2O_3) and boron oxide (B_2O_3)*] and high content of high-Z element as concrete and Fe in sample #10 . This indicates that the neutron shielding mechanism is complex, and that high-Z elements are effective in neutron shielding, especially in the fast neutron region. Moreover, as hydrogen and boron atoms are required, this means that the combination of iron and boron with high content of hydrogen in the matrix (rubber) can improve the neutron shielding capability while at the same time offering more physical flexibility than the others.



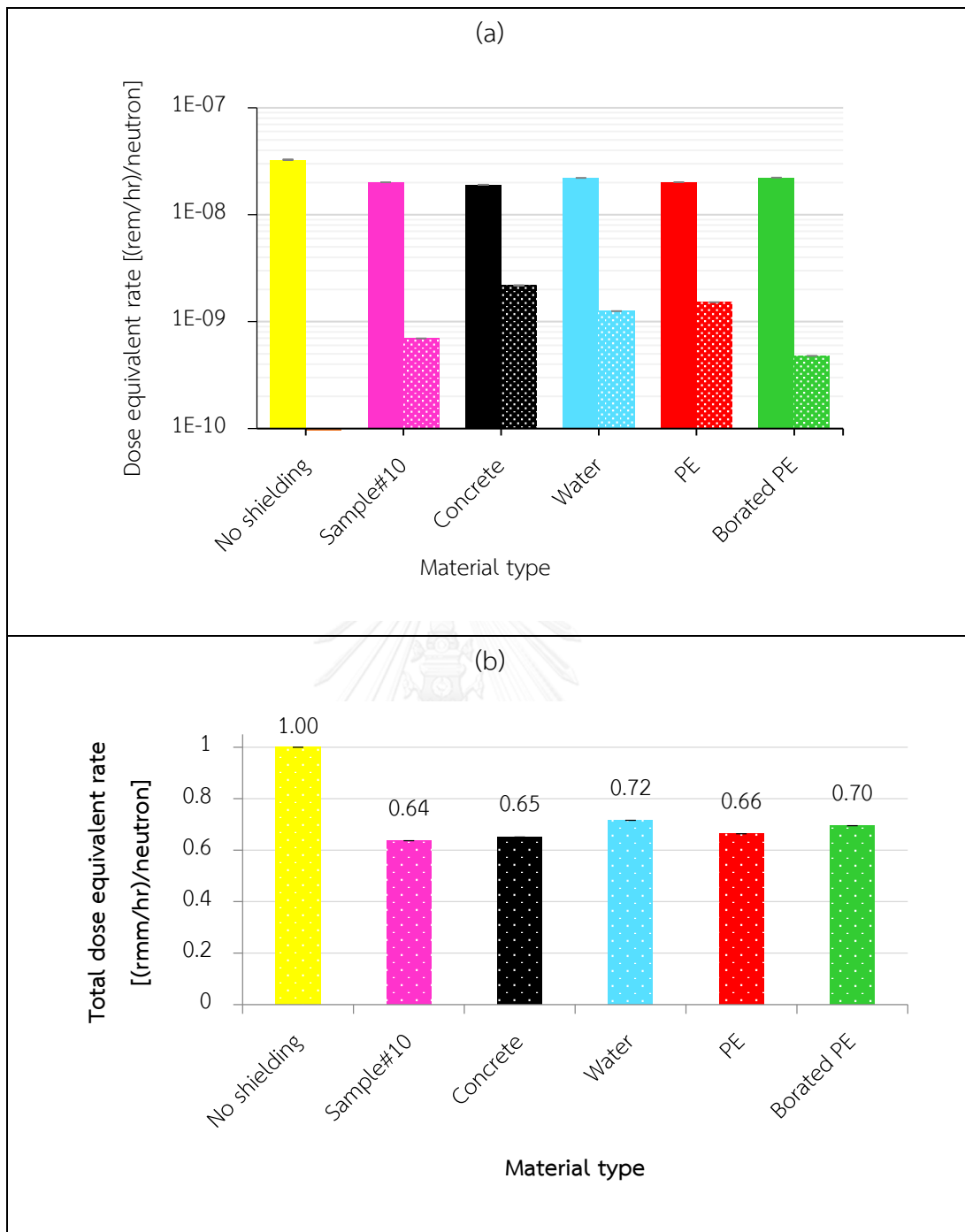


Figure 30: (a) The neutron and secondary gamma (photon) dose equivalent rate (from entire energy neutron source; $10^{-8} - 100$ MeV) and (b) transmission factor (I/I_0) of total dose equivalent rate on the outer surface of 10 cm radius sphere shielding materials.

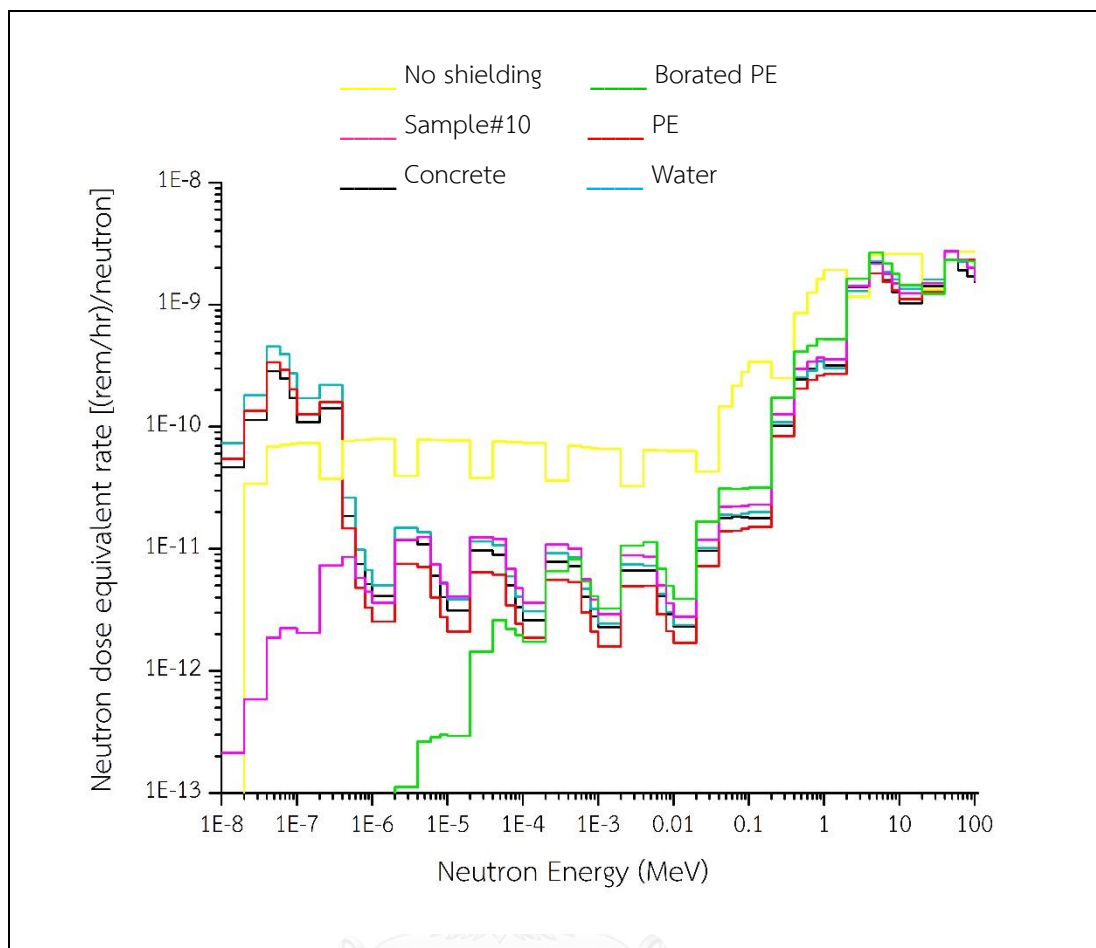


Figure 31: Neutron dose equivalent rate $[(\text{rem}/\text{hr})/\text{neutron}]$ spectra at the outer surface of 10 cm thick ordinary neutron shielding materials and the innovative neutron shielding material (sample #10)

Table 10: The calculated transmission factor of various neutron shielding material

Material	Density (g/cm ³)	Transmission factor (I/I ₀)	
		1 cm thick for Thermal neutron	10 cm thick for neutron energy range 10 ⁻⁸ -100 MeV
Sample#2	1.29	0.7140	0.6494
Sample#10	1.37	1.0500	0.6366
Regular concrete	2.30	1.2600	0.6511
Water	1.00	1.2400	0.7157
Polyethylene (PE)	0.93	1.2800	0.6634
Borated PE	1.00	0.5350	0.6953
B ₄ C 20 phr/NR and carbon black 40 phr (8)	1.181	0.9050	-
H ₃ BO ₃ 30 phr/NR and carbon black 40 phr (9)	1.453	0.7550	-

4.2.4 Additional material for improving the total neutron shielding performance

Each of the following 1 mm thick metal sheets: Cadmium (Cd), Iron (Fe), Tin (Sn), Copper (Cu), Lead (Pb) and Bismuth (Bi) was added to the innovative neutron shielding sample #10 to improve the neutron and secondary gamma ray shielding efficiency. The MCNP result revealed that adding 1 mm thick Cd sheets on both sides reduced both neutron dose and secondary gamma ray by about 2%, which was the most compared to other metal sheets as shown in Figure 32. This slight dose reduction was because Cd has high absorption cross section for thermal neutron only ($\sigma_a; E=0.0253 \text{ eV} = 2462 \text{ barn}$). Although other metal sheets containing high-Z materials have large absorption cross sections in the fast neutron region, their layer thickness was less than the mean free path of fast neutron.

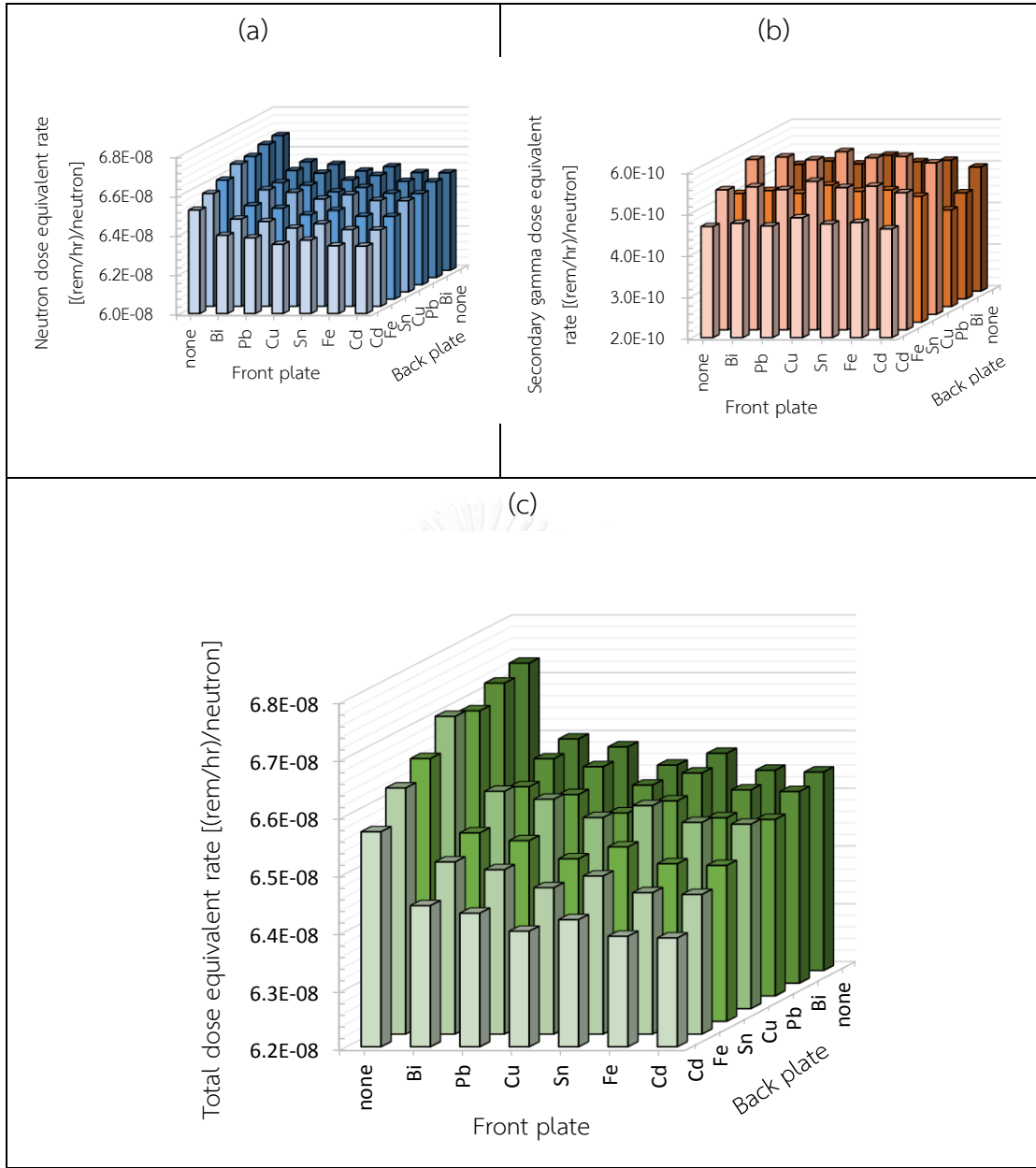


Figure 32: The column chart of dose equivalent rate for (a) entire energy of neutron, (b) secondary gamma ray and (c) total dose of neutron and gamma ray with various additional metal plates

4.2.5 Different shapes of neutron shielding material.

The radiation shielding performances for different shapes of sample #10 material with the same volume (see Figure 33) with and without 1 mm Cd sheets on both sides (from the result in Section 4.2.4) were simulated by the MCNP transport

code. The result revealed that the spherical shape material with and without Cd sheets offered the best radiation shielding with the transmission factor from entire neutron energy source of 0.6082 and 0.6298, respectively, as shown in Figure 34. This is because the spherical shape material has the most thickness compared to cylindrical and cubical shapes. In addition, all neutron particles had to go through the same thickness of the shielding material for the spherical case, while for cubical and cylindrical shapes, the interaction distance was largest from the center to corners. Therefore, the spherical shape material is most effective for neutron source shielding. The neutron dose distribution at each plane ($15 \times 15 \text{ cm}^2$) of cube detector around each shielding shape was shown in Figure 35.

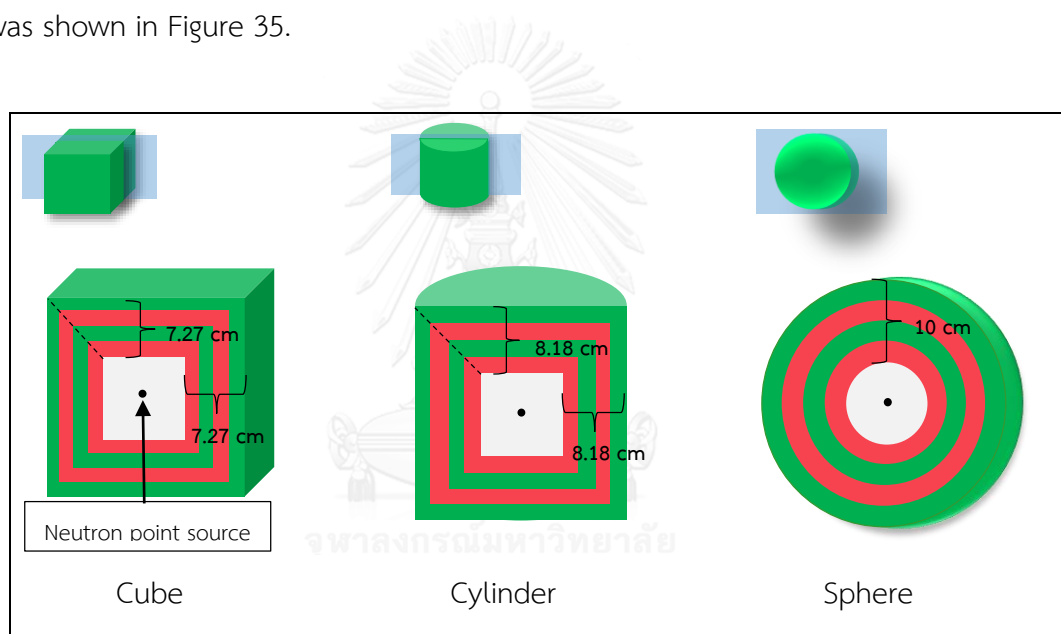


Figure 33: Drawing of cross section of various shapes for neutron shielding material sample #10 for MCNP modeling

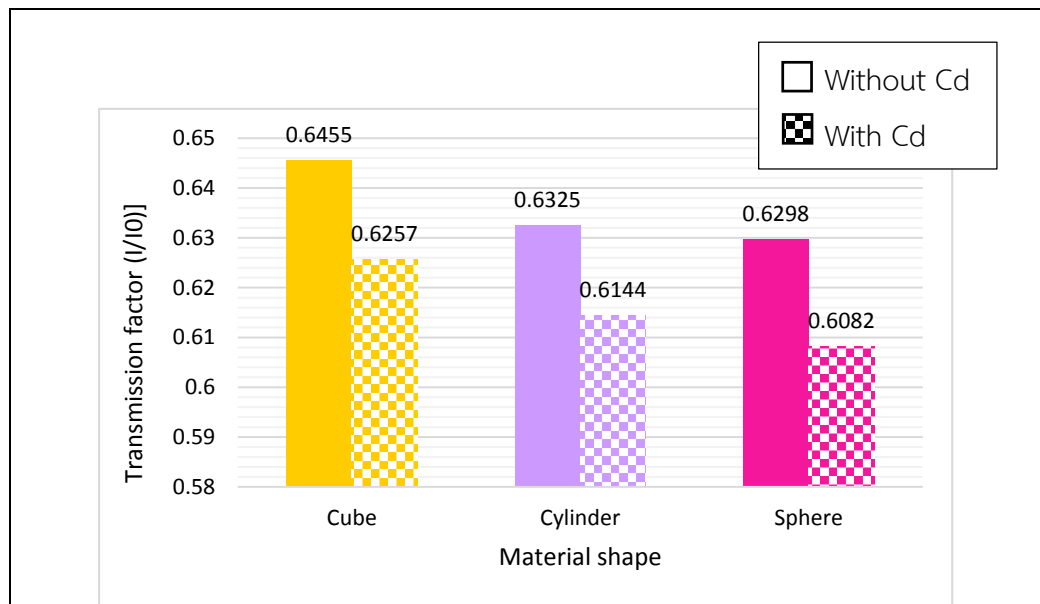


Figure 34: The transmission factor of various shapes of neutron shielding material with and without cadmium sheets

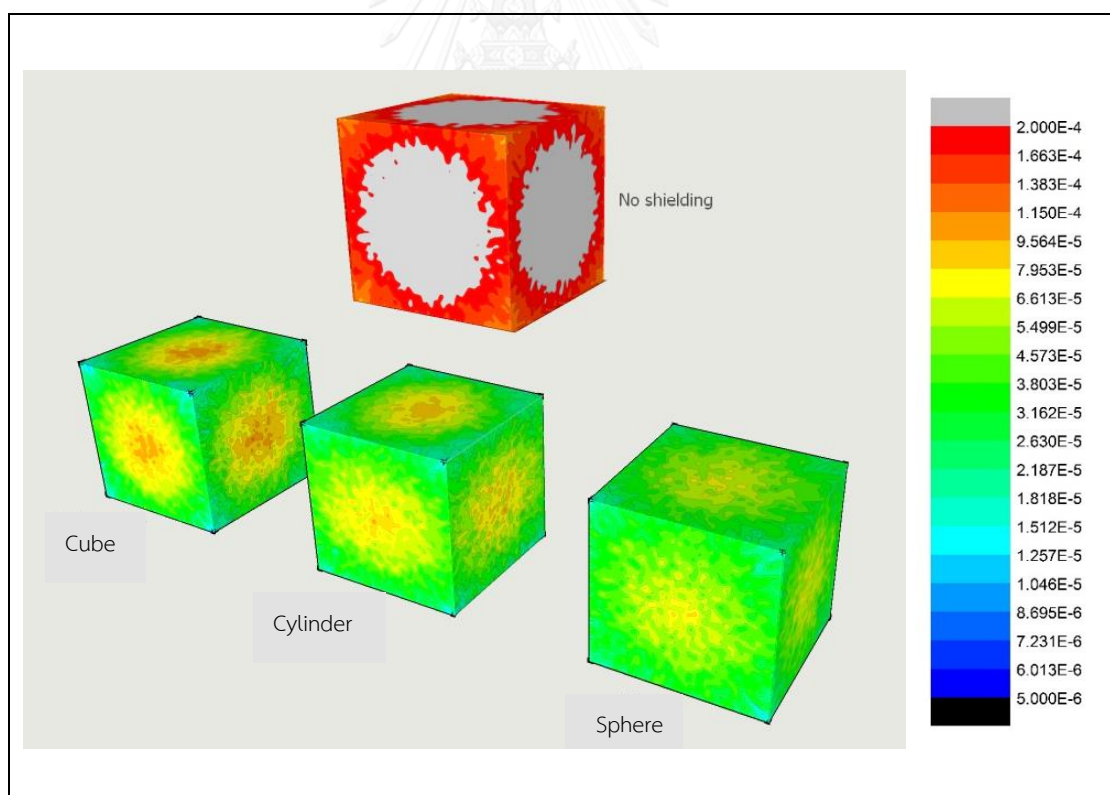


Figure 35: The neutron dose distribution at each plane ($15 \times 15 \text{ cm}^2$) of cube detector around each shielding shape.

4.3. Fabrication of rubber compound

The optimized designs according to the MCNP simulation were fabricated by trial and error. Various recipes of vulcanized rubber (No. 2, 2.1, 4 and 4.1) were tested to investigate the rubber properties for tensile strength and tear strength as shown in Table 10. The properties of vulcanized rubber No. 2 were better than those of No. 2.1. This was because styrene in the molecule of styrene butadiene rubber (SBR) was more resistant to B_2O_3 , which was more acidic ($pH \sim 4$) than natural rubber (NR). Comparison of the rubber properties between the vulcanized rubber No. 4 and 4.1 revealed that rubber properties of No. 4.1 was better than that of No. 4, because normally rubber properties of NR is better than that of SBR without reinforcing filler (such as carbon black). Moreover, Fe_2O_3 powder is not a poison to rubber. Therefore, samples No. 2 and No. 4.1 were chosen to be alternating layers of the neutron shielding material.

The successfully-fabricated shielding materials with slab geometry are shown in Figures 36(a) and 37(a). Homogeneity was one of several factors determining the suitability of the fabricated shielding materials. In reality, for the rubber compounds of samples #2 and #10, if they were left exposed to moisture in room condition, B_2O_3 would quickly react with water vapor in the atmosphere, turning into boric acid crystals, causing a problem with homogeneity. Thus, the samples must be completely encased in a thin layer of conventional rubber compound. Therefore, Figure 36(a) represents the rubber compound encased in the green conventional rubber. In Figure 40(a), because the rubber with iron oxide didn't require any encasement, the red slab represented the actual rubber compound. The corresponding neutron radiographs displayed in Figures 36(b) including intensities profile in Figure 38 for sample #2 exhibiting a very even color tone indicated that the neutron absorbing/scattering materials (B_2O_3 or Fe_2O_3) can be homogenously dispersed in the rubber compounds of NR and SBR. The neutron radiograph profiles of sample #10 shown in Figure 41 can be indicative that particles were homogenously dispersed as well.

Table 11: Properties of vulcanized rubber sample

Properties	Sample No.				Method
	2	2.1	4	4.1	
Tensile strength (MPa)	3.1	4.2	4.5	11.5	ASTM D412-06ae2 (Die C)
Tear strength (N/mm)	15.0	16.2	18.4	27	ISO 34-1:2010
Aging at 100°C, 22 h					
Tensile strength (MPa)	2.9	3.5	3.1	3.1	ASTM D412-06ae2 (Die C)
Tear strength (N/mm)	15.8	17.1	15.7	22.6	ISO 34-1:2010

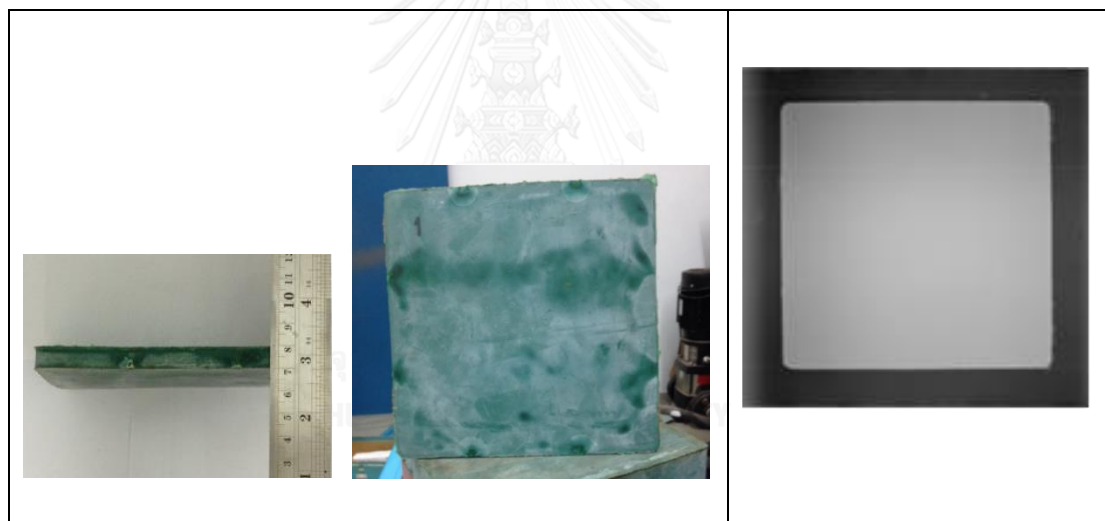


Figure 36: (a) Front view and (b) side view of 1 cm (NR+SBR+B₂O₃ 60 PHR: sample #2) shielding material samples trial-produced to fabricate slab shape. (c) Neutron radiograph of this shielding material (front view).

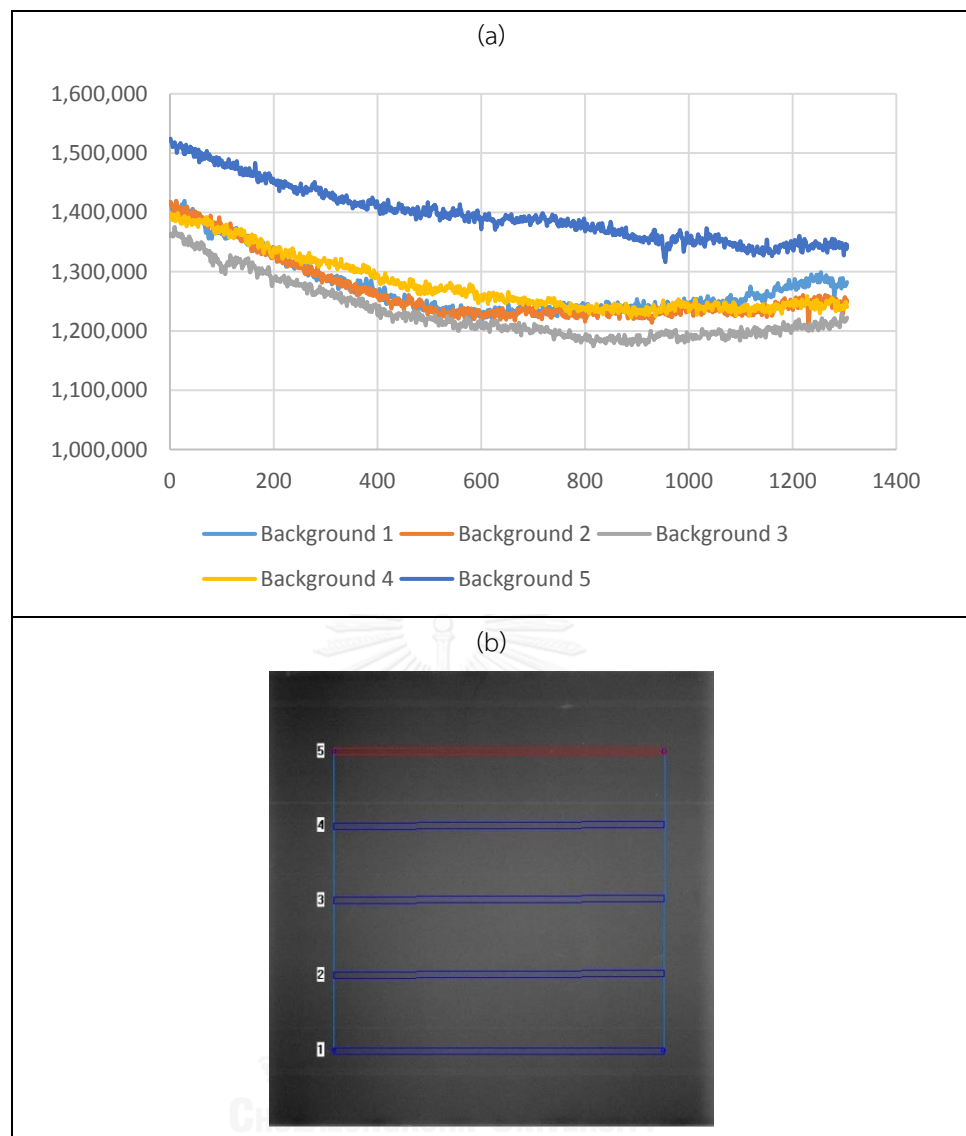


Figure 37: (a) The background counting intensity profile at various positions on the image plate (no material) and (b) the neutron radiograph with indicated profile's positions.

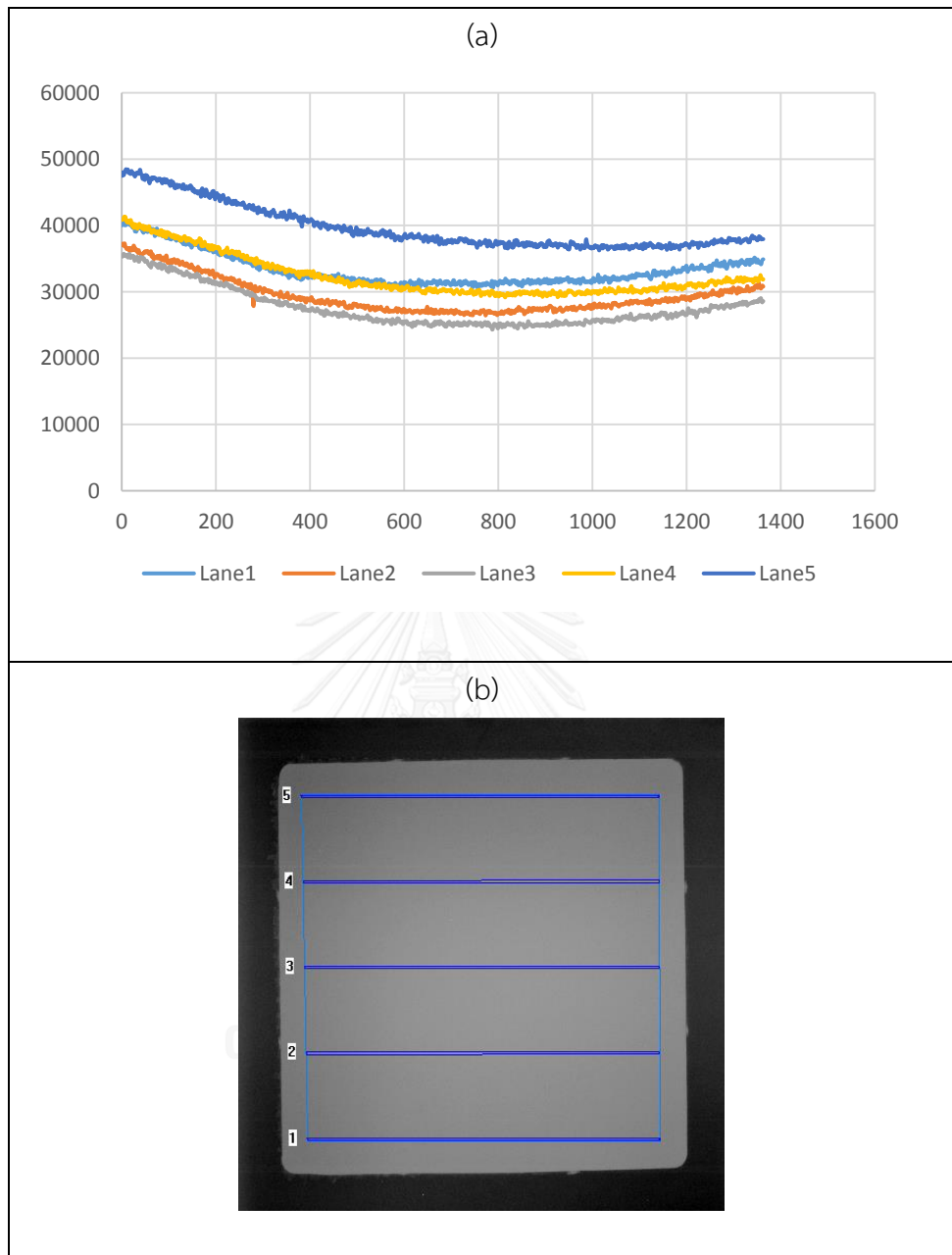


Figure 38: (a) The counting intensity profile at various positions on 1 cm thick sample #10 and (b) neutron radiograph with indicated profile's positions.

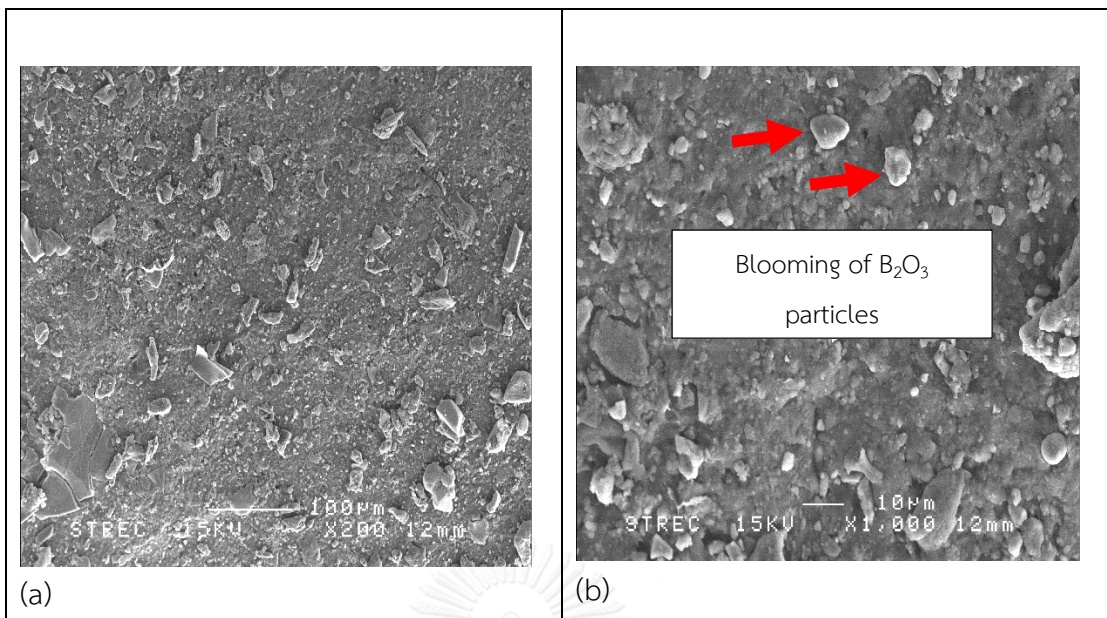
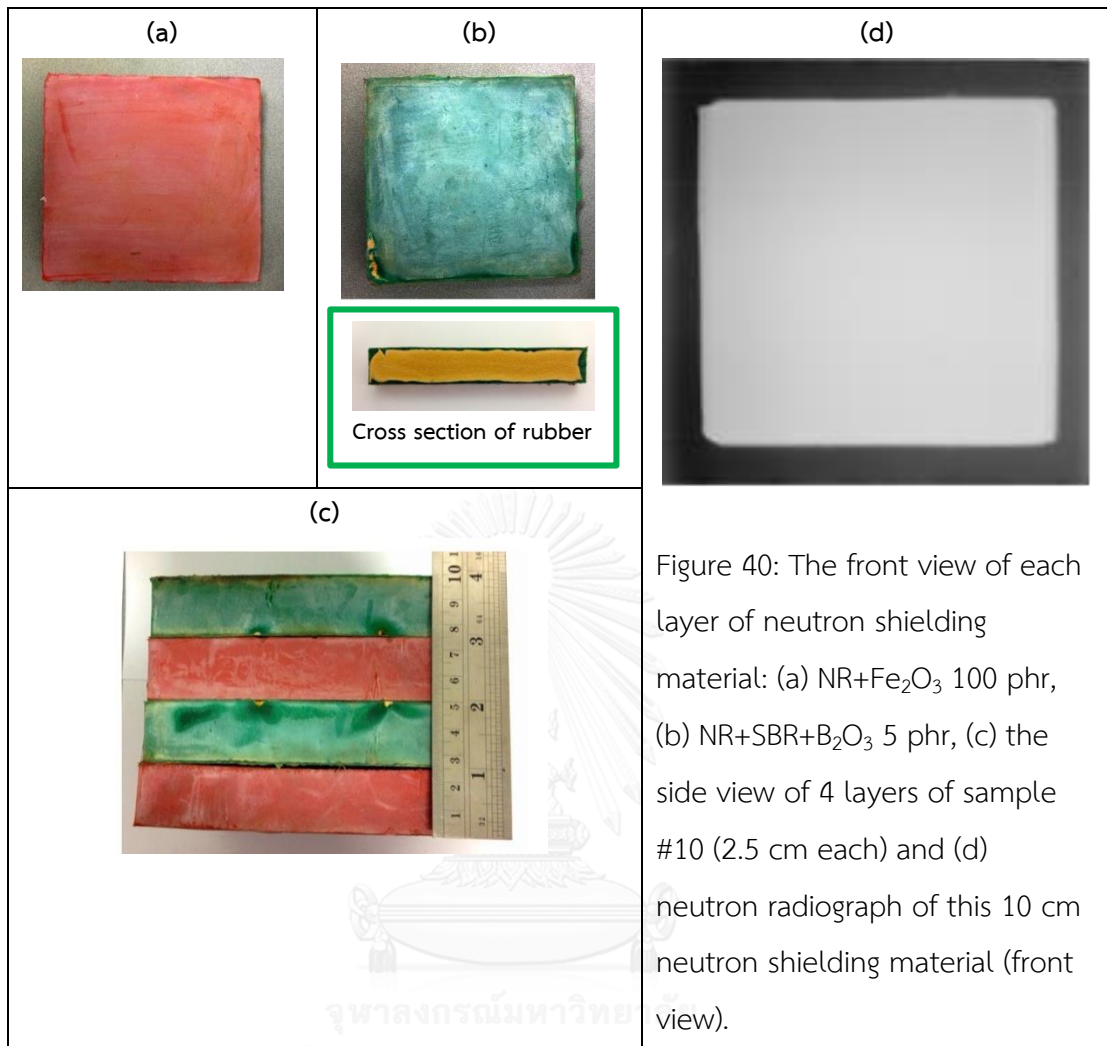


Figure 39: SEM micrographs of the surface of the vulcanized rubber (NR+SBR+ B_2O_3 60 PHR) for magnifications of 200x (a) and 1,000x (b) showing the blooming of B_2O_3 particles (and boric acid) (red arrows) on the rubber surface without encasing in a thin layer of conventional rubber compound.



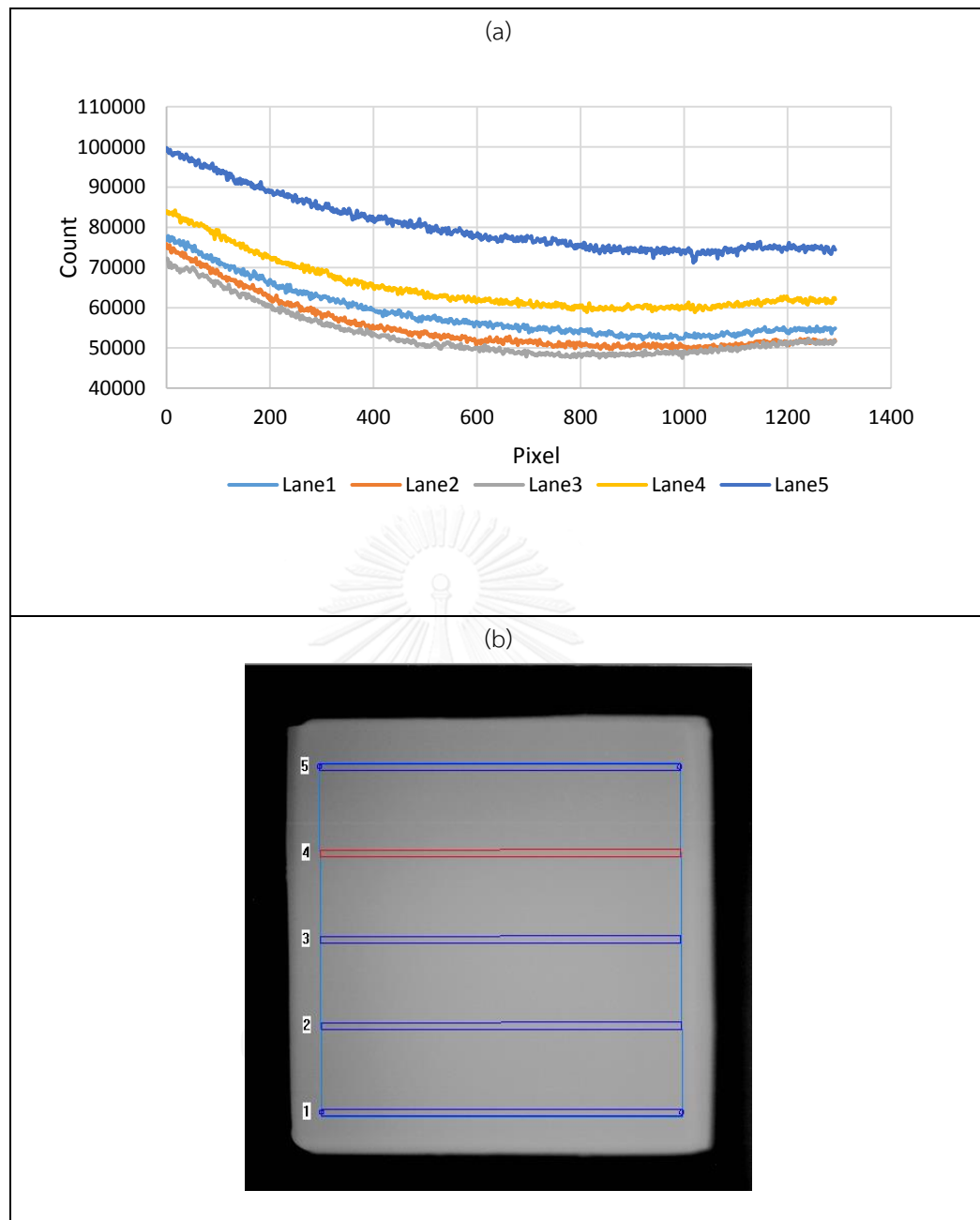


Figure 41: (a) The counting intensity profile at various positions on 10 cm thick sample #10 and (b) neutron radiograph with indicated profile's positions.

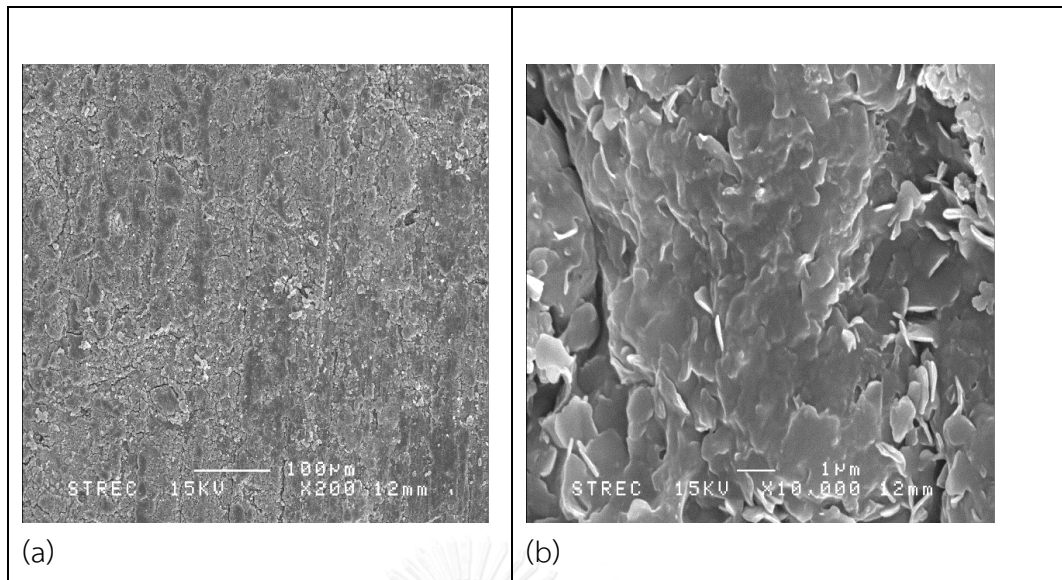


Figure 42: SEM micrographs of the surface of the vulcanized rubber (NR+SBR+ Fe_2O_3 100 PHR) for magnifications of 200x (a) and 10,000x (b).

4.4. Neutron transmission test

From the neutron transmission test, the 1 cm rubber compound with 60 phr B_2O_3 can reduce the neutron dose from the Am-Be source by $53.91 \pm 6.37\%$ with total macroscopic cross section of 0.076 cm^{-1} . The 10 cm rubber compound composing of 4 alternating layers with 100 phr Fe_2O_3 and 10 phr B_2O_3 can reduce the neutron dose by $72.56 \pm 5.95\%$.

The comparison of neutron transmission fluxes between experiments and MCNP simulation is displayed in Figure 43. The experimental data agreed well with the MCNP simulation. However, the trend lines of the simulation and the experiment were slightly different. This was because in the MCNP simulation, the neutron absorber and the scattering powder were homogeneously mixed with the rubber matrix, while in the real samples the powder material was dispersed as discrete particles in the rubber matrix.

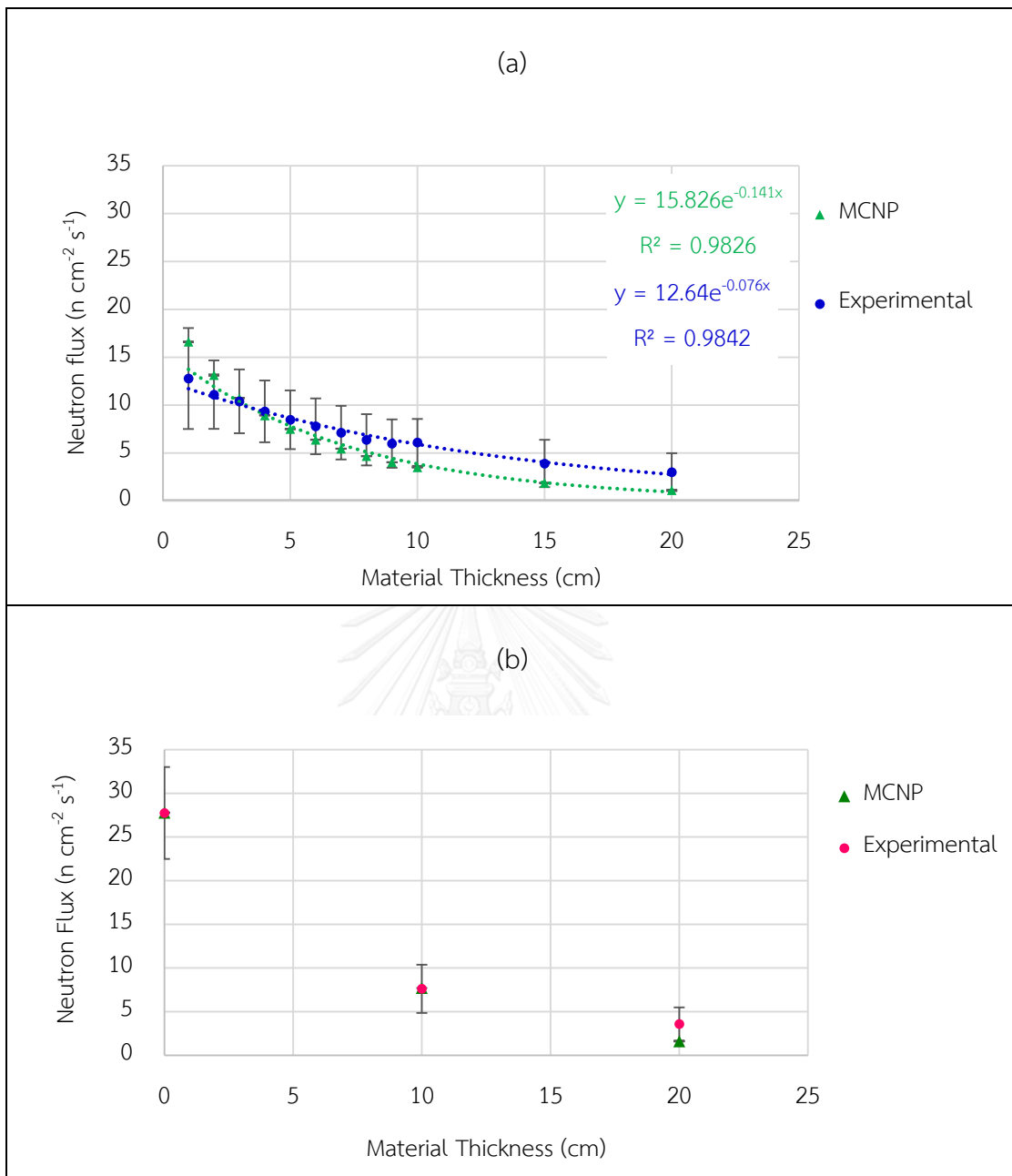
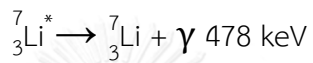
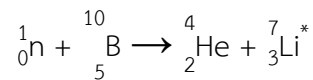


Figure 43: The relationship between transmitted neutron and material thickness of
(a) sample #2 and (b) sample #10.

4.5 Secondary gamma radiation determination

Samples #2 and #10 were continuously irradiated with a neutron beam from ^{241}Am -Be source for 1 hr. The constituent elements of the samples absorbed some of these neutrons and emitted prompt gamma rays which were measured using a HPGe gamma ray spectrometer. The spectrum of these secondary gamma rays is shown in Figure 44(b). The peak at 478 keV was produced from boron-10 interaction as follows:



In Figure 44(b), the intensity profile for sample #10 was lower than that of sample #2 everywhere. This was because of the larger thickness of sample #10 and the high Fe content that attenuated the gamma ray also. As these secondary gamma rays were of low intensities according to the MCNP result, using an additional thin layer of high-Z material would completely shield against these gamma rays.



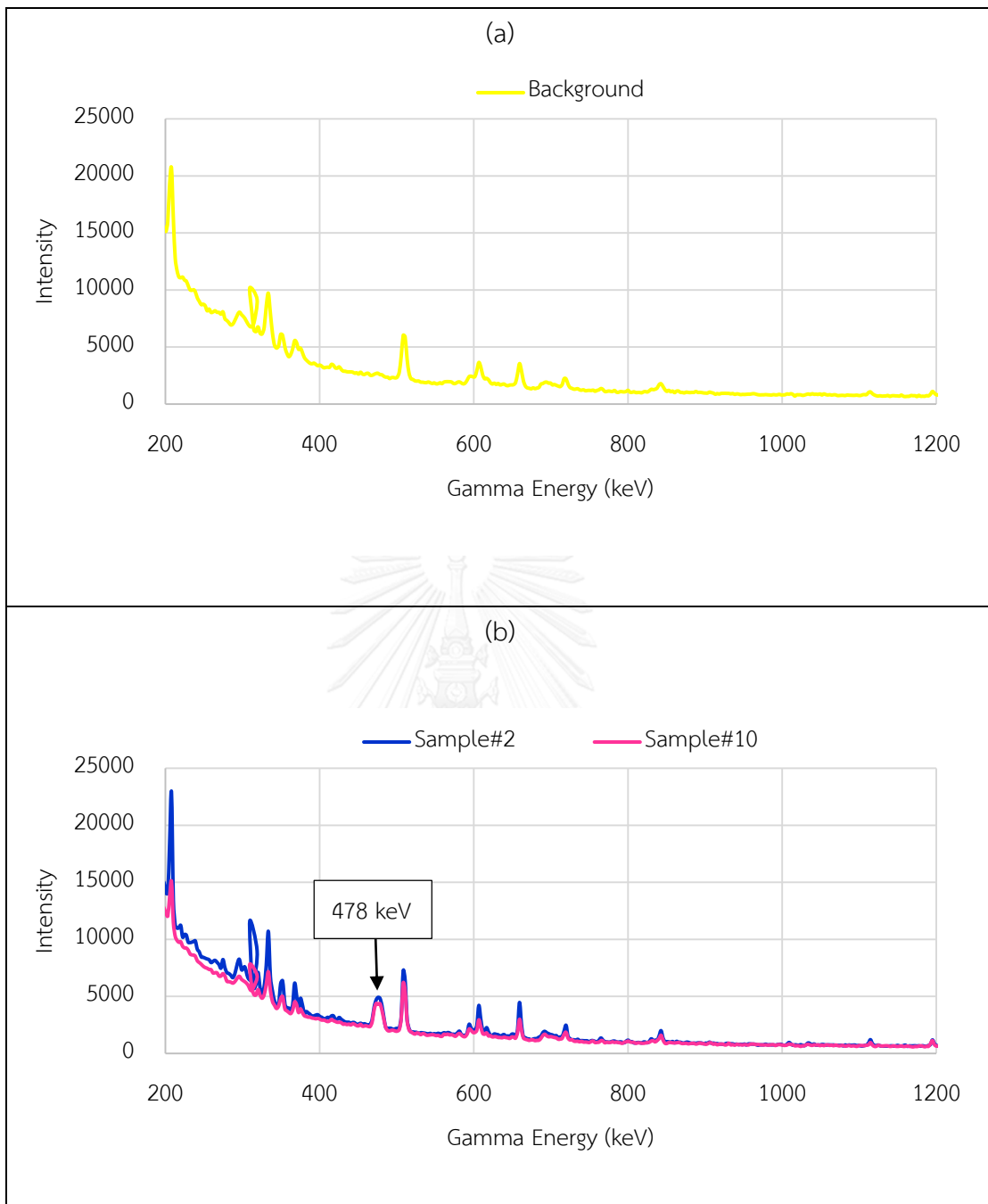


Figure 44: (a) Gamma ray spectrum of $^{241}\text{AmBe}$ neutron source (background) and (b) secondary gamma ray spectrum from neutron interaction with sample #2 and sample #10

CHAPTER 5

CONCLUSION

5.1 Conclusion

Optimized flexible and lightweight neutron shielding materials were designed using the MCNP transport code. The neutron shielding materials with thicknesses of 1 cm and 10 cm were examined for neutron shielding performances. Simulation results indicate that the 1 cm shielding material of NR and SBR blend (1:1) with 60 phr B_2O_3 (sample #2), and the 10 cm shielding material having 4 alternating layers of NR with 100 phr Fe_2O_3 and of NR and SBR blend (1:1) with 10 phr B_2O_3 (sample #10) were most suitable for thermal neutron shielding and entire energy neutron shielding, respectively.

The 1 cm thick sample #2 offered a better thermal neutron shielding performance than concrete, water and polyethylene (PE) with the same thickness. The transmission factors of sample #2, concrete, water, PE and borated PE were 0.71, 1.26, 1.24, 1.28 and 0.54, respectively. The borated PE offered a better shielding performance than sample #2 because of a higher hydrogen content present in the material. However, sample #2 offered more physical flexibility than borated PE.

The entire energy neutron (10^{-8} - 100 MeV) shielding performance of 10 cm thick, composing of 4 layers each 2.5 cm in thickness, sample #10 was the best when compared with those of other ordinary neutron shielding materials. This was due to the effect of fast neutron undergoing inelastic scattering with Fe (present in the layer of Fe_2O_3 rubber compound) and elastic scattering with hydrogen atoms (present in the rubber molecule) to become the low energy neutron or thermal neutron that could be absorbed by boron-10 in the layer of B_2O_3 rubber compound. The total dose (both neutron and secondary gamma) transmission factors of sample #10, concrete, water, PE and borated PE were 0.64, 0.65, 0.72, 0.66 and 0.70, respectively. Even though the radiation transmission factor of sample #10 was slightly less than that of concrete, it was physically lighter by approximately 1.35 times. Therefore, the combination of iron and boron with high hydrogen content matrix material as rubber can improve the neutron shielding capability, while offering more physical flexibility than others.

The innovative neutron shielding material of sample #10 with added 1 mm cadmium (Cd) sheets on both sides could reduce the total dose from neutron source of entire energies by an additional $\sim 2\%$ compared to materials without any additional Cd sheet. Moreover, some secondary gamma ray could be attenuated by the Cd sheets as well.

The neutron shielding performance of various shapes (rectangle, cylinder and sphere) of the shielding material was evaluated. Results revealed that the spherical shape material offered the best shielding performance, and that the transmission factors with and without the Cd sheets on both sides were 0.6082 and 0.6298, respectively. This spherical shielding material could be utilized as a neutron shielding container.

The optimized neutron shielding that was designed according to MCNP simulations having 1 cm thickness for thermal neutron shielding and 10 cm thickness for shielding neutron in the entire energy spectrum were fabricated into a slab geometry by the compression molding machine at 160 ± 2 °C and 4 MPa after all compositions were mixed by the two roll mill rubber mixture. The rubber compound that contained B_2O_3 was completely encased in a thin layer of conventional rubber compound to avoid contact with moisture in the air, which may turn B_2O_3 into boric acid crystals, causing problem with homogeneity.

The neutron radiography was carried out to verify the homogeneity of neutron shielding materials. Neutron radiograph profiles at various positions for each material were investigated using the Multi-gauge program. Results revealed that the particles of B_2O_3 and Fe_2O_3 were homogenously dispersed in the fabricated rubber compound.

The neutron transmission experiment was carried out to verify the shielding efficiency of these optimal designs. The 1 cm thick rubber compound with 60 phr B_2O_3 can reduce the neutron dose from the Am-Be source by $53.91 \pm 6.37\%$ with the total macroscopic cross section (Σ_t) of 0.076 cm^{-1} . The 10 cm thick rubber compound composing of 4 alternating layers with 100 phr Fe_2O_3 and 10 phr B_2O_3 can reduce the neutron dose by $72.56 \pm 5.95\%$ with Σ_t of 0.1293 cm^{-1} . The secondary gamma ray produced by the interaction between neutron and neutron shielding material was

determined by the prompt gamma neutron activation analysis method. The result revealed that a small amount of 478 keV gamma ray was generated. Therefore, a material with high atomic mass would be necessary to attenuate these gamma radiations.

The designed shielding materials are highly suitable for applications in nuclear science and technology. Not only is the production of these neutron shielding materials useful for neutron-related work, but they also utilize domestic resource

5.2 Suggestion and future studies

- 5.2.1 Determine the shelf life of the neutron shielding material.
- 5.2.2 Determine the degradation of the neutron shielding material under neutron fluence.
- 5.2.3 Use enriched boron-10 compound for the neutron absorber.

Use radiation for rubber vulcanization.





APPENDIX A

Neutron cross sections of common materials (24)

Material	Atomic or Molecular Weight Density (g/cm ³)	Cross Section								
		E = 0.0253 eV				E = 1 MeV				
		σ_t (barn)	σ_a (barn)	Σ_t (cm ⁻¹)	Σ_a (cm ⁻¹)	σ_t (barn)	σ_a (barn)	Σ_t (cm ⁻¹)	Σ_a (cm ⁻¹)	
Al	27	2.7	1.61	0.232	0.097	0.014	2.37	0.000	0.143	0.000
B	10	2.3	3845	3843	533	532	2.68	0.189	0.371	0.026
B	11	2.3	5.28	0.005	0.655	0.0006	2.13	0.000	0.268	0.000
Be	9	9	6.35	0.01	3.82	0.006	3.25	0.003	1.96	0.002
C	12	1.9	4.95	0.003	0.472	0.0003	2.58	0.000	0.246	0.000
Nat Ca	40.08	1.55	3.46	0.433	0.081	0.101	1.14	0.004	0.027	0.000
Cd	112	8.7	2470	2462	115.5	115.2	6.5	0.058	0.304	0.003
Nat Cl	34.45	Gas	50.2	33.4	Gas	Gas	2.3	0.001	Gas	Gas
Nat Cu	63.55	8.94	12.5	3.8	1.06	0.322	3.4	0.011	0.288	0.001
F	19	Gas	3.72	0.01	Gas	Gas	3.15	0.000	Gas	Gas
Fe	56	7.9	14.07	2.56	1.19	0.217	5.19	0.003	0.441	0.000
Nat Gd	157.25	7.95	49153	48981	1496	1491	7.33	0.223	0.223	0.007
H	1	Gas	30.62	0.33	Gas	Gas	4.26	0.000	Gas	Gas
H	2	Gas	4.25	0	Gas	Gas	2.87	0.000	Gas	Gas
He	3	Gas	5337	5336	Gas	Gas	2.87	0.879	Gas	Gas
He	4	Gas	0.86	0	Gas	Gas	7.08	0.000	Gas	Gas
Li	6	0.534	938	937	50.3	50.2	1.28	0.230	0.069	0.012
Li	7	0.534	1.16	0.036	0.053	0.0017	1.57	0.000	0.072	0.000
Nat Mg	24.31	1.74	3.47	0.063	0.15	0.0027	2.66	0.001	0.115	0.000
Mn	55	7.2	14.5	13.2	1.14	1.04	3.17	0.003	0.25	0.000

Material	Atomic or Molecular Weight	Density (g/cm ³)	Cross Section							
			E = 0.0253 eV				E = 1 MeV			
			σ_t (barn)	σ_a (barn)	Σ_t (cm ⁻¹)	Σ_a (cm ⁻¹)	σ_t (barn)	σ_a (barn)	Σ_t (cm ⁻¹)	Σ_a (cm ⁻¹)
N	14	Gas	12.22	1.9	Gas	Gas	2.39	0.021	Gas	Gas
Na	23	0.971	3.92	0.529	0.1	0.0134	3.17	0.000	0.081	0.000
Ni	59	8.9	23.08	4.58	2.1	0.416	3.66	0.001	0.322	0.000
O	16	Gas	3.87	0.000	Gas	Gas	8.22	0.000	Gas	Gas
Pb	204	11.34	11.40	0.18	0.381	0.006	4.39	0.003	0.147	0.000
Pu	238.05	19.6	599.3	562.0	29.72	27.87	6.66	0.190	0.330	0.0094
Pu	239.05	19.6	1021	270	50.4	13.3	7.01	0.026	0.364	0.0013
Pu	240.05	19.6	294	293	14.5	14.4	7.15	0.108	0.352	0.0053
Pu	241.06	19.6	1390	362	68.1	17.7	7.98	0.117	0.391	0.0057
Pu	242.06	19.6	26.7	18.9	1.30	0.922	7.31	0.098	0.357	0.0048
Nat Si	28.09	2.42	2.24	0.161	0.116	0.0084	4.43	0.01	0.230	0.0001
Th	232	11.3	20.4	7.50	0.598	0.220	7.00	0.135	0.205	0.0040
U	233.04	19.1	587	45.8	29.0	2.26	6.78	0.069	0.335	0.0034
U	234.04	19.1	116	103	5.70	5.07	8.02	0.363	0.394	0.0178
U	235.04	19.1	703	96.9	34.3	4.74	6.84	0.117	0.335	0.0057
U	236.05	19.1	13.3	5.16	0.648	0.251	7.73	0.363	0.377	0.177
U	237.05	19.1	487.5	476.4	23.6	23.1	6.72	0.135	0.326	0.0066
U	238.05	19.1	11.63	2.71	0.562	0.131	7.10	0.123	0.343	0.0059
Nat U	238.05	19.1	16.49	3.39	0.797	0.1637	7.01	0.120	0.343	0.0058
Nat W	183.85	19.3	23.08	18.05	1.459	1.141	6.95	0.057	0.439	0.0036
CH ₂	14	0.94			2.68	0.027			0.449	0.000
H ₂ O	18	1.0			2.18	0.022			0.560	0.000
D ₂ O	20	1.1			0.410	0.000			0.420	0.000

Material	Atomic or Molecular Weight Density (g/cm ³)	Cross Section							
		E = 0.0253 eV				E = 1 MeV			
		σ_t (barn)	σ_a (barn)	Σ_t (cm ⁻¹)	Σ_a (cm ⁻¹)	σ_t (barn)	σ_a (barn)	Σ_t (cm ⁻¹)	Σ_a (cm ⁻¹)
Average Fission Products of:									
²³⁵ U	117	4496	4486			7.43	0.0004		
²³⁹ Pu	119	2087	2086			7.48	0.0009		



APPENDIX B

Neutron Flux-to-Dose Rate Conversion Factors and Quality Factors

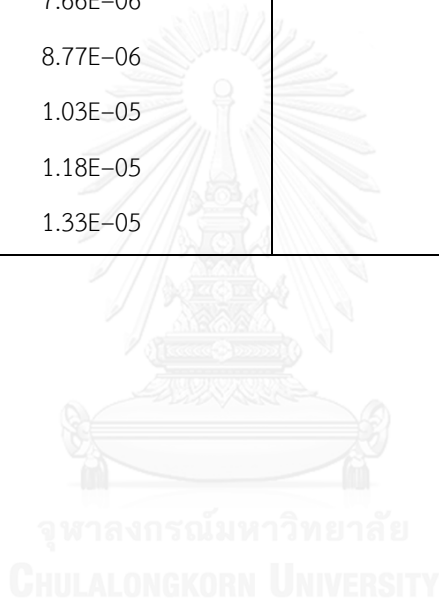
NCRP-38, ANSI/ANS-6.1.1-1977*			ICRP-21	
Energy, E (MeV)	DF(E) (rem/hr)/(n/cm ² -s)	Quality Factor	DF(E) (rem/hr)/(n/cm ² -s)	Quality Factor
2.5E-08	3.67E-06	2.0	3.85E-06	2.3
1.0E-07	3.67E-06	2.0	4.17E-06	2.0
1.0E-06	4.46E-06	2.0	4.55E-06	2.0
1.0E-05	4.54E-06	2.0	4.35E-06	2.0
1.0E-04	4.18E-06	2.0	4.17E-06	2.0
1.0E-03	3.76E-06	2.0	3.70E-06	2.0
1.0E-02	3.56E-06	2.5	3.57E-06	2.0
1.0E-01	2.17E-05	7.5	2.08E-05	7.4
5.0E-01	9.26E-05	11.0	7.14E-05	11.0
1.0	1.32E-04	11.0	1.18E-04	10.6
2.0			1.43E-04	9.3
2.5	1.25E-04	9.0		
5.0	1.56E-04	8.0	1.47E-04	7.8
7.0	1.47E-04	7.0		
10.0	1.47E-04	6.5	1.47E-04	6.8
14.0	2.08E-04	7.5		
20.0	2.27E-04	8.0	1.54E-04	6.0

*Extracted from American National Standard ANSI/ANS-6.1.1-1977 with permission of the publisher, the American Nuclear Society.

Photon Flux-to-Dose Rate Conversion Factors

ANSI/ANS-6.1.1-1977		ICRP-21	
Energy, E (MeV)	DF(E) (rem/hr)/(p/cm ² -s)	Energy, E (MeV)	DF(E) (rem/hr)/(p/cm ² -s)
0.01	3.96E-06	0.01	2.78E-06
0.03	5.82E-07	0.015	1.11E-06
0.05	2.90E-07	0.02	5.88E-07
0.07	2.58E-07	0.03	2.56E-07
0.1	2.83E-07	0.04	1.56E-07
0.15	3.79E-07	0.05	1.20E-07
0.2	5.01E-07	0.06	1.11E-07
0.25	6.31E-07	0.08	1.20E-07
0.3	7.59E-07	0.1	1.47E-07
0.35	8.78E-07	0.15	2.38E-07
0.4	9.85E-07	0.2	3.45E-07
0.45	1.08E-06	0.3	5.56E-07
0.5	1.17E-06	0.4	7.69E-07
0.55	1.27E-06	0.5	9.09E-07
0.6	1.36E-06	0.6	1.14E-06
0.65	1.44E-06	0.8	1.47E-06
0.7	1.52E-06	1	1.79E-06
0.8	1.68E-06	1.5	2.44E-06
1	1.98E-06	2	3.03E-06
1.4	2.51E-06	3	4.00E-06
1.8	2.99E-06	4	4.76E-06
2.2	3.42E-06	5	5.56E-06
2.6	3.82E-06	6	6.25E-06
2.8	4.01E-06	8	7.69E-06
3.25	4.41E-06	10	9.09E-06
3.75	4.83E-06		
4.25	5.23E-06		

ANSI/ANS-6.1.1-1977		ICRP-21	
Energy, E (MeV)	DF(E) (rem/hr)/(p/cm ² -s)	Energy, E (MeV)	DF(E) (rem/hr)/(p/cm ² -s)
4.75	5.60E-06		
5	5.80E-06		
5.25	6.01E-06		
5.75	6.37E-06		
6.25	6.74E-06		
6.75	7.11E-06		
7.5	7.66E-06		
9	8.77E-06		
11	1.03E-05		
13	1.18E-05		
15	1.33E-05		

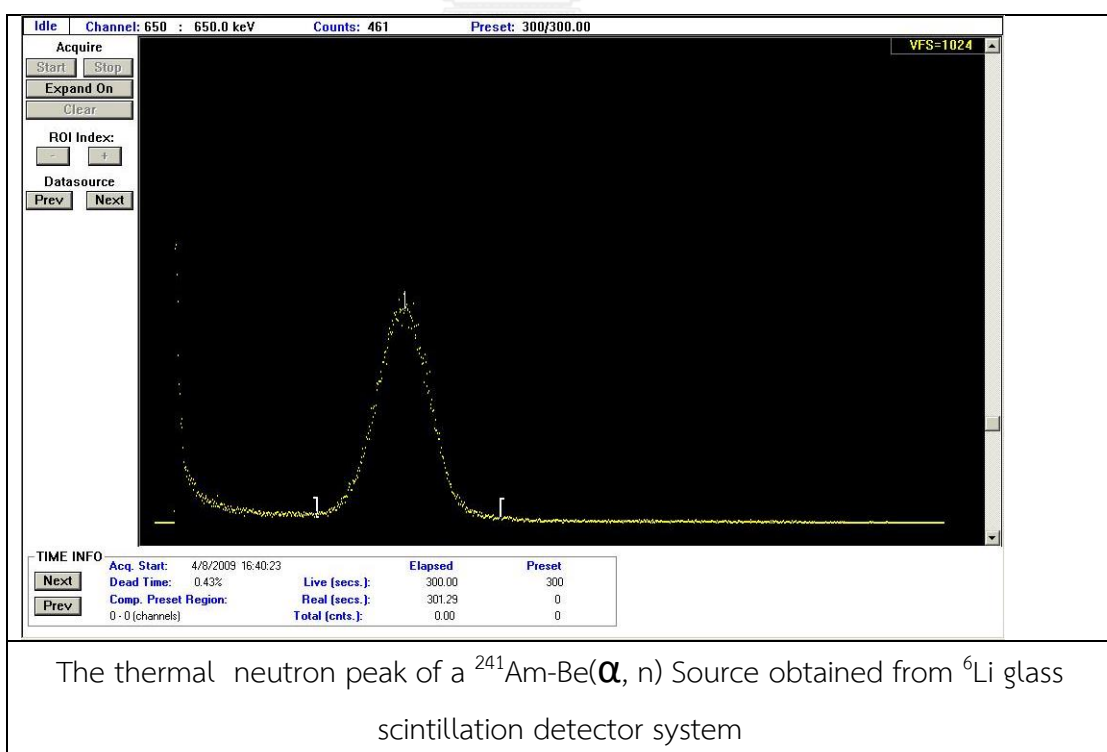
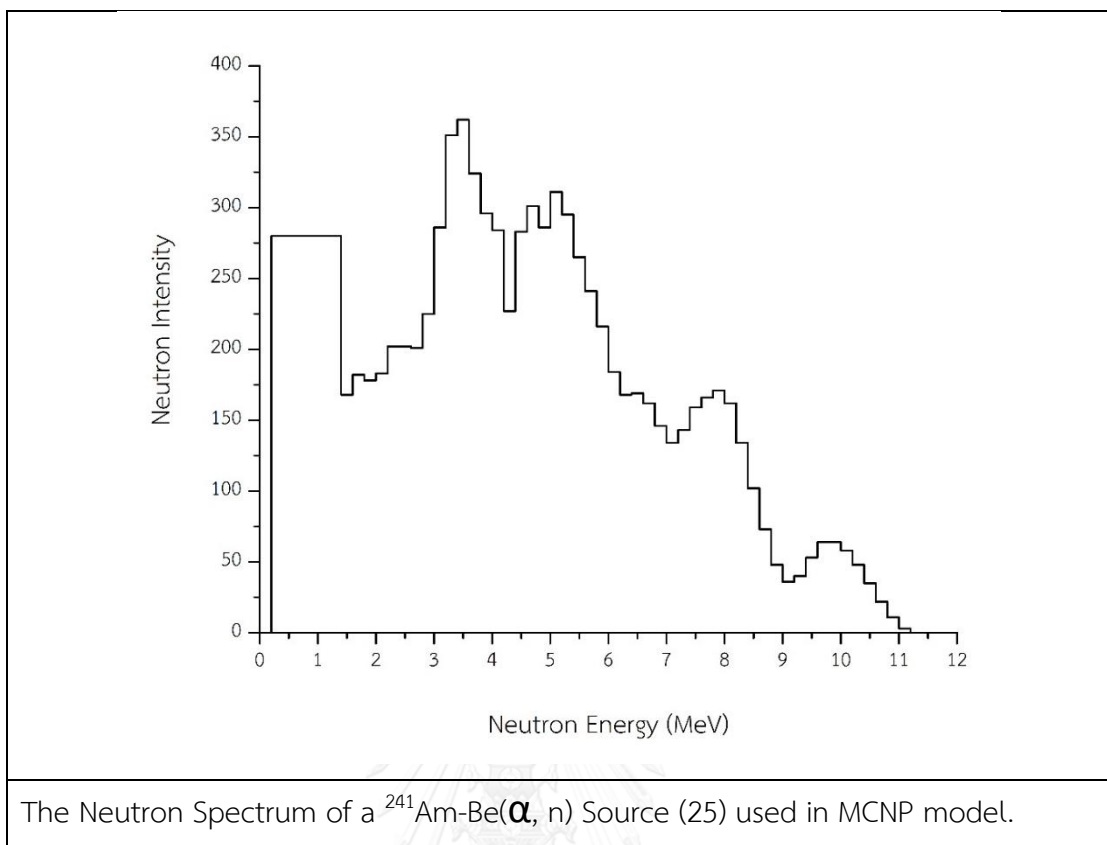


APPENDIX C

NEUTRON SOURCE

$^{241}\text{Am-Be}$ Neutron energy distribution.(25)

Median Energy (MeV)	Neutron Intensity (N _n)	Median Energy (MeV)	Neutron Intensity (N _n)	Median Energy (MeV)	Neutron Intensity (N _n)
0	0	4	284	8	162
0.2	280	4.2	227	8.2	134
0.4	280	4.4	283	8.4	102
0.6	280	4.6	301	8.6	73
0.8	280	4.8	286	8.8	48
1	280	5	311	9	36
1.2	280	5.2	295	9.2	40
1.4	168	5.4	265	9.4	53
1.6	182	5.6	241	9.6	64
1.8	178	5.8	216	9.8	64
2	183	6	184	10	58
2.2	202	6.2	168	10.2	48
2.4	202	6.4	169	10.4	35
2.6	201	6.6	162	10.6	22
2.8	225	6.8	146	10.8	11
3	286	7	134	11	3
3.2	351	7.2	143	11.2	1
3.4	362	7.4	159		
3.6	324	7.6	166		
3.8	296	7.8	171		$\Sigma N_n = 10,000$



APPENDIX D

EXAMPLE OF MCNP INPUT FILE

1. Sample#2 with B₂O₃ 40 phr (thickness = 1 cm)

MCNP input file

C Sphere (NR+SBR+B2O3 10 mm)

C Cell Card

21 21 -1.21 -21 imp:n,p=1 \$ NR+SBR+B2O3

90 30 -0.001205 -90 21 -999 imp:n,p=1 \$ surrounding air

999 0 999 imp:n,p=0

C Surface card

21 SPH 0 0 150 1 \$neutron shielding

90 RPP -150 150 -150 150 0 300

999 RPP -150 150 -150 150 0 300

C Data Card

mode n p

m10 1001 -0.143716 6000 -0.856284

m13 48000 -1

m21 1001 -10.378 6012 -89.622 8016 -27.577 5010 -2.46 5011 -9.963 \$ NR+SBR+B2O3

m30 8016 -0.501077 12000 -0.024121 13027 -0.095265 14000 -0.261764

m31 13027 -1

sdef par=1 pos=0 0 150 erg=d1 \$ dir=1 vec= 0 0 1

SI1 1E-8 1E-7 1E-6 1E-5 1E-4 1E-3 1E-2 1E-1 1 10 100

SP1 0 100 100 100 100 100 100 100 100 100 100

NPS 100000000

F2:N 21

F12:n 21

DE2 2.5e-8 1.0e-7 1.0e-6 1.0e-5 1.0e-4 1.0e-3 1.0e-2 1.0e-1 &

0.5 1.0 2.0 5.0 10.0 20.0

DF2 3.85e-6 4.17e-6 4.5e-6 4.35e-6 4.17e-6 3.7e-6 3.57e-6 &

2.08e-5 7.14e-5 1.18e-4 1.43e-4 1.47e-4 1.47e-4 1.54e-4

F22:P 21

F32:p 21

DE22 0.01 0.015 0.02 0.03 0.04 0.05 0.06 0.08 0.1 0.15 0.2 0.3 0.4 &
 0.5 0.6 0.8 1.0 1.5 2.0 3.0 4.0 5.0 6.0 8.0 10.0
 DF22 2.78e-6 1.11e-6 5.88e-7 2.56e-7 1.56e-7 1.20e-7 1.11e-7 1.20e-7 &
 1.47e-7 2.38e-7 3.45e-7 5.56e-7 7.69e-7 9.09e-7 1.14e-6 1.47e-6 1.79e-6 &
 2.44e-6 3.03e-6 4.00e-6 4.76e-6 5.56e-6 6.25e-6 7.69e-6 9.09e-6

2. Sample#10 with Fe₂O₃ 20 phr and B₂O₃ 20 phr (thickness = 10 cm)

MCNP input file

C Sphere (4layers NR+SBR+B2O3 2.5 cm/NR+SBR+Fe2O3 2.5 cm =10cm)

C Cell Card

```
21 22 -1.300744417 -21      imp:n,p=1 $ NR+SBR+Fe2O3
22 21 -1.21 -22  21        imp:n,p=1 $ NR+SBR+B2O3
23 22 -1.300744417 -23  22 imp:n,p=1 $ NR+SBR+Fe2O3
24 21 -1.21 -24  23        imp:n,p=1 $ NR+SBR+B2O3
30 30 -0.001205 -30 24      imp:n,p=1 $ air volume
31 30 -0.001205 -31 30      imp:n,p=1 $ middle air
90 30 -0.001205 -90  21 22 23 24 30 31 -999 imp:n,p=1 $ surrounding air
999 0 999                  imp:n,p=0
```

C Surface card

```
21 SPH 0 0 150 0.25 $neutron shielding B2O3
22 SPH 0 0 150 0.5 $neutron shielding B2O3
23 SPH 0 0 150 0.75 $neutron shielding B2O3
24 SPH 0 0 150 1 $neutron shielding B2O3
30 SPH 0 0 150 2 $ source to detector = 30cm
31 SPH 0 0 150 3
90 RPP -150 150 -150 150  0 300
999 RPP -150 150 -150 150  0 300
```

C Data Card

mode n p

m10 1001 -0.143716 6000 -0.856284

m13 48000 -1

m21 1001 -10.378 6012 -89.622 8016 -27.577 5010 -2.46 5011 -9.963 \$ NR+SBR+B2O3

m22 1001 -10.378 6012 -89.622 8016 -12.023 26000 -27.9767 \$ NR+SBR+Fe2O3
 m30 8016 -0.501077 12000 -0.024121 13027 -0.095265 14000 -0.261764
 m31 13027 -1
 sdef par=1 pos=0 0 150 erg=d1 \$ dir=1 vec= 0 0 1
 SI1 1E-8 1E-7 1E-6 1E-5 1E-4 1E-3 1E-2 1E-1 1 10 100
 SP1 0 100 100 100 100 100 100 100 100 100 100 100
 NPS 100000
 F4:n 31
 F14:n 31
 F2:N 24
 F12:n 24
 DE4 2.5e-8 1.0e-7 1.0e-6 1.0e-5 1.0e-4 1.0e-3 1.0e-2 1.0e-1 &
 0.5 1.0 2.0 5.0 10.0 20.0
 DF4 3.85e-6 4.17e-6 4.5e-6 4.35e-6 4.17e-6 3.7e-6 3.57e-6 &
 2.08e-5 7.14e-5 1.18e-4 1.43e-4 1.47e-4 1.47e-4 1.54e-4
 DE2 2.5e-8 1.0e-7 1.0e-6 1.0e-5 1.0e-4 1.0e-3 1.0e-2 1.0e-1 &
 0.5 1.0 2.0 5.0 10.0 20.0
 DF2 3.85e-6 4.17e-6 4.5e-6 4.35e-6 4.17e-6 3.7e-6 3.57e-6 &
 2.08e-5 7.14e-5 1.18e-4 1.43e-4 1.47e-4 1.47e-4 1.54e-4
 F24:p 31
 F34:p 31
 F22:P 24
 F32:p 24
 DE24 0.01 0.015 0.02 0.03 0.04 0.05 0.06 0.08 0.1 0.15 0.2 0.3 0.4 &
 0.5 0.6 0.8 1.0 1.5 2.0 3.0 4.0 5.0 6.0 8.0 10.0
 DF24 2.78e-6 1.11e-6 5.88e-7 2.56e-7 1.56e-7 1.20e-7 1.11e-7 1.20e-7 &
 1.47e-7 2.38e-7 3.45e-7 5.56e-7 7.69e-7 9.09e-7 1.14e-6 1.47e-6 1.79e-6 &
 2.44e-6 3.03e-6 4.00e-6 4.76e-6 5.56e-6 6.25e-6 7.69e-6 9.09e-6
 DE22 0.01 0.015 0.02 0.03 0.04 0.05 0.06 0.08 0.1 0.15 0.2 0.3 0.4 &
 0.5 0.6 0.8 1.0 1.5 2.0 3.0 4.0 5.0 6.0 8.0 10.0
 DF22 2.78e-6 1.11e-6 5.88e-7 2.56e-7 1.56e-7 1.20e-7 1.11e-7 1.20e-7 &
 1.47e-7 2.38e-7 3.45e-7 5.56e-7 7.69e-7 9.09e-7 1.14e-6 1.47e-6 1.79e-6 &
 2.44e-6 3.03e-6 4.00e-6 4.76e-6 5.56e-6 6.25e-6 7.69e-6 9.09e-6

3. Sample#2 with B₂O₃ 60 phr

MCNP input file

C NR+SBR+ B2O3 60 phr

C Cell Card

21 21 -1.295 -21 imp:n,p=1 \$ NR+SBR+B2O3

90 30 -0.001205 -90 21 -999 imp:n,p=1 \$ surrounding air

999 0 999 imp:n,p=0

C Surface card

21 SPH 0 0 150 1.1 \$neutron shielding B2O3

90 RPP -150 150 -150 150 0 300

999 RPP -150 150 -150 150 0 300

C Data Card

mode n p

m10 1001 -0.143716 6000 -0.856284

m13 48000 -1

m21 1001 -10.378 6012 -89.622 8016 -41.366 5010 -3.690 5011 -14.945 \$ NR+SBR+B2O3

m30 8016 -0.501077 12000 -0.024121 13027 -0.095265 14000 -0.261764

m31 13027 -1

sdef par=1 pos=0 0 150 erg=d1 \$ dir=1 vec= 0 0 1

SI1 1E-8 1E-7 1E-6 1E-5 1E-4 1E-3 1E-2 \$ thermal neutron source

SP1 0 100 100 100 100 100 100

NPS 100000000

F2:N 25

F12:n 25

E2 1E-8 2E-8 4E-8 6E-8 8E-8 1E-7 2E-7 4E-7 6E-7 8E-7 1E-6 2E-6 4E-6 6E-6 &

8E-6 1E-5 2E-5 4E-5 6E-5 8E-5 1E-4 2E-4 4E-4 6E-4 8E-4 1E-3 2E-3 4E-3 6E-3 &

8E-3 1E-2 2E-2 4E-2 6E-2 8E-2 1E-1 2E-1 4E-1 6E-1 8E-1 1 2 4 6 8 10 20 40 &

60 80 100

E12 1E-8 2E-8 4E-8 6E-8 8E-8 1E-7 2E-7 4E-7 6E-7 8E-7 1E-6 2E-6 4E-6 6E-6 &

8E-6 1E-5 2E-5 4E-5 6E-5 8E-5 1E-4 2E-4 4E-4 6E-4 8E-4 1E-3 2E-3 4E-3 6E-3 &

8E-3 1E-2 2E-2 4E-2 6E-2 8E-2 1E-1 2E-1 4E-1 6E-1 8E-1 1 2 4 6 8 10 20 40 &

60 80 100

DE2 2.5e-8 1.0e-7 1.0e-6 1.0e-5 1.0e-4 1.0e-3 1.0e-2 1.0e-1 &
 0.5 1.0 2.0 5.0 10.0 20.0
 DF2 3.85e-6 4.17e-6 4.5e-6 4.35e-6 4.17e-6 3.7e-6 3.57e-6 &
 2.08e-5 7.14e-5 1.18e-4 1.43e-4 1.47e-4 1.47e-4 1.54e-4
 F22:P 25
 F32:p 25
 E22 1E-8 2E-8 4E-8 6E-8 8E-8 1E-7 2E-7 4E-7 6E-7 8E-7 1E-6 2E-6 4E-6 6E-6 &
 8E-6 1E-5 2E-5 4E-5 6E-5 8E-5 1E-4 2E-4 4E-4 6E-4 8E-4 1E-3 2E-3 4E-3 6E-3 &
 8E-3 1E-2 2E-2 4E-2 6E-2 8E-2 1E-1 2E-1 4E-1 6E-1 8E-1 1 2 4 6 8 10 20 40 &
 60 80 100
 E32 1E-8 2E-8 4E-8 6E-8 8E-8 1E-7 2E-7 4E-7 6E-7 8E-7 1E-6 2E-6 4E-6 6E-6 &
 8E-6 1E-5 2E-5 4E-5 6E-5 8E-5 1E-4 2E-4 4E-4 6E-4 8E-4 1E-3 2E-3 4E-3 6E-3 &
 8E-3 1E-2 2E-2 4E-2 6E-2 8E-2 1E-1 2E-1 4E-1 6E-1 8E-1 1 2 4 6 8 10 20 40 &
 60 80 100
 DE22 0.01 0.015 0.02 0.03 0.04 0.05 0.06 0.08 0.1 0.15 0.2 0.3 0.4 &
 0.5 0.6 0.8 1.0 1.5 2.0 3.0 4.0 5.0 6.0 8.0 10.0
 DF22 2.78e-6 1.11e-6 5.88e-7 2.56e-7 1.56e-7 1.20e-7 1.11e-7 1.20e-7 &
 1.47e-7 2.38e-7 3.45e-7 5.56e-7 7.69e-7 9.09e-7 1.14e-6 1.47e-6 1.79e-6 &
 2.44e-6 3.03e-6 4.00e-6 4.76e-6 5.56e-6 6.25e-6 7.69e-6 9.09e-6

4. Sample#10 with Fe₂O₃ 100 phr and B₂O₃ 10 phr (with both side of Cd)

MCNP input file

C Sphere (4layers NR+SBR+B2O3 2.5cm/NR+SBR+Fe2O3 2.5cm =10cm)

C Cell Card

```

20 20 -8.65 -20      imp:n,p=1 $ Cd
21 22 -1.67959 -21 20  imp:n,p=1 $ NR+SBR+Fe2O3
22 21 -1.058 -22  21  imp:n,p=1 $ NR+SBR+B2O3
23 22 -1.67959 -23  22 imp:n,p=1 $ NR+SBR+Fe2O3
24 21 -1.058 -24  23  imp:n,p=1 $ NR+SBR+B2O3
25 20 -8.65 -25 24  imp:n,p=1 $ Cd
90 30 -0.001205 -90 20 21 22 23 24 25 -999 imp:n,p=1 $ surrounding air
999 0 999 imp:n,p=0
  
```

C Surface card

20 SPH 0 0 150 0.1 \$ Cd

21 SPH 0 0 150 2.6 \$neutron shielding B2O3
 22 SPH 0 0 150 5.1 \$neutron shielding B2O3
 23 SPH 0 0 150 7.6 \$neutron shielding B2O3
 24 SPH 0 0 150 10.1 \$neutron shielding B2O3
 25 SPH 0 0 150 10.2 \$ Cd
 90 RPP -150 150 -150 150 0 300
 999 RPP -150 150 -150 150 0 300

C Data Card

mode n p

m10 1001 -0.143716 6000 -0.856284

m13 48000 -1

m20 48000 -1 \$ CD

m21 1001 -10.378 6012 -89.622 8016 -6.894 5010 -0.615 5011 -2.491 \$ NR+SBR+B2O3

m22 1001 -10.378 6012 -89.622 8016 -30.057 26000 -69.942 \$ NR+SBR+Fe2O3

m30 8016 -0.501077 12000 -0.024121 13027 -0.095265 14000 -0.261764

m31 13027 -1

sdef par=1 pos=0 0 150 erg=d1 \$ dir=1 vec= 0 0 1

SI1 1E-8 1E-7 1E-6 1E-5 1E-4 1E-3 1E-2 1E-1 1 10 100 \$ entire neutron energy source

SP1 0 100 100 100 100 100 100 100 100 100 100 100

NPS 100000000

F2:N 25

F12:n 25

E2 1E-8 2E-8 4E-8 6E-8 8E-8 1E-7 2E-7 4E-7 6E-7 8E-7 1E-6 2E-6 4E-6 6E-6 &

8E-6 1E-5 2E-5 4E-5 6E-5 8E-5 1E-4 2E-4 4E-4 6E-4 8E-4 1E-3 2E-3 4E-3 6E-3 &

8E-3 1E-2 2E-2 4E-2 6E-2 8E-2 1E-1 2E-1 4E-1 6E-1 8E-1 1 2 4 6 8 10 20 40 &

60 80 100

E12 1E-8 2E-8 4E-8 6E-8 8E-8 1E-7 2E-7 4E-7 6E-7 8E-7 1E-6 2E-6 4E-6 6E-6 &

8E-6 1E-5 2E-5 4E-5 6E-5 8E-5 1E-4 2E-4 4E-4 6E-4 8E-4 1E-3 2E-3 4E-3 6E-3 &

8E-3 1E-2 2E-2 4E-2 6E-2 8E-2 1E-1 2E-1 4E-1 6E-1 8E-1 1 2 4 6 8 10 20 40 &

60 80 100

DE2 2.5e-8 1.0e-7 1.0e-6 1.0e-5 1.0e-4 1.0e-3 1.0e-2 1.0e-1 &

0.5 1.0 2.0 5.0 10.0 20.0

DF2 3.85e-6 4.17e-6 4.5e-6 4.35e-6 4.17e-6 3.7e-6 3.57e-6 &

2.08e-5 7.14e-5 1.18e-4 1.43e-4 1.47e-4 1.47e-4 1.54e-4

F22:P 25

F32:p 25

E22 1E-8 2E-8 4E-8 6E-8 8E-8 1E-7 2E-7 4E-7 6E-7 8E-7 1E-6 2E-6 4E-6 6E-6 &
8E-6 1E-5 2E-5 4E-5 6E-5 8E-5 1E-4 2E-4 4E-4 6E-4 8E-4 1E-3 2E-3 4E-3 6E-3 &
8E-3 1E-2 2E-2 4E-2 6E-2 8E-2 1E-1 2E-1 4E-1 6E-1 8E-1 1 2 4 6 8 10 20 40 &
60 80 100

E32 1E-8 2E-8 4E-8 6E-8 8E-8 1E-7 2E-7 4E-7 6E-7 8E-7 1E-6 2E-6 4E-6 6E-6 &
8E-6 1E-5 2E-5 4E-5 6E-5 8E-5 1E-4 2E-4 4E-4 6E-4 8E-4 1E-3 2E-3 4E-3 6E-3 &
8E-3 1E-2 2E-2 4E-2 6E-2 8E-2 1E-1 2E-1 4E-1 6E-1 8E-1 1 2 4 6 8 10 20 40 &
60 80 100

DE22 0.01 0.015 0.02 0.03 0.04 0.05 0.06 0.08 0.1 0.15 0.2 0.3 0.4 &

0.5 0.6 0.8 1.0 1.5 2.0 3.0 4.0 5.0 6.0 8.0 10.0

DF22 2.78e-6 1.11e-6 5.88e-7 2.56e-7 1.56e-7 1.20e-7 1.11e-7 1.20e-7 &
1.47e-7 2.38e-7 3.45e-7 5.56e-7 7.69e-7 9.09e-7 1.14e-6 1.47e-6 1.79e-6 &
2.44e-6 3.03e-6 4.00e-6 4.76e-6 5.56e-6 6.25e-6 7.69e-6 9.09e-6

5. Slab material transmission test (sample#2 20 cm)

MCNP input file

C NR+SBR+B2O3

C Cell Card

```
10 10 -3 -10 12      imp:n,p=1 $ Parafin
12 12 -0.001205 -12   imp:n,p=1 $ air pocket
21 21 -1.295 -21     imp:n,p =1 $ shielding
31 31 -8.65 -31 32    imp:n,p =1 $ cadmium sheet
32 12 -0.001205 -32   imp:n,p=1 $ air pocket
50 50 -2.48 -50       imp:n,p=1 $ glass scintillator detector NE905
90 12 -0.001205 10 21 31 32 50 -999 imp:n,p=1 $ surrounding air
999 0 999 imp:n,p=0
```

C Surface card

10 RCC 0 0 0 0 0 16 8 \$ Height = 16 radius = 8

12 RCC 0 0 4 0 0 12 1.6 \$ start = 4 radius = 1.6

21 RPP -7.5 7.5 -7.5 7.5 16.1 36.1 \$ NR+SBR+B2O3 60phr

31 RCC 0 0 16 0 0 0.1 8

32 RCC 0 0 16 0 0 0.1 1.6
 50 RCC 0 0 44.1 0 0 1 1.25
 60 Pz 36.1
 999 RPP -100 100 -100 100 0 150

C Data Card
 mode n p
 m10 1001 -143.7 6012 -856.3
 m12 6000 -0.000124 7014 -0.755268 8016 -0.231781 18000 -0.012827 \$ air \$ air
 m21 1001 -10.378 6012 -89.622 8016 -41.366 5010 -3.690 5011 -14.945 \$ NR+SBR+H3BO3+B
 m31 48000 -8.65 \$ Cd sheet
 m50 8016 -0.501077 12000 -0.024121 13027 -0.095265 14000 -0.261764 \$detector NE905
 sdef par=1 pos=0 0 4.1 erg=d1 \$ dir = 1 vec = 0 0 1
 SI1 L 0 0.2 0.4 0.6 0.8 1.0 1.2 1.4 1.6 1.8 2.0 2.2 &
 2.4 2.6 2.8 3.0 3.2 3.4 3.6 3.8 4.0 4.2 4.4 4.6 4.8 &
 5.0 5.2 5.4 5.6 5.8 6.0 6.2 6.4 6.6 6.8 7.0 7.2 7.4 &
 7.6 7.8 8.0 8.2 8.4 8.6 8.8 9.0 9.2 9.4 9.6 9.8 10.0 &
 10.2 10.4 10.6 10.8 11.0 11.2 \$ AmBe neutron source
 SP1 0 280 280 280 280 280 168 182 &
 178 183 202 202 201 225 286 351 362 &
 324 296 284 277 283 301 286 311 295 &
 265 241 216 184 168 169 162 146 134 &
 143 159 166 171 162 134 102 73 48 &
 36 40 53 64 64 58 48 35 22 11 3 1
 NPS 1000000000
 F4:n 50
 F14:n 50
 F2:n 60
 E4 1E-8 2E-8 4E-8 6E-8 8E-8 1E-7 2E-7 4E-7 6E-7 8E-7 1E-6 2E-6 4E-6 6E-6 &
 8E-6 1E-5 2E-5 4E-5 6E-5 8E-5 1E-4 2E-4 4E-4 6E-4 8E-4 1E-3 2E-3 4E-3 6E-3 &
 8E-3 1E-2 2E-2 4E-2 6E-2 8E-2 1E-1 2E-1 4E-1 6E-1 8E-1 1 2 4 6 8 10 20 40 &
 60 80 100
 E14 1E-8 2E-8 4E-8 6E-8 8E-8 1E-7 2E-7 4E-7 6E-7 8E-7 1E-6 2E-6 4E-6 6E-6 &
 8E-6 1E-5 2E-5 4E-5 6E-5 8E-5 1E-4 2E-4 4E-4 6E-4 8E-4 1E-3 2E-3 4E-3 6E-3 &
 8E-3 1E-2 2E-2 4E-2 6E-2 8E-2 1E-1 2E-1 4E-1 6E-1 8E-1 1 2 4 6 8 10 20 40 &

60 80 100

E2 1E-8 2E-8 4E-8 6E-8 8E-8 1E-7 2E-7 4E-7 6E-7 8E-7 1E-6 2E-6 4E-6 6E-6 &
8E-6 1E-5 2E-5 4E-5 6E-5 8E-5 1E-4 2E-4 4E-4 6E-4 8E-4 1E-3 2E-3 4E-3 6E-3 &

8E-3 1E-2 2E-2 4E-2 6E-2 8E-2 1E-1 2E-1 4E-1 6E-1 8E-1 1 2 4 6 8 10 20 40 &

60 80 100

DE4 2.5e-8 1.0e-7 1.0e-6 1.0e-5 1.0e-4 1.0e-3 1.0e-2 1.0e-1 &

0.5 1.0 2.0 5.0 10.0 20.0

DF4 3.85e-6 4.17e-6 4.5e-6 4.35e-6 4.17e-6 3.7e-6 3.57e-6 &

2.08e-5 7.14e-5 1.18e-4 1.43e-4 1.47e-4 1.47e-4 1.54e-4

F24:p 50

F34:p 50

F12:P 60

E24 1E-8 2E-8 4E-8 6E-8 8E-8 1E-7 2E-7 4E-7 6E-7 8E-7 1E-6 2E-6 4E-6 6E-6 &

8E-6 1E-5 2E-5 4E-5 6E-5 8E-5 1E-4 2E-4 4E-4 6E-4 8E-4 1E-3 2E-3 4E-3 6E-3 &

8E-3 1E-2 2E-2 4E-2 6E-2 8E-2 1E-1 2E-1 4E-1 6E-1 8E-1 1 2 4 6 8 10 20 40 &

60 80 100

E34 1E-8 2E-8 4E-8 6E-8 8E-8 1E-7 2E-7 4E-7 6E-7 8E-7 1E-6 2E-6 4E-6 6E-6 &

8E-6 1E-5 2E-5 4E-5 6E-5 8E-5 1E-4 2E-4 4E-4 6E-4 8E-4 1E-3 2E-3 4E-3 6E-3 &

8E-3 1E-2 2E-2 4E-2 6E-2 8E-2 1E-1 2E-1 4E-1 6E-1 8E-1 1 2 4 6 8 10 20 40 &

60 80 100

E12 1E-8 2E-8 4E-8 6E-8 8E-8 1E-7 2E-7 4E-7 6E-7 8E-7 1E-6 2E-6 4E-6 6E-6 &

8E-6 1E-5 2E-5 4E-5 6E-5 8E-5 1E-4 2E-4 4E-4 6E-4 8E-4 1E-3 2E-3 4E-3 6E-3 &

8E-3 1E-2 2E-2 4E-2 6E-2 8E-2 1E-1 2E-1 4E-1 6E-1 8E-1 1 2 4 6 8 10 20 40 &

60 80 100

DE24 2.5e-8 1.0e-7 1.0e-6 1.0e-5 1.0e-4 1.0e-3 1.0e-2 1.0e-1 &

0.5 1.0 2.0 5.0 10.0 20.0

DF24 3.85e-6 4.17e-6 4.5e-6 4.35e-6 4.17e-6 3.7e-6 3.57e-6 &

2.08e-5 7.14e-5 1.18e-4 1.43e-4 1.47e-4 1.47e-4 1.54e-4

REFERENCES

- 1) J. Kenneth Shultis REF. Radiation Shielding and Radiological Protection. In: Cacuci DG, editor. Handbook of nuclear engineering. 1: Springer Science & Business Media, 2010; 2010. p. 1313.
- (2) Faw JKSARE. Radiation shielding: Prentice Hall PTR; 1996. 533 p.
- (3) A. El-Sayed Abdo MAE-S, F.A. Gaber. Utilization of ilmenite/epoxy composite for neutrons and gamma rays attenuation. Annals of Nuclear Energy. 2003;30:175–87.
- (4) Okuno K. Neutron shielding material based on colemanite and epoxy resin. Radiation Protection Dosimetry. 2005;115(1-4):258-61.
- (5) Osman Gencel WB, Cengiz Ozel and Mümin Filiz. An investigation on the concrete properties containing colemanite. International Journal of Physical Sciences. 2010;5(3):216-25.
- (6) Osman Gençel MN, Ömer Çelik, Kadir Yalman and Dilek Bayram. Selenium and vitamin E modulates radiation-induced liver toxicity in pregnant and nonpregnant rat : effects of colemanite and hematite shielding. Biol Trace Elem Res. 2010;135:253-63.
- (7) Gencel O. 5. Gamma and neutron shielding characteristics of concretes containing different colemanite proportions. Nuclear Science and Technology. 2012;41-9.
- (8) S.E. Gwaily MMB, H.H. Hassan, M. Madani Natural rubber composites as thermal neutron radiation shields I. B_4C/NR composites Polymer Testing. 2002;21:123-33.
- (9) S.E. Gwaily HHH, M.M. Badawy, M. Madani Natural rubber composites as thermal neutron radiation shields II — H_3BO_3/NR composites. Polymer Testing. 2002; 21:513–7.
- (10) Chayanit Jumpee DW. Innovative neutron shielding materials composed of natural rubber-styrene butadiene rubber blends, boron oxide and iron(III) oxide Journal of Physics : conference Series. 2015;1(611).
- (11) Huasi Hu QW, Juan Qin, Yuelei Wu, Tiankui Zhang, Zhongsheng Xie, Xinbiao Jiang,, Guoguang Zhang HX, Xiangyang Zheng, Jing Zhang, Wenhao Liu, Zhenghong Li, Boping Zhang,, Linbo Li ZS, Xiaoping Ouyang, Jun Zhu, Yaolin Zhao, Xiaoqin Mi,

- Zhengping Dong, Cheng Li,, Zhenyu Jiang aYZ. Study on composite material for shielding mixed neutron and γ -Rays. IEEE Transactions on nuclear science. 2008;55.
- (12) Elbio Calzada F, BurkhardSchillinger, HaraldTurck Reusable shielding material for neutron and gamma radiation. Nuclear Instruments and Methods in Physics Research A. 2011:77-80.
- (13) L'Annunziata MF. Chapter 1 - Radiation Physics and Radionuclide Decay. In: L'Annunziata MF, editor. Handbook of Radioactivity Analysis (Third Edition). Amsterdam: Academic Press; 2012. p. 1-162.
- (14) Knoll G. Radiation Detection and Measurement. Toronto: John Wiley & Sons, Inc; 1979.
- (15) Lamarsch JR. Introduction to nuclear reactor theory. [Ithaca, N. Y.]1961. v. p.
- (16) ENDF/B-VII.1 Incident-Neutron Data [Internet]. Los Alamos National Security, LLC for the U.S. Department of Energy's NNSA. 2011. Available from: <https://t2.lanl.gov/nis/data/endf/endfvii.1-n-pdf/u235.pdf>.
- (17) Team X-MC. MCNP — A General Monte Carlo
N-Particle Transport Code, Version 5
Volume I: Overview and Theory: University of California, Los Alamos National Laboratory; 2003. 340 p.
- (18) Team X-MC. MCNP — A General Monte Carlo
N-Particle Transport Code, Version 5
Volume II: User's Guide: University of California, Los Alamos National Laboratory; 2003.
- (19) แซ่ อุย พ. ยา : ชนิด สมบัติ และการใช้งาน. กรุงเทพมหานคร: ชีเอ็ด จำกัด; 2548.
20. Mineralszone.com. Borate.
- (21) RJ McConn Jr CG, RT Pagh, RA Rucker, RG Williams III Radiation Portal Monitor : Project Compendium of Material Composition Data for Radiation Transport Modeling. Washington: The U.S. Department of Homeland Security U.S. Customs and Border Protection and Domestic Nuclear Detection Office 2011. p. 18.
- (22) Crosby KS. Geology of the Udon Thani Potash (Sylvinitite) Deposits with an Overview for Development of a Sustainable Potassium Resource for Thailand.

Proceedings of the International Conference on Geology of Thailand: Towards Sustainable Development and Sufficiency Economy. 2007:96-103.

(23) Suwanich P. Geology and geological structure of potash and rock salt deposits in Chalerm Phrakiat district, Nakhon Ratchasima province in Northeastern Thailand. Kasetart J (Nat Sci). 2010;44:1058 - 68.

(24) Rinard PM. Neutron Interactions with Matter. In: Kreiner S, editor. Passive Nondestructive Assay of Nuclear Materials. Washington, DC: Office of Nuclear Regulatory Research, U.S. Nuclear Regulatory Commission; 1991. p. 368.

(25) ZWAN KWGaLVD. The Neutron Spectrum of a $^{241}\text{Am-Be}(\alpha, n)$ Source as Simulated by Accelerator Produced α -Particles. International Journal of Applied Radiation and Isotope. 1970;21:7.



VITA

NAME: Ms. Chayanit Jumpee

SEX: Female

NATIONALITY: Thai

DATE OF BIRTH: 20 January 1984

PLACE OF BIRTH: Chiangrai, Thailand

INSTITUTIONS ATTENDED:

Chiangmai University,

2002-2006: Bachelor of Science (Radiological Technology)

Chulalongkorn University,

2008-2010: Master of Science (Nuclear Technology)

Chulalongkorn University,

2010-2015: Doctoral of Engineering (Nuclear Engineering)

HOME ADDRESS: 94 Moo 15 Wiang, Thoeng district, Chiangrai, Thailand,
57160, Tel. 089-2651692

Email: bullterrier_amp@hotmail.com